UNIVERSITY OF CALIFORNIA
SANTA CRUZ

THE FLAVOR PROGRAM: SPANNING SCALES AND RARE NEW PHYSICS

A dissertation submitted in partial satisfaction of the
requirements for the degree of

DOCTOR OF PHILOSOPHY

in

PHYSICS

by

Sri Aditya Gadam

June 2025

The Dissertation of Sri Aditya Gadam
is approved:

DocuSigned by:
Wolfgang Altmannshofer
6970CA890CB7417...
Professor Wolfgang Altmannshofer, Chair

DocuSigned by:
Stefano Profumo
795D46FB8122492...
Professor Stefano Profumo

DocuSigned by:
Stefania Gori
06F1E70FBCB24FE...
Professor Stefania Gori

Dean Peter Biehl
Vice Provost and Dean of Graduate Studies

Contents

List of Figures

List of Tables

Abstract

The Flavor Program: Spanning Scales and Rare New Physics

by

Sri Aditya Gadam

This dissertation presents novel approaches to probing physics beyond the Standard Model through precision flavor physics. It comprises four major studies: (1) A supersymmetric extension of the Standard Model that explains the muon g-2 anomaly with multi-TeV sleptons; (2) A supersymmetric flavor clockwork model addressing both the flavor puzzle and making predictions for flavor violation in the supersymmetric sector; (3) An investigation of bottom-strange production at future muon colliders as a probe of the same new physics that might explain current B-decay anomalies; and (4) A study of rare Λ_b decays at future Z-factories, introducing new observables that exploit baryon polarization to provide unique sensitivity to new physics. Together, these works demonstrate the extraordinary power of precision measurements to probe physics at energy scales far beyond the direct reach of current colliders.

To life and nature!

Acknowledgments

I would like to express my sincere gratitude to my advisor, Professor Wolfgang Altmannshofer, for his guidance, support, and mentorship throughout my doctoral studies. His insights, enthusiasm, and dedication to physics have been truly inspirational. He has genuinely been the best advisor one could ask for, and it is my hope that others will learn from him.

I am also deeply grateful to my committee members, Professor Stefano Profumo and Professor Stefania Gori, for their valuable feedback and encouragement. Their expertise and perspectives have significantly enriched my research, and my collaborations with them have taught me a lot.

My collaborations with Nick Hamer and Kevin Toner have been both productive and enjoyable. I thank them for their contributions to the work presented in this dissertation.

I would like to acknowledge Professors Howard Haber, Jason Nielsen, and Onuttom Narayan for being exceptional teachers and valuable resources during my PhD. Their wisdom and willingness to help have been instrumental in my growth as a physicist.

I would like to acknowledge the vibrant intellectual environment at the Santa Cruz Institute for Particle Physics, which has been instrumental in shaping my development as a physicist.

My deepest gratitude goes to Kiley Mayford, my wonderful partner, whose unwavering support, patience, and encouragement have sustained me throughout this journey. They have helped make me a better me.

Finally, I extend my heartfelt thanks to my parents and friends for their constant support throughout this challenging and rewarding experience.

Chapter 1

Introduction: The Standard Model and Beyond

1.1 The Standard Model: Triumphs and Limitations

The Standard Model (SM) of particle physics stands as one of the most successful theoretical frameworks in the history of science. Over the past half-century, it has withstood countless experimental tests, culminating in the discovery of the Higgs boson at the Large Hadron Collider (LHC) in 2012 [8, 229]. The SM provides a quantum field theoretical description of three of the four fundamental forces in nature—the electromagnetic, weak, and strong interactions—through an elegant mathematical structure based on the gauge symmetry group $\mathrm{SU}(3)_C \times \mathrm{SU}(2)_L \times \mathrm{U}(1)_Y$. It successfully describes the properties and interactions of all known elementary particles: the spin-1/2 fermions (quarks and leptons), the spin-1 gauge bosons that mediate the forces, and the spin-0 Higgs boson responsible for the mechanism of electroweak symmetry breaking [329, 506, 474].

The predictive power of the SM is remarkable. It accurately accounts for phenomena spanning an enormous range of energy scales, from the atomic to the TeV regime. The measured properties of the electroweak gauge bosons match

theoretical predictions with extraordinary precision [513, 476]. The discovery of the top quark with a mass close to theoretical expectations [57, 47] and the Higgs boson with properties consistent with SM predictions [9, 401] further cemented the model's credibility. The SM even successfully describes subtle quantum effects such as CP violation in kaon and B-meson systems [121, 206] and the running of the gauge couplings with energy [169, 496].

Despite these impressive successes, there exists compelling evidence that the SM cannot be the complete theory of fundamental physics. Several profound questions remain unanswered within the SM framework, pointing to the existence of "New Physics" (NP) beyond its scope. These shortcomings can be broadly categorized into observational inconsistencies, theoretical puzzles, and unexplained phenomena.

1.1.1 The Hierarchy Problem

One of the most pressing theoretical issues within the SM is the hierarchy problem [512, 370, 495]. The Higgs boson mass receives quantum corrections that are quadratically sensitive to the highest energy scale at which the theory remains valid. If this scale is the Planck scale ($M_{Pl} \sim 10^{19}$ GeV), where gravity becomes important, then the "natural" value for the Higgs mass would be approximately M_{Pl}. However, the observed Higgs mass is approximately 125 GeV [6, 487], some 17 orders of magnitude smaller.

This extreme discrepancy requires an extraordinary degree of fine-tuning in the bare parameters of the theory to cancel these large quantum corrections—a situation widely considered unnatural. This fine-tuning problem suggests there should be new physics at a scale not too far above the electroweak scale that provides a more natural explanation for the observed Higgs mass. Proposed solutions include supersymmetry [427, 510, 447], which introduces partner particles that provide cancellations in quantum corrections; extra dimensions [462, 136, 129], which dilute gravity's strength; and technicolor models [508, 495, 363], which generate masses dynamically through new strong interactions.

1.1.2 Matter-Antimatter Asymmetry

The observed universe contains significantly more matter than antimatter, agreed upon by theoretical and experimental work [287, 463, 288]. This asymmetry cannot be explained within the SM framework, which predicts nearly equal amounts of matter and antimatter should have been produced in the early universe. While the SM incorporates CP violation through the complex phase in the Cabibbo-Kobayashi-Maskawa (CKM) matrix [215, 408], this source is quantitatively insufficient to explain the observed baryon asymmetry as demonstrated by [313, 378, 314].

Generating the observed matter-antimatter asymmetry requires satisfying the three Sakharov conditions [471, 472]: baryon number violation, C and CP violation, and interactions out of thermal equilibrium. Although the SM contains mechanisms for all three, they are too weak to produce the observed asymmetry. Additional sources of CP violation beyond the SM are therefore necessary, potentially arising in the neutrino sector [309, 273], in extensions of the Higgs sector [499, 463], or through new heavy particles at high energy scales [202, 273, 242].

1.1.3 Dark Matter

Astrophysical and cosmological observations provide overwhelming evidence for the existence of dark matter, which accounts for approximately 27% of the energy content of the universe [70, 69]. Dark matter's gravitational effects have been observed in galaxy rotation curves [466, 467, 250], gravitational lensing [244, 432, 444], and the cosmic microwave background [70, 69].

The SM contains no particle that could serve as a dark matter candidate. The required particle must be stable, electrically neutral, and interact only weakly with ordinary matter. Proposed candidates include Weakly Interacting Massive Particles (WIMPs) [393, 168, 302], axions [455, 511, 403], sterile neutrinos [51, 50], and primordial black holes [221, 222], all of which require physics beyond the SM.

1.1.4 Experimental Anomalies

In addition to these fundamental questions, several experimental measurements show persistent deviations from SM predictions. While individual discrepancies must be treated with caution, patterns of related anomalies could provide crucial insights into the nature of physics beyond the SM.

1.2 Flavor Physics Anomalies

Flavor physics, which studies the transitions between different quark and lepton flavors, offers a powerful indirect probe of new physics. The highly suppressed nature of many flavor-changing processes in the SM makes them particularly sensitive to new physics contributions. Over the past decade, several intriguing anomalies have emerged in flavor physics measurements, particularly in semileptonic B-meson decays.

1.2.1 The $b \to s\ell^+\ell^-$ Anomalies

Among the most prominent flavor anomalies are discrepancies observed in $b \to s\mu^+\mu^-$ transitions [17, 22, 23]. The LHCb experiment has reported several measurements of $B \to K^{(*)}\mu^+\mu^-$ and $B_s \to \phi\mu^+\mu^-$ decays that consistently deviate from SM predictions. These include:

1. Branching ratio deficits in $B \to K\mu^+\mu^-$, $B \to K^*\mu^+\mu^-$, and $B_s \to \phi\mu^+\mu^-$ [18, 23, 34, 37], where the measured rates are lower than SM predictions by approximately 30%.

2. Angular distribution anomalies in $B \to K^*\mu^+\mu^-$ [29, 32, 38], particularly in the so-called P_5' observable, which shows discrepancies of approximately 3σ from SM predictions in certain q^2 bins.

Until recently, these deviations were complemented by hints of lepton flavor universality violation in the ratios $R_K = \frac{\mathcal{B}(B^+\to K^+\mu^+\mu^-)}{\mathcal{B}(B^+\to K^+e^+e^-)}$ and $R_{K^*} = \frac{\mathcal{B}(B^0\to K^{*0}\mu^+\mu^-)}{\mathcal{B}(B^0\to K^{*0}e^+e^-)}$.

Early measurements by LHCb indicated values of R_K and R_{K^*} that were approximately 2.5σ below the SM prediction of nearly unity [19, 25, 28].

However, the landscape of these anomalies has evolved with more recent measurements. In 2022, LHCb released updated results for R_K and R_{K^*} with significantly improved precision [40, 38]. These new measurements are in excellent agreement with the SM predictions, effectively resolving the lepton universality puzzle in $b \to s\ell^+\ell^-$ transitions. This resolution demonstrates the importance of accumulating statistics and refining experimental techniques before drawing definitive conclusions about potential new physics.

Despite this resolution, the branching ratio deficits and angular anomalies in $b \to s\mu^+\mu^-$ transitions persist. These remaining discrepancies could potentially be explained by underestimated hadronic uncertainties in the SM predictions [239, 343, 341], or they might indeed point to new physics effects that are lepton-flavor universal [116, 112]. Global fits to the data suggest that a new physics contribution to the Wilson coefficient C_9 provides a consistent explanation of the observed pattern of deviations [77, 380, 240, 76, 333].

1.2.2 The Muon $g-2$ Anomaly

Another long-standing discrepancy exists in the measurement of the muon anomalous magnetic moment, $(g-2)_\mu$. The Fermilab Muon g-2 experiment recently confirmed the earlier Brookhaven measurement, finding a value that exceeds the SM prediction by 4.2σ [60, 75]. The combined experimental result is

$$a_\mu^{\text{exp}} = (116592061 \pm 41) \times 10^{-11}, \tag{1.1}$$

while the SM prediction is

$$a_\mu^{\text{SM}} = (116591810 \pm 43) \times 10^{-11}, \tag{1.2}$$

leading to a discrepancy of

$$\Delta a_\mu = (251 \pm 59) \times 10^{-11}. \tag{1.3}$$

This persistent deviation could indicate new physics that couples preferentially to muons, such as new gauge bosons [459, 184], leptoquarks [173, 290], or supersymmetric particles [102, 141, 226]. However, recent lattice QCD calculations of the hadronic vacuum polarization contribution to $(g-2)_\mu$ have challenged the standard evaluation based on $e^+e^- \to$ hadrons data [193, 414, 263]. This situation remains unresolved, highlighting the importance of further theoretical work and independent experimental verification.

1.2.3 Evidence for $B^+ \to K^+\nu\bar{\nu}$

Very recently, the Belle II experiment reported evidence for the rare decay $B^+ \to K^+\nu\bar{\nu}$ with a significance of 3.1σ and a measured branching ratio of $(2.0^{+0.7}_{-0.6}) \times 10^{-5}$ [65, 99]. This result is approximately 2.8σ above the SM prediction of $(0.42 \pm 0.05) \times 10^{-5}$ [205, 451, 170]. While the statistical significance is not yet definitive, this measurement is particularly interesting because the $b \to s\nu\bar{\nu}$ transition is theoretically cleaner than $b \to s\ell^+\ell^-$, being free from complications due to non-local hadronic effects.

If confirmed with higher precision, this discrepancy could provide a crucial new piece in the flavor physics puzzle, potentially indicating new physics that couples to both charged leptons and neutrinos, as expected in scenarios with left-handed new physics currents related by $\mathrm{SU}(2)_L$ symmetry [216, 96, 163, 82].

1.3 The Flavor Puzzle

Beyond these specific anomalies lies the broader "flavor puzzle" of the Standard Model—the unexplained pattern of fermion masses and mixing angles [335, 303, 305, 101]. The SM accommodates these patterns through Yukawa couplings but provides no explanation for their highly hierarchical structure.

The quark masses span five orders of magnitude, from the up quark at a few MeV to the top quark at 173 GeV. Similarly, the CKM matrix elements exhibit a clear hierarchical pattern, with off-diagonal elements becoming progressively

smaller away from the diagonal. In the lepton sector, the charged lepton masses a range of 3-4 orders of magnitude, and the neutrino mixing angles are large compared to quark mixing angles.

This flavor structure suggests an underlying organizing principle beyond the SM. Proposed explanations include flavor symmetries [307, 415, 416, 303], extra dimensions with localized fermion profiles [138, 319, 334], radiative mass generation [507, 156, 149], and the clockwork mechanism [453, 101, 325]. Understanding the origin of flavor could provide crucial insights into physics at very high energy scales, potentially linking the flavor puzzle to other outstanding questions in particle physics.

1.4 Effective Field Theory Approach to New Physics

Given the lack of direct evidence for new particles at the LHC, an effective field theory (EFT) approach provides a powerful model-independent framework for studying potential new physics effects [337, 203, 323]. In this approach, the effects of heavy new particles are parameterized through higher-dimensional operators added to the SM Lagrangian:

$$\mathcal{L}_{\text{eff}} = \mathcal{L}_{\text{SM}} + \sum_i \frac{C_i}{\Lambda^2} \mathcal{O}_i^{(6)} + \dots \tag{1.4}$$

where Λ represents the scale of new physics, $\mathcal{O}_i^{(6)}$ are dimension-six operators, and C_i are the corresponding Wilson coefficients.

For energies well below Λ, this approach captures the effects of any new physics model that reduces to the SM at low energies. In the context of flavor physics, the relevant EFT is typically a low-energy effective theory where the top quark, W, Z, and Higgs are integrated out, such as the weak effective theory for $b \to s$ transitions [201, **?**, 114, 171].

This approach allows us to:

1. Identify patterns in observed deviations across different processes.

2. Translate experimental constraints into bounds on new physics scales.

3. Make predictions for correlations between different observables.

4. Connect low-energy flavor observables with potential direct searches at high-energy colliders.

1.5 Structure of the Dissertation

In the following chapters, I present my contributions to this field through several published works. Each chapter begins with a brief introduction contextualizing the specific research problem within the broader framework outlined above, followed by the publication in its original form.

Chapter 2 introduces a supersymmetric extension of the Standard Model in which the new physics contributions to the anomalous magnetic moment of the muon can be more than an order of magnitude larger than in the minimal supersymmetric Standard Model (MSSM) [102]. This model can comfortably explain the experimentally confirmed discrepancy in $(g-2)_\mu$ even with sleptons in the multi-TeV mass range.

In Chapter 3, I present a supersymmetric version of a flavor model based on the clockwork mechanism [101]. The model not only addresses the flavor hierarchies in the Standard Model but also makes specific predictions for the flavor structure of supersymmetric particles, with important implications for rare flavor-changing processes.

Chapter 4 explores the potential of a high-energy muon collider to probe new physics through the process $\mu^+\mu^- \to bs$ [104]. This work demonstrates that such a facility could provide a complementary approach to studying the same underlying new physics that might be responsible for the $b \to s\ell^+\ell^-$ anomalies, with sensitivity to energy scales approaching 100 TeV.

Finally, Chapter 5 examines new physics sensitivity of the rare decay $\Lambda_b \to \Lambda\nu\bar{\nu}$, which will be accessible at future Z-pole machines like FCC-ee and CEPC [105]. This work introduces a novel observable, the forward-backward asymmetry $A_{FB}^{\uparrow}$, arising from the longitudinal polarization of Λ_b baryons produced in

Z decays, which provides complementary sensitivity to the chirality structure of potential new physics interactions.

Together, these works demonstrate how precision measurements of rare processes can provide powerful constraints on new physics models, complementing direct searches at high-energy colliders. The effective field theory framework allows us to interpret these constraints in a model-independent manner, providing crucial guidance in our ongoing quest to understand physics beyond the Standard Model.

Chapter 2

Explaining $(g-2)_\mu$ with Multi-TeV Sleptons

2.1 Introduction to the Chapter

The anomalous magnetic moment of the muon, $(g-2)_\mu$, stands as one of the most precisely measured quantities in particle physics and provides a powerful probe of new physics beyond the Standard Model. For more than a decade, there has existed a persistent discrepancy between experimental measurements and Standard Model predictions of this quantity, suggesting the presence of new particles or interactions that couple preferentially to muons.

In this chapter, I present a supersymmetric extension of the Standard Model that can naturally accommodate the experimentally observed discrepancy in $(g-2)_\mu$ even with sleptons in the multi-TeV mass range. Unlike the Minimal Supersymmetric Standard Model (MSSM), where an explanation of the muon $g-2$ anomaly typically requires light superpartners with masses below 1 TeV, our model—the Flavorful Supersymmetric Standard Model (FSSM)—can generate contributions to $(g-2)_\mu$ that are more than an order of magnitude larger than in the MSSM.

The key innovation of the FSSM is its extended electroweak symmetry breaking sector with a rich Higgs and Higgsino structure. This setup allows for Hig-

gsinos with $\mathcal{O}(1)$ couplings to muons, leading to a significant enhancement of the one-loop contributions to $(g-2)_\mu$. Notably, this enhancement is achieved in a framework that preserves the natural stabilization of the electroweak scale provided by supersymmetry, while simultaneously keeping all superpartners at mass scales that are consistent with the null results from direct searches at the LHC.

This work connects to the broader flavor program by showing how extensions of the minimal supersymmetric framework can address precision anomalies while respecting direct search constraints. The FSSM not only explains the muon g-2 discrepancy with multi-TeV superpartners but also offers a framework where the same extended Higgs sector could potentially address the hierarchical pattern of fermion masses. This establishes a direct link between precision flavor measurements and potential discoveries at future high-energy colliders.

The following analysis involves supersymmetric loop calculations contributing to the muon anomalous magnetic moment. For readers interested in a pedagogical introduction to supersymmetric loop calculations, we refer to the comprehensive review by Haber and Haskins [345], which provides the necessary background for understanding the derivations presented in this section.

The following publication details the theoretical framework of the FSSM, provides a comprehensive analysis of its contributions to $(g-2)_\mu$, and explores additional phenomenological implications, including potential signatures in lepton flavor violating processes and at future colliders.

2.2 Original Publication

Wolfgang Altmannshofer[a], Sri Aditya Gadam[a], Stefania Gori[a], Nick Hamer[a]

[a] *Santa Cruz Institute for Particle Physics and Department of Physics, University of California, Santa Cruz, 1156 High Street, Santa Cruz, CA 95064, USA*

waltmann@ucsc.edu sgori@ucsc.edu sgadam@ucsc.edu nhamer@ucsc.edu

Abstract. We present a supersymmetric extension of the Standard Model in which the new physics contributions to the anomalous magnetic moment of the muon can be more than an order of magnitude larger than in the minimal supersymmetric Standard Model. The extended electroweak symmetry breaking sector of the model can consistently accommodate Higgs bosons and Higgsinos with $O(1)$ couplings to muons. We find that sleptons with masses in the multi-TeV range can comfortably explain the recently confirmed discrepancy in the anomalous magnetic moment of the muon. We discuss additional phenomenological aspects of the model, including its effects on tau flavor changing decays.

2.2.1 Introduction

The Higgs discovery and the subsequent measurements of its properties at the LHC have been a crucial confirmation of the Standard Model (SM) of particle physics. Using data from Run I and Run II of the LHC, we know that the Higgs has SM-like properties and that its couplings to SM gauge bosons and third generation fermions agree with the SM predictions at the $10\% - 20\%$ level [10, 485]. Much less is known about the Higgs couplings to first and second generation fermions. Only recently, the LHC showed the first evidence for the Higgs coupling to muons [13, 490]. There is no evidence yet for the Higgs couplings to light quarks and electrons.

At the same time, the origin of the large hierarchies in the SM fermion masses, as well as the hierarchical structure of the CKM quark mixing matrix, constitute a long-standing open question in particle physics: the so-called SM flavor puzzle.

One dynamical approach to this puzzle is to couple the first two generations exclusively to a new subleading source of electroweak symmetry breaking, in the form of a second Higgs doublet or some strong dynamics [106, 320, 194] (see also [268, 181, 293] for related ideas). Such a scenario adds new sources of flavor universality breaking to the SM. This is an experimentally viable option due to our lack of knowledge of the Higgs couplings to first and second generations. One concrete realization of this scenario is the Flavorful-Two-Higgs-Doublet-Model (F2HDM) [98].

Recently, new measurements involving muons have been reported by precision experiments. The LHCb collaboration has reported updated results on the ratio R_K of the rare B meson decay rates $B \to K\mu\mu$ and $B \to Kee$ [35], confirming earlier hints [19, 15, 28] for lepton flavor universality violation in rare B decays. In addition, a new measurement of the muon anomalous magnetic moment $a_\mu \equiv (g_\mu - 2)/2$ has been very recently reported by the Fermilab Muon g-2 collaboration, $a_\mu^{\rm FNAL} = 116\ 592\ 040(54) \times 10^{-11}$ [60]. This measurement is consistent with the previous measurement by the E821 experiment at BNL, $a_\mu^{\rm BNL} = 116\ 592\ 089(63) \times 10^{-11}$ [165]. The quoted combination of experimental results is $a_\mu^{\rm exp} = 116\ 592\ 061(41) \times 10^{-11}$ and deviates by 4.2σ from the SM prediction reported by the white paper of the g-2 theory initiative, $a_\mu^{\rm SM} = 116\ 591\ 810(43) \times 10^{-11}$ [132], based on [275, 399, 248, 367, 274, 400, 409, 228, 192, 182, 327, 477, 276, 316, 145, 328, 438, 431, 247, 368, 317, 174, 245, 454, 265, 389, 407, 294, 464, 246, 183, 133, 134, 262, 330], where the main uncertainty of the SM prediction comes from the hadronic vacuum polarization contribution. This leads to

$$\Delta a_\mu = a_\mu^{\rm exp} - a_\mu^{\rm SM} = (251 \pm 59) \times 10^{-11}\,. \tag{2.1}$$

Although further scrutiny of this anomaly is needed (see e.g. [260, 193, 414, 249]), it is interesting to ask what this anomaly may imply for new physics [261, 388, 421]. In the SM, the contributions to the muon anomalous magnetic moment are chirally suppressed by the muon mass. Such a suppression can be lifted in the presence of new physics opening up the possibility to indirectly probe high new physics scales. Known examples include lepto-quark contributions that in some models

can be enhanced by the ratio of top mass to muon mass, m_t/m_μ, or contributions in the minimal supersymmetric Standard Model (MSSM) that are enhanced by $\tan\beta$, the ratio of the vacuum expectation values (vevs) of the two Higgs doublets of the MSSM. Still, the typical scale of supersymmetric (SUSY) particles required to fully address the anomaly is in the few hundred GeV range. A crucial limiting factor in the MSSM is an upper bound on $\tan\beta$ that arises from demanding perturbative Yukawa couplings of the bottom quark and the tau lepton.

In this paper, we formulate a new SUSY scenario, the flavorful supersymmetric Standard Model (FSSM). In this scenario, the contributions to a_μ can be more than an order of magnitude larger than in the MSSM. The scenario corresponds to the supersymmetrized version of the F2HDM. Its richer Higgs sector can consistently accommodate Higgsinos with $O(1)$ couplings to muons, leading to a strong enhancement of 1-loop SUSY contributions to a_μ. The paper is organized as follows: In section 2.2.2, we briefly review the MSSM contributions to a_μ and show that sleptons in the few hundred GeV mass range are generically preferred. In section 2.2.3, we present our model, a SUSY version of the SM with an extended scalar sector, and discuss the features most relevant in the context of $(g-2)_\mu$. In section 2.2.4 we detail the contributions to a_μ in our model and show that smuons as heavy as 6 TeV can be responsible for the observed discrepancy. In section 2.2.5 we comment on further phenomenological implications of the model. We cover both indirect probes like lepton flavor violating tau decays and direct searches for electroweak SUSY particles at the LHC. Section 5.2.6 is reserved for conclusions and an outlook. In appendix 2.2.6, we collect the loop functions entering the several contributions to $(g-2)_\mu$.

2.2.2 Muon Anomalous Magnetic Moment in the MSSM

We start by briefly reviewing the well known 1-loop slepton contributions to the anomalous magnetic moment of the muon in the MSSM [230, 442]. We will neglect possible CP violating phases as they are strongly constrained by the non-observation of an electric dipole moment of the electron. We will also assume that

the slepton soft masses are flavor conserving. Large flavor mixing between smuons and staus could in principle lead to chirally enhanced contributions to the anomalous magnetic moment of the muon [430, 321]. However, taking into account the stringent constraints from $\tau \to \mu\gamma$ [144, 55] it is found that flavor changing effects are negligibly small [322]. In presenting the MSSM contributions, it is convenient to distinguish loops with binos and winos. For masses of supersymmetric particles $m^2_{\rm SUSY} \gg m_Z^2$, one finds to a very good approximation that the two contributions are given by

$$\Delta a_\mu^{\rm MSSM} = \Delta a_\mu^{\tilde b} + \Delta a_\mu^{\tilde w} \ , \tag{2.2}$$

$$\Delta a_\mu^{\tilde b} = \frac{g'^2}{192\pi^2}\frac{m_\mu^2}{m^2_{\tilde\mu_L}}\frac{M_1\mu}{m^2_{\tilde\mu_L}}\frac{t_\beta}{1+\epsilon_\ell t_\beta}\left(2f_1(x_1,x_R)+f_2(x_1,x_\mu)-\frac{2}{x_R^2}f_2(y_1,y_\mu)\right) \tag{2.3}$$

$$\Delta a_\mu^{\tilde w} = \frac{5g^2}{192\pi^2}\frac{m_\mu^2}{m^2_{\tilde\mu_L}}\frac{M_2\mu}{m^2_{\tilde\mu_L}}\frac{t_\beta}{1+\epsilon_\ell t_\beta}f_3(x_2,x_\mu) \ , \tag{2.4}$$

where, in the last equation, we have used the $SU(2)_L$ condition on the muon sneutrino mass $m_{\tilde\nu_\mu} = m_{\tilde\mu_L}$. The mass ratios are given by $x_1 = M_1^2/m^2_{\tilde\mu_L}$, $y_1 = M_1^2/m^2_{\tilde\mu_R}$, $x_\mu = \mu^2/m^2_{\tilde\mu_L}$, $y_\mu = \mu^2/m^2_{\tilde\mu_R}$, $x_2 = M_2^2/m^2_{\tilde\mu_L}$, and $x_R = m^2_{\tilde\mu_R}/m^2_{\tilde\mu_L}$. In the above expressions g and g' denote the $SU(2)_L$ and $U(1)_Y$ gauge couplings, M_2 and M_1 are the corresponding gaugino masses, μ is the Higgsino mass, and $m_{\tilde\mu_L}$, $m_{\tilde\mu_R}$ are the soft masses of the second generation slepton doublet and singlet, respectively. The parameter $\tan\beta = t_\beta = v_u/v_d$ is the ratio of the two Higgs vevs. We normalize the loop functions such that $f_1(1,1) = f_2(1,1) = f_3(1,1) = 1$. For completeness, their explicit expressions are given in the appendix 2.2.6. The parameter ϵ_ℓ arises from $\tan\beta$-enhanced threshold corrections to the muon mass. It is given by [426, 151] (see also [348, 361, 220, 457])

$$\epsilon_\ell = \frac{g'^2}{64\pi^2}\frac{M_1\mu}{m^2_{\tilde\mu_L}}\left(2g(x_1,x_R)+g(x_1,x_\mu)-\frac{2}{x_R}g(y_1,y_\mu)\right) - \frac{3g^2}{64\pi^2}\frac{M_2\mu}{m^2_{\tilde\mu_L}}g(x_2,x_\mu) \ , \tag{2.5}$$

where the loop function is given in the appendix 2.2.6 and it is normalized such that $g(1,1) = 1$. For a generic point in MSSM parameter space $\epsilon_\ell \sim 10^{-3}$, and its effect becomes relevant only for very large $\tan\beta$.

The dominant contribution to $(g-2)_\mu$ typically comes from the wino loops. In the limit that all SUSY masses are equal and neglecting the threshold corrections,

the above expressions give

$$\Delta a_\mu^{\rm MSSM} \simeq 260 \times 10^{-11} \times \left(\frac{t_\beta}{50}\right) \times \left(\frac{500\,{\rm GeV}}{m_{\rm SUSY}}\right)^2 \,. \tag{2.6}$$

As it is evident from the above equation, even for large values of $\tan\beta \simeq 50$, the typical mass scale of the involved supersymmetric particles (sleptons and electroweakinos) is below 1 TeV. This is confirmed by our numerical results in Figure 2.2 (see the blue and purple shaded regions). The fact that an explanation of $(g-2)_\mu$ prefers a light spectrum of sleptons and electroweakinos has been re-emphasized recently in several studies of the MSSM [84, 295, 387, 338, 500, 515, 504, 226, 252, 350, 161, 143, 61, 227, 374] and of MSSM extensions [56, 360]. It is possible to accommodate the preferred value for Δa_μ for a somewhat heavier spectrum ($m_{\rm SUSY} \gtrsim 1$ TeV) in corners of parameter space with either a very large μ term [295, 338, 143] or with very large values of $\tan\beta$. However, for large values of μ, the MSSM scalar potential can develop charge breaking minima and vacuum stability considerations strongly constrain the parameter space. For very large values of $\tan\beta \gtrsim 70$ the bottom and tau Yukawa couplings develop Landau poles before the GUT scale, see e.g. [118].

In the following, we present a supersymmetric extension of the Standard Model that can accommodate the measured $(g-2)_\mu$ with multi-TeV sleptons. The corresponding region of parameter space is completely safe from vacuum stability constraints and all Yukawa couplings remain perturbative.

2.2.3 The MSSM with a Flavorful Higgs Sector

We supersymmetrize the flavorful 2HDM. Instead of the usual two chiral superfields $\hat{H}_u, \hat{H}_d$ of the MSSM, we introduce four chiral superfields $\hat{H}_u, \hat{H}'_u, \hat{H}_d, \hat{H}'_d$ (see also [296, 396, 292] for other models with more than two Higgs doublets). Under the $SU(3)_c \times SU(2)_L \times U(1)_Y$ gauge symmetry, these superfields transform as $\hat{H}_u, \hat{H}'_u \sim (\mathbf{1},\mathbf{2})_{+\frac{1}{2}}$ and $\hat{H}_d, \hat{H}'_d \sim (\mathbf{1},\mathbf{2})_{-\frac{1}{2}}$. The superpotential of the model is given by

$$W = \mu_1 \hat{H}_u \hat{H}_d + \mu_2 \hat{H}'_u \hat{H}'_d + \mu_3 \hat{H}'_u \hat{H}_d + \mu_4 \hat{H}_u \hat{H}'_d$$

$$+ (Y_u \hat{H}_u + Y'_u \hat{H}'_u)\hat{Q}\hat{U}^c + (Y_d \hat{H}_d + Y'_d \hat{H}'_d)\hat{Q}\hat{D}^c + (Y_\ell \hat{H}_d + Y'_\ell \hat{H}'_d)\hat{L}\hat{E}^c \,. \quad (2.7)$$

It contains four independent μ-terms as well as the Yukawa couplings Y_f and Y'_f of the Higgs doublets to the matter superfields. In the following we will denote this model as the flavorful supersymmetric Standard Model or FSSM.

We assume that the neutral components of the Higgs scalars acquire vevs given by v_u, v'_u, v_d, and v'_d, such that $v_u^2 + v_d^2 + v_u'^2 + v_d'^2 = v^2 = (246\,\text{GeV})^2$. In addition to the usual vev ratio $\tan\beta = t_\beta = v_u/v_d$, we also introduce the ratios $\tan\beta_u = t_{\beta_u} = v_u/v'_u$ and $\tan\beta_d = t_{\beta_d} = v_d/v'_d$. Generic Yukawa couplings Y_f and Y'_f violate the principle of natural flavor conservation. They can lead to large neutral Higgs mediated flavor changing neutral currents and are therefore strongly constrained. In the following we will consider the "flavorful" ansatz for the Yukawa couplings as suggested in [106] that avoids the most stringent flavor constraints due to an approximate flavor symmetry [106]. In this ansatz, the doublets $\hat{H}_u$, $\hat{H}_d$ couple exclusively to third generation fermions, while $\hat{H}'_u$, $\hat{H}'_d$ provide masses for the first and second generations. In particular, the muon mass is proportional to the vev v'_d and the corresponding muon Yukawa coupling $Y'_{\mu\mu}$. The muon Yukawa is thus enhanced by a factor $\tan\beta\tan\beta_d$ compared to the usual $\tan\beta$ enhancement present in the MSSM.

In the case of all three leptons, we have (neglecting SUSY threshold effects)[1]

$$Y'_\ell \simeq \frac{\sqrt{2}}{v'_d}\begin{pmatrix} m_e & x_{e\mu}m_e & x_{e\tau}m_e \\ x_{\mu e}m_e & m_\mu & x_{\mu\tau}m_\mu \\ x_{\tau e}m_e & x_{\tau\mu}m_\mu & x_{\tau\tau}m_\mu \end{pmatrix}, \qquad Y_\ell \simeq \frac{\sqrt{2}}{v_d}\begin{pmatrix} 0 & 0 & 0 \\ 0 & 0 & 0 \\ 0 & 0 & m_\tau \end{pmatrix}. \quad (2.8)$$

The rank-1 Yukawa coupling Y_ℓ preserves an $SU(2)^2 = SU(2)_L \times SU(2)_E$ flavor symmetry acting of the first two generations of left-handed and right-handed lepton fields. The structure of the second Yukawa coupling Y'_ℓ follows the ansatz in [106]: a 2×2 block with entries of the order of the muon mass with the remaining entries of the order of the electron mass. The x_{ij} parameters indicate how much the Yukawa coupling Y'_ℓ differs from such an ansatz. Generically, one might expect the x_{ij} are of order one, but they can be much smaller as well. Assuming

[1] A similar structure can be implemented in the quark sector.

that soft SUSY breaking is flavor universal, the $SU(2)^2$ flavor symmetry is minimally broken by the second Yukawa coupling Y'_ℓ, implying that flavor changing effects between the second and first generation leptons are strongly suppressed. The parameters $x_{\tau\mu}$ and $x_{\mu\tau}$ can be constrained by the experimental bounds on flavor violating tau decays like $\tau \to \mu\gamma$ and $\tau \to 3\mu$, while the corresponding parameters with electrons, $x_{\tau e}$ and $x_{e\tau}$, can be constrained from data on $\tau \to e$ transitions. Due to the $SU(2)^2$ flavor symmetry, the parameters $x_{\mu e}$ and $x_{e\mu}$ are unobservable. Effects in the highly constrained $\mu \to e$ transitions like $\mu \to e\gamma$ can be expected only if the products $x_{\mu\tau}x_{\tau e}$ or $x_{e\tau}x_{\tau\mu}$ are sizable (see section 2.2.5 for more details).

In addition to the leptonic Yukawa couplings shown above, the most relevant ingredients for the discussion of $(g-2)_\mu$ are the smuon masses as well as the chargino and neutralino masses. For the smuon mass matrix we find after electroweak symmetry breaking

$$M^2_{\tilde{\mu}} = \begin{pmatrix} m^2_{\tilde{\mu}_L} & -m_\mu t_\beta t_{\beta_d}(\mu_4 + \mu_2/t_{\beta_u}) \\ -m_\mu t_\beta t_{\beta_d}(\mu_4 + \mu_2/t_{\beta_u}) & m^2_{\tilde{\mu}_R} \end{pmatrix}, \tag{2.9}$$

where we have neglected the small D-term contributions, as well as the contributions from soft trilinear terms. Neglecting the trilinear terms is a good approximation as long as $v'_d \ll v_u$. Note that in eq. (2.9) we neglected left-right mixing between smuons and staus proportional to $x_{\tau\mu}$ and $x_{\mu\tau}$. Such mixing is of no relevance to the calculation of $(g-2)_\mu$. We will comment on its effect on $\tau \to \mu\gamma$ in section 2.2.5.

The model features an extended electroweakino sector, because of the additional Higgsinos. It contains three charginos and six neutralinos with the following

mass matrices

$$M_{\chi^\pm} = \begin{pmatrix} M_2 & \frac{g}{\sqrt{2}}v_u & \frac{g}{\sqrt{2}}v'_u \\ \frac{g}{\sqrt{2}}v_d & \mu_1 & \mu_3 \\ \frac{g}{\sqrt{2}}v'_d & \mu_4 & \mu_2 \end{pmatrix}, \quad M_{\chi^0} = \begin{pmatrix} M_1 & 0 & -\frac{g'}{2}v_d & \frac{g'}{2}v_u & -\frac{g'}{2}v'_d & \frac{g'}{2}v'_u \\ 0 & M_2 & \frac{g}{2}v_d & -\frac{g}{2}v_u & \frac{g}{2}v'_d & -\frac{g}{2}v'_u \\ -\frac{g'}{2}v_d & \frac{g}{2}v_d & 0 & -\mu_1 & 0 & -\mu_3 \\ \frac{g'}{2}v_u & -\frac{g}{2}v_u & -\mu_1 & 0 & -\mu_4 & 0 \\ -\frac{g'}{2}v'_d & \frac{g}{2}v'_d & 0 & -\mu_4 & 0 & -\mu_2 \\ \frac{g'}{2}v'_u & -\frac{g}{2}v'_u & -\mu_3 & 0 & -\mu_2 & 0 \end{pmatrix}, \tag{2.10}$$

where we have considered the basis $(\tilde{W}^\pm, \tilde{H}^\pm, \tilde{H}'^\pm)$ and $(\tilde{B}, \tilde{W}^0, \tilde{H}^0_d, \tilde{H}^0_u, \tilde{H}'^0_d, \tilde{H}'^0_u)$ for charginos and neutralinos, respectively. For the calculation of $(g-2)_\mu$ it is convenient to rotate the Higgsino states to diagonalize the 2×2 Higgsino submatrix:

$$\begin{pmatrix} c_d & s_d \\ -s_d & c_d \end{pmatrix} \begin{pmatrix} \mu_1 & \mu_3 \\ \mu_4 & \mu_2 \end{pmatrix} \begin{pmatrix} c_u & s_u \\ -s_u & c_u \end{pmatrix} = \begin{pmatrix} \mu & 0 \\ 0 & \tilde{\mu} \end{pmatrix}, \tag{2.11}$$

where we have introduced the mixing angles $c_{d,u} \equiv \cos\theta_{d,u}$, $s_{d,u} \equiv \sin\theta_{d,u}$. For gaugino and Higgsino masses sufficiently above the electroweak scale, the masses of the three charginos and of the six neutralinos are approximately $m_{\chi^\pm_i} \simeq (M_2, \mu, \tilde{\mu})$ and $m_{\chi^0_i} \simeq (M_1, M_2, \mu, \mu, \tilde{\mu}, \tilde{\mu})$. In the following section we will report the contributions to the anomalous magnetic moment of the muon in terms of the Higgsino parameters θ_u, θ_d and $\mu, \tilde{\mu}$.

2.2.4 FSSM Contributions to $(g-2)_\mu$

Similar to the MSSM, it is possible to split the contributions to the anomalous magnetic moment of the muon into bino mediated and wino mediated contributions. For supersymmetric particles that are sufficiently heavier than the electroweak scale, $m^2_{\text{SUSY}} \gg m^2_Z$, we find

$$\Delta a_\mu^{\text{FSSM}} = \Delta a_\mu^{\tilde{b}} + \Delta a_\mu^{\tilde{w}}\,, \tag{2.12}$$

$$\Delta a_\mu^{\tilde{b}} = \frac{g'^2}{192\pi^2}\frac{m^2_\mu}{m^2_{\tilde{\mu}_L}}\frac{t_\beta t_{\beta_d}}{1+\epsilon_\ell t_\beta t_{\beta_d}} \tag{2.13}$$
$$\times \left[s_d \left(c_u - \frac{s_u}{t_{\beta_u}} \right) \frac{M_1 \mu}{m^2_{\tilde{\mu}_L}} \left(2f_1(x_1, x_R) + f_2(x_1, x_\mu) - \frac{2}{x^2_R} f_2(y_1, y_\mu) \right) \right.$$

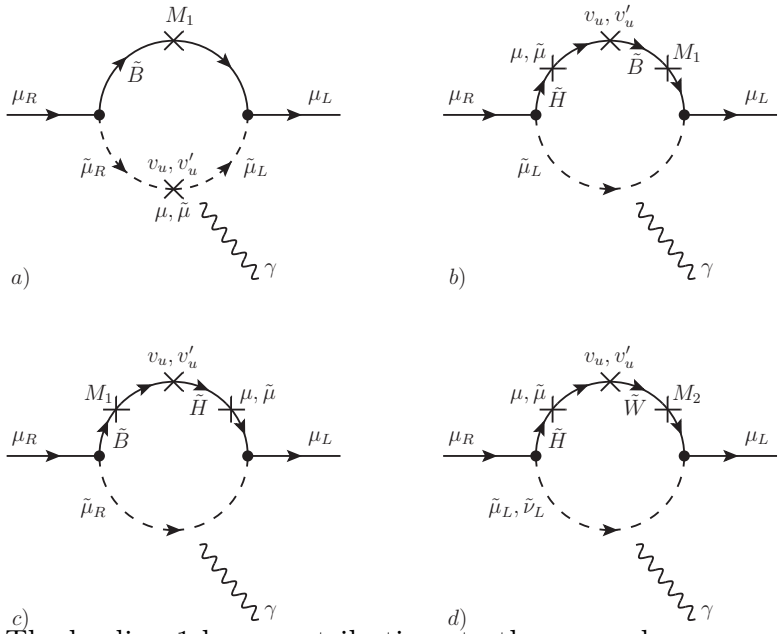

Figure 2.1: The leading 1-loop contributions to the anomalous magnetic moment of the muon. The external photon has to be attached in all possible ways to the loops. Diagrams a), b), and c) involve binos, while diagram d) involves winos. The threshold corrections to the muon mass correspond to analogous diagrams without the external photon.

$$+c_d\left(s_u+\frac{c_u}{t_{\beta_u}}\right)\frac{M_1\tilde{\mu}}{m^2_{\tilde{\mu}_L}}\left(2f_1(x_1,x_R)+f_2(x_1,x_{\tilde{\mu}})-\frac{2}{x_R^2}f_2(y_1,y_{\tilde{\mu}})\right)\Bigg]\ ,$$

$$\Delta a_\mu^{\tilde{w}}=\frac{5g^2}{192\pi^2}\frac{m_\mu^2}{m^2_{\tilde{\mu}_L}}\frac{t_\beta t_{\beta_d}}{1+\epsilon_\ell t_\beta t_{\beta_d}}\Bigg[s_d\left(c_u-\frac{s_u}{t_{\beta_u}}\right)\frac{M_2\mu}{m^2_{\tilde{\mu}_L}}f_3(x_2,x_\mu) \tag{2.14}$$

$$+c_d\left(s_u+\frac{c_u}{t_{\beta_u}}\right)\frac{M_2\tilde{\mu}}{m^2_{\tilde{\mu}_L}}f_3(x_2,x_{\tilde{\mu}})\Bigg]\ ,$$

with the threshold correction parameter ϵ_ℓ given by

$$\epsilon_\ell=\frac{g'^2}{64\pi^2}\Bigg[s_d\left(c_u-\frac{s_u}{t_{\beta_u}}\right)\frac{M_1\mu}{m^2_{\tilde{\mu}_L}}\left(2g(x_1,x_R)+g(x_1,x_\mu)-\frac{2}{x_R}g(y_1,y_\mu)\right)$$

$$+c_d\left(s_u+\frac{c_u}{t_{\beta_u}}\right)\frac{M_1\tilde{\mu}}{m^2_{\tilde{\mu}_L}}\left(2g(x_1,x_R)+g(x_1,x_{\tilde{\mu}})-\frac{2}{x_R}g(y_1,y_{\tilde{\mu}})\right)\Bigg]$$

$$-\frac{3g^2}{64\pi^2}\left[s_d\left(c_u-\frac{s_u}{t_{\beta_u}}\right)\frac{M_2\mu}{m^2_{\tilde{\mu}_L}}g(x_2,x_\mu)+c_d\left(s_u+\frac{c_u}{t_{\beta_u}}\right)\frac{M_2\tilde{\mu}}{m^2_{\tilde{\mu}_L}}g(x_2,x_{\tilde{\mu}})\right]\ , \tag{2.15}$$

where, similarly to x_μ and y_μ, we have defined $x_{\tilde{\mu}}=\tilde{\mu}^2/m^2_{\tilde{\mu}_L}$ and $y_{\tilde{\mu}}=\tilde{\mu}^2/m^2_{\tilde{\mu}_R}$. Note that the loop functions are identical to the MSSM case. In fact, the expres-

sions above largely resemble the MSSM result shown in section 2.2.2. The relevant Feynman diagrams containing Higgsinos, binos, winos, and sleptons are shown in Figure 2.1[2]. As in the MSSM, the dominant contribution typically comes from the loops containing a wino. If all SUSY masses are set equal, the wino loops dominate over the bino loops by a factor $5g^2/g'^2 \simeq 17$. In contrast to the MSSM, we find two sets of contributions that are proportional to either one of the Higgsino mass eigenvalues μ and $\tilde{\mu}$. The main difference to the MSSM is the overall proportionality to the product of the vev ratios $\tan\beta \times \tan\beta_d = v_u/v'_d$. The additional factor $\tan\beta_d$ can increase the contributions in our setup by an order of magnitude or more compared to the MSSM. Note that the threshold correction remains of order $\epsilon_\ell \sim 10^{-3}$ in our setup. However, as it is multiplied by the product $\tan\beta \times \tan\beta_d$ (see Eqs. (2.12), (2.14)), it can have an $O(1)$ impact on the contribution to the $(g-2)_\mu$ (we show its effect explicitly in Figure 2.2 below). Setting all SUSY masses equal and assuming maximal mixing in the Higgsino sector $s_d = c_d = s_u = c_u = 1/\sqrt{2}$, the threshold correction corresponds to the following 1-loop correction to the muon mass

$$\frac{\Delta m_\mu^{\text{1-loop}}}{m_\mu^{\text{tree}}} = \epsilon_\ell t_\beta t_{\beta_d} \simeq -0.54 \times \left(\frac{t_\beta}{20}\right) \times \left(\frac{t_{\beta_d}}{15}\right) \ . \tag{2.16}$$

Note that for this benchmark case, the correction is identical to the correction in the MSSM (see e.g. [151]) up to the additional factor $\tan\beta_d$. Away from the limit $s_d = c_d = s_u = c_u = 1/\sqrt{2}$, the correction to the muon mass is modified by the factor $(s_d(c_u - s_u/t_{\beta_u}) + c_d(s_u + c_u/t_{\beta_u})) \sim \mathcal{O}(1)$.

A relevant bound on the size of $\tan\beta_d$ is given by perturbativity considerations. Yukawa couplings that are larger than $O(1)$ at the TeV scale develop Landau poles before reaching the GUT scale. Requiring that the muon Yukawa of the Higgs

[2] In addition, the model also predicts contributions from 1-loop diagrams containing leptons and Higgs bosons. However, such contributions to Δa_μ are not chirally enhanced by $\tan\beta$ factors and therefore can be neglected.

field H'_d stay perturbative up to the GUT scale, leads to the approximate bound[3]

$$Y'_{\mu\mu} \simeq \frac{\sqrt{2} m_\mu}{v} \frac{t_\beta t_{\beta_d}}{1 + \epsilon_\ell t_\beta t_{\beta_d}} \lesssim 0.7 \ . \tag{2.17}$$

Differently from the MSSM, the requirement of perturbativity of the tau and bottom Yukawa couplings sets weaker bounds on the values of $\tan\beta$ and $\tan\beta_d$. In the limit that all SUSY masses are equal and assuming maximal mixing in the Higgsino sector $s_d = c_d = s_u = c_u = 1/\sqrt{2}$, we find

$$\Delta a_\mu \simeq 220 \times 10^{-11} \times \left(\frac{t_\beta}{20}\right) \times \left(\frac{t_{\beta_d}}{15}\right) \times \left(\frac{0.46}{1 + \epsilon_\ell t_\beta t_{\beta_d}}\right) \times \left(\frac{2.0\,\text{TeV}}{m_{\text{SUSY}}}\right)^2 \tag{2.18}$$

$$\simeq 240 \times 10^{-11} \times \left(\frac{Y'_{\mu\mu}}{0.7}\right) \times \left(\frac{2.5\,\text{TeV}}{m_{\text{SUSY}}}\right)^2 \ . \tag{2.19}$$

Analogously to the corrections to the muon mass in (2.16), for generic $O(1)$ mixing of the FSSM Higgsinos, the results in (2.18) and (2.19) have to be multiplied by the factor $s_d(c_u - s_u/t_{\beta_u}) + c_d(s_u + c_u/t_{\beta_u})$. In the MSSM, similar equations for Δa_μ hold up to the additional factor $\tan\beta_d$. Comparably large contributions to Δa_μ are therefore in principle possible in the MSSM in the ultra-large $\tan\beta$ limit (see e.g. [151]). However, as mentioned in section 2.2.2, the required values of $\tan\beta$ for multi-TeV SUSY particles are very strongly constrained by perturbativity considerations [118]. Those constraints are relaxed in the FSSM, and very large values for the product $\tan\beta \tan\beta_d$ are viable.

Keeping in mind the estimated bound on the muon Yukawa discussed above, we find that the generic scale of supersymmetric particles can be larger by a factor of $\simeq 5$ compared to the MSSM, while still producing the desired effect in the anomalous magnetic moment of the muon.

In Figure 2.2, we show the regions of SUSY masses that are preferred by the anomalous magnetic moment of the muon in several benchmark cases. For

[3] We estimate that the perturbativity bound on the muon Yukawa in our model will be similar to the bound on the tau Yukawa in the MSSM. In Eq. (2.17), we therefore quote the bound on the tau Yukawa coupling at a scale of 1 TeV that has been found in the MSSM requiring the Yukawa coupling to be smaller than $\sqrt{4\pi}$ at the GUT scale [118]. A dedicated renormalization group study of the full set of third and second generation Yukawa couplings and of the gauge couplings would be required to establish a precise bound on the muon Yukawa coupling in our model, but we do not expect the result to change significantly.

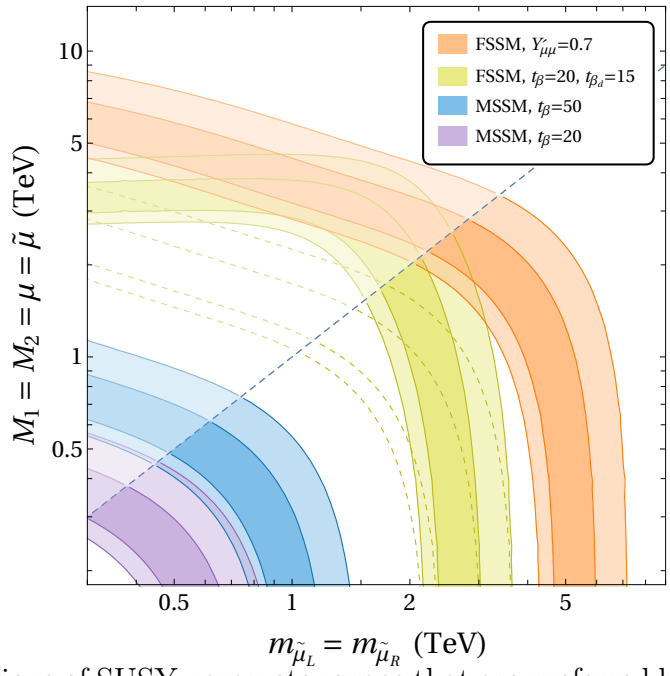

Figure 2.2: Regions of SUSY parameter space that are preferred by the anomalous magnetic moment of the muon at the 1σ and 2σ level in several benchmark models. Above the dashed diagonal line, the smuons are lighter than any of the gauginos and Higgsinos. In blue and purple, we present two MSSM scenarios; in yellow and orange two FSSM scenarios. The dashed yellow lines show the corresponding FSSM scenario neglecting the SUSY threshold corrections to the muon mass.

simplicity, we assume that the masses of the left-handed and right-handed smuons are equal, as do we for the masses of the bino, the wino, and the Higgsinos. In the colored bands we find agreement with (2.1) at the 1σ and 2σ level. The purple and blue bands correspond to the MSSM with $\tan\beta = 20$ and $\tan\beta = 50$, respectively. We see that for $\tan\beta = 50$, sleptons can be at most at around 1 TeV, if gauginos and Higgsinos are in the few hundred GeV range. The yellow and orange bands show two benchmark scenarios in the FSSM assuming a generic $O(1)$ mixing in the Higgsino sector $s_d \sim c_d \sim s_u \sim c_u \sim 1/\sqrt{2}$. The yellow band corresponds to moderate values for $\tan\beta = 20$ and $\tan\beta_d = 15$. In such a scenario the smuons can be as heavy as 3 TeV while still explaining $(g-2)_\mu$. The dashed yellow lines show the region favored by $(g-2)_\mu$ in this FSSM scenario neglecting the SUSY threshold corrections to the muon mass (i.e. ϵ_ℓ is set to zero). We clearly see

that the threshold corrections have an order 1 impact and cannot be neglected.[4] Finally, the orange band shows a scenario in which we choose a large muon Yukawa coupling, $Y'_{\mu\mu} = 0.7$, that we estimate to be close to the bound from demanding perturbativity up to the GUT scale. In this case, smuons can be as heavy as 6 TeV.

2.2.5 Phenomenological Implications

In addition to the contributions to Δa_μ, the FSSM predicts contributions to the anomalous magnetic moments of the electron and of the tau, Δa_e and Δa_τ. Due to the minimally broken $SU(2)^2$ lepton symmetry, the setup predicts the relation

$$\Delta a_e \simeq \frac{m_e^2}{m_\mu^2} \Delta a_\mu \simeq 5.8 \times 10^{-14} \times \left(\frac{\Delta a_\mu}{251 \times 10^{-11}} \right) , \tag{2.20}$$

which is almost an order of magnitude smaller than the uncertainties of the experimental determination [353], as well as the uncertainties of the SM prediction that depends crucially on the value of the fine structure constant [450, 441]. There is no strict correlation of Δa_μ and Δa_τ, but generically we expect

$$\Delta a_\tau \sim \frac{m_\tau^2}{m_\mu^2} \frac{1}{t_{\beta_d}} \Delta a_\mu \simeq 4.7 \times 10^{-8} \times \left(\frac{15}{t_{\beta_d}} \right) \times \left(\frac{\Delta a_\mu}{251 \times 10^{-11}} \right) , \tag{2.21}$$

which is far below foreseeable experimental sensitivities [53].

Similar to the 1-loop slepton contributions to anomalous magnetic moments, the FSSM setup also gives contributions to the radiative lepton decays $\tau \to \mu\gamma$, $\tau \to e\gamma$, and $\mu \to e\gamma$. While the relevant off-diagonal couplings $x_{\tau e}$, $x_{e\tau}$, $x_{\tau\mu}$, and $x_{\mu\tau}$ in the lepton Yukawa matrix (2.8) do not enter the predictions for Δa_μ at the considered level of accuracy, it is nonetheless interesting to explore their implications. In the limit in which both left-handed and right-handed smuons and staus have equal masses we find simple relations between the 1-loop slepton

[4] In this context, it might be interesting to consider a scenario in which the entire muon mass is radiatively generated. In such a case one expects that the $(g-2)_\mu$ anomaly can be explained with new physics masses at around 2 TeV. The radiative muon mass scenario has been analyzed in the MSSM [151, 258] and it is strongly constrained by perturbativity arguments.

contributions to the anomalous magnetic moment of the muon and the branching ratios of the decays $\tau \to \mu\gamma$, $\tau \to e\gamma$, and $\mu \to e\gamma$

$$\begin{aligned}
\mathrm{BR}(\tau \to \mu\gamma) &\simeq 24\pi^3 \alpha_{\mathrm{em}} \frac{v^4}{m_\mu^4} (\Delta a_\mu)^2 \left(x_{\tau\mu}^2 + x_{\mu\tau}^2\right) \times \mathrm{BR}(\tau \to \mu\nu_\tau\bar{\nu}_\mu) \\
&\simeq 1.7 \times 10^{-8} \times \left(\frac{\Delta a_\mu}{251 \times 10^{-11}}\right)^2 \left[\left(\frac{x_{\tau\mu}}{0.01}\right)^2 + \left(\frac{x_{\mu\tau}}{0.01}\right)^2\right] , \quad (2.22) \\
\mathrm{BR}(\tau \to e\gamma) &\simeq 24\pi^3 \alpha_{\mathrm{em}} \frac{v^4}{m_\mu^4} \frac{m_e^2}{m_\mu^2} (\Delta a_\mu)^2 \left(x_{\tau e}^2 + x_{\mu e}^2\right) \times \mathrm{BR}(\tau \to e\nu_\tau\bar{\nu}_\mu) \\
&\simeq 4.1 \times 10^{-9} \times \left(\frac{\Delta a_\mu}{251 \times 10^{-11}}\right)^2 \left[\left(\frac{x_{\tau e}}{1.0}\right)^2 + \left(\frac{x_{e\tau}}{1.0}\right)^2\right] , \quad (2.23) \\
\mathrm{BR}(\mu \to e\gamma) &\simeq 24\pi^3 \alpha_{\mathrm{em}} \frac{v^4}{m_\mu^4} \frac{m_e^2}{m_\tau^2} (\Delta a_\mu)^2 \left(x_{e\tau}^2 x_{\tau\mu}^2 + x_{\mu\tau}^2 x_{\tau e}^2\right) \\
&\simeq 8.2 \times 10^{-15} \times \left(\frac{\Delta a_\mu}{2.51 \times 10^{-9}}\right)^2 \left[\left(\frac{x_{e\tau} x_{\tau\mu}}{0.01}\right)^2 + \left(\frac{x_{\mu\tau} x_{\tau e}}{0.01}\right)^2\right] \quad (2.24)
\end{aligned}$$

where we used $\mathrm{BR}(\tau \to \mu\nu_\tau\bar{\nu}_\mu) \simeq 17.4\%$ and $\mathrm{BR}(\tau \to e\nu_\tau\bar{\nu}_\mu) \simeq 17.8\%$ [516].

We can compare these predictions to the current experimental bounds. From the bound $\mathrm{BR}(\tau \to \mu\gamma)_{\mathrm{exp}} < 4.2 \times 10^{-8}$ [144, 55] we see that the couplings $x_{\tau\mu}$ and $x_{\mu\tau}$ have to be of order 10^{-2} in order not to violate the bound from $\tau \to \mu\gamma$. The smallness of these couplings suggests that an additional lepton flavor symmetry gives structure to the lepton Yukawa coupling Y'_ℓ. If the coupling $x_{\tau e}$ or $x_{e\tau}$ is of order 1, the branching ratio of $\tau \to e\gamma$ is predicted below the current bound, $\mathrm{BR}(\tau \to e\gamma)_{\mathrm{exp}} < 3.3 \times 10^{-8}$ [144, 55], but in reach of the Belle II experiment [91]. Once the bound from $\mathrm{BR}(\tau \to \mu\gamma)$ is taken into account, the $\mu \to e\gamma$ branching ratio is predicted well below the current constraint $\mathrm{BR}(\mu \to e\gamma)_{\mathrm{exp}} < 4.2 \times 10^{-13}$ [157].

In the FSSM, we also find tree level neutral Higgs contributions to lepton flavor violating decays $\tau \to 3\mu$, $\tau \to 3e$, and $\mu \to 3e$. The most constraining decay is expected to be $\tau \to 3\mu$ as it involves the largest Yukawa couplings enhanced by the product $t_\beta t_{\beta_d}$. Neglecting mixing among the Higgs bosons and using the results from [449], we find

$$\mathrm{BR}(\tau \to 3\mu) \simeq \frac{m_\mu^4}{4m_{H'_d}^4} \frac{t_\beta^4 t_{\beta_d}^4}{(1 + \epsilon_\ell t_\beta t_{\beta_d})^4} \left(x_{\tau\mu}^2 + x_{\mu\tau}^2\right) \times \mathrm{BR}(\tau \to \mu\nu_\tau\bar{\nu}_\mu)$$

$$\simeq \; 1.0 \times 10^{-9} \times \left(\frac{Y'_{\mu\mu}}{0.7}\right)^4 \left(\frac{1.0\,\text{TeV}}{m_{H'_d}}\right)^4 \left[\left(\frac{x_{\tau\mu}}{0.01}\right)^2 + \left(\frac{x_{\mu\tau}}{0.01}\right)^2\right] \quad (2.25)$$

Comparing to the experimental bound obtained by the Belle collaboration, $\text{BR}(\tau \to 3\mu)_{\text{exp}} < 2.1 \times 10^{-8}$ [355] (see also [412, 21]), we see that TeV scale Higgs bosons are viable and could lead to branching ratios that are accessible at Belle II and LHCb [91, 14].

Finally, we comment on the prospects of testing the SUSY parameter space favored by $(g-2)_\mu$ at the LHC. The sleptons necessary for addressing the $(g-2)_\mu$ anomaly are being searched for by the ATLAS and CMS collaborations. Particularly, the most relevant slepton signature is the slepton pair production $pp \to \tilde{\ell}\tilde{\ell}$, followed by the decay into a lepton and the lightest neutralino $\tilde{\ell}\tilde{\ell} \to (\ell\tilde{\chi}^0)(\ell\tilde{\chi}^0)$. The most stringent bounds on the slepton parameter space come from the analyses [489, 11] performed with the full Run II data set. These searches show that, in the case of degenerate left-handed and right-handed smuons, slepton masses as large as ~ 600 GeV are now generically probed if the mass splitting with the lightest neutralino $m_{\tilde{\ell}} - m_{\tilde{\chi}^0}$ is sufficiently large. In the case of a compressed spectrum, the limits are weaker and allow sleptons as light as ~ 250 GeV for mass splitting $m_{\tilde{\ell}} - m_{\tilde{\chi}^0} \lesssim 30$ GeV [12].

The existing searches probe already part of the MSSM parameter space that is able to explain the $(g-2)_\mu$ anomaly. However, depending on the specific electroweakino spectrum, sizable regions of parameter space are left unexplored. For example, for the specific spectrum fixed in Figure 2.2 ($M_1 = M_2 = \mu$), the aforementioned LHC slepton searches can only set a weak bound because of the dilution of the branching ratio of the slepton into the lightest neutralino and a lepton. For that spectrum, additional slepton decay modes arise including $\tilde{\mu} \to \mu\tilde{\chi}^0_2, \nu\tilde{\chi}^\pm_{1,2}$ with the subsequent decay of $\tilde{\chi}^0_2$ and $\tilde{\chi}^\pm_{1,2}$ to the lightest neutralino and jets or leptons. It will be interesting to search for these new slepton cascade decays in the coming years at the LHC to probe further regions of MSSM parameter space that can address the $(g-2)_\mu$ anomaly.

The slepton phenomenology in the FSSM is even richer. Due to the extended electroweakino sector, several cascade decays are possible, giving rise to signa-

tures with multi-leptons (or jets) and missing energy. We leave the study of such signatures for future work. Due to the generically heavier slepton masses in the FSSM to address the $(g-2)_\mu$ anomaly, the sleptons that we considered in this paper are outside the reach of the LHC. We expect some of the scenarios favored by $(g-2)_\mu$ to be probed at a 100 TeV collider through a $pp \to \tilde{\ell}\tilde{\ell} \to (\ell\tilde{\chi}^0)(\ell\tilde{\chi}^0)$ search [155].

2.2.6 Conclusions and Outlook

The recent result of the Fermilab Muon g-2 collaboration confirms the long-standing discrepancy in the anomalous magnetic moment of the muon, $(g-2)_\mu$. Motivated by this result, we constructed a supersymmetric extension of the Standard Model that can give more than an order of magnitude larger contributions to the $(g-2)_\mu$ than the MSSM. The model, that we dub flavorful supersymmetric Standard Model (FSSM), is based on an extended electroweak breaking sector with Yukawa couplings that follow the flavorful ansatz suggested in [106].

One set of Higgs doublets couples exclusively to the third generation through a rank-1 Yukawa coupling, while a second set of Higgs doublets couples also to the first and second generations. One of the Higgs fields can have an $O(1)$ coupling to muons. Loop contributions to $(g-2)_\mu$ that contain the corresponding Higgsino state are strongly enhanced. In contrast to the MSSM, where the SUSY particles generically have to be below the 1 TeV scale, in the FSSM, the $(g-2)_\mu$ result can be comfortably explained by sleptons in the multi-TeV mass range.

We explored further phenomenological implications of the model, in particular for the anomalous magnetic moments of the electron and the tau, as well as for lepton flavor violation. We found that existing bounds on $\tau \to \mu\gamma$ already give relevant constraints on the lepton flavor violating Yukawa couplings of the model. The $\tau \to 3\mu$ and $\tau \to e\gamma$ decays might be in reach of running experiments.

While LHC searches for sleptons already constrain some of the MSSM explanations of the $(g-2)_\mu$ discrepancy, directly probing the multi-TeV sleptons of the FSSM will require a future higher energy collider.

There are several possible future directions to further explore the FSSM. The rank-1 ansatz for the Yukawa couplings has been successfully implemented in the quark sector in non-supersymmetric versions of the model [106, 98, 110, 111, 108]. It has been shown that in the considered scenarios quark flavor changing neutral currents can be relatively easily in agreement with experimental bounds. In a supersymmetric version, we expect interesting Higgsino mediated effects in chirality suppressed processes like $b \to s\gamma$ and $B_s \to \mu^+\mu^-$ and possibly even for the lepton flavor universality ratios R_K and R_{K^*}. A study of those effects will be presented elsewhere.

If the rank-1 ansatz for the Yukawa couplings is implemented both in the lepton and quark sectors, a scenario with $\tan\beta \sim 50$, $\tan\beta_u \sim 100$, and $\tan\beta_d \sim 10$ can address all hierarchies among the third and second generation quark and lepton masses without any pronounced hierarchy in Yukawa couplings. These are the values of $\tan\beta$ and $\tan\beta_d$ that allow multi-TeV sleptons to address the $(g-2)_\mu$ anomaly. In such a region of parameter space, third and second generation Yukawa unification might be possible at the GUT scale. For the first generation, one could entertain the possibility of radiative mass generation to explain the smallness of the up quark, down quark, and electron mass. We leave these studies to future work.

Acknowledgements

We thank Kaustubh Agashe for discussions. The research of W. A. is supported by the U.S. Department of Energy grant number DE-SC0010107. The research of SG is supported in part by the National Science Foundation CAREER grant PHY- 1915852 and by the National Science Foundation under Grant No. NSF PHY-1748958.

Appendix: Loop Functions

In this appendix, we collect the loop functions that enter the expressions for the SUSY contributions to $(g-2)_\mu$ discussed in sections 2.2.2 and 2.2.4

$$f_1(x,y) = \frac{6(y-3x^2+x(1+y))}{(1-x)^2(x-y)^2} - \frac{12x(x^3+y-3xy+y^2)\log x}{(1-x)^3(x-y)^3} + \frac{12xy\log y}{(1-y)(x-y)^3}, \tag{2.26}$$

$$f_2(x,y) = \frac{6(x+y+xy-3)}{(1-x)^2(1-y)^2} - \frac{12x\log x}{(1-x)^3(x-y)} + \frac{12y\log y}{(1-y)^3(x-y)}, \tag{2.27}$$

$$f_3(x,y) = \frac{6(13-7(x+y)+xy)}{5(1-x)^2(1-y)^2} + \frac{12(2+x)\log x}{5(1-x)^3(x-y)} - \frac{12(2+y)\log y}{5(1-y)^3(x-y)}. \tag{2.28}$$

The loop function entering the threshold corrections to the muon mass reads

$$g(x,y) = \frac{2x\log x}{(1-x)(y-x)} - \frac{2y\log y}{(1-y)(y-x)}\ . \tag{2.29}$$

2.3 Chapter Conclusion

In this chapter, I have presented the Flavorful Supersymmetric Standard Model as a framework for explaining the muon g-2 anomaly with superpartners at the multi-TeV scale. This work advances the goals of this dissertation by demonstrating how extended Higgs sectors can significantly enhance loop contributions to precision observables while maintaining consistency with direct search constraints. The FSSM establishes a connection between the flavor structure of the Higgs sector and the enhancement of dipole operators, providing a potential link between the flavor puzzle and precision measurements. The predictions for lepton flavor violating processes offer concrete avenues for testing this model, further enriching the experimental program aimed at uncovering the origins of flavor.

Chapter 3

A Supersymmetric Flavor Clockwork

3.1 Introduction to the Chapter

The hierarchical structure of fermion masses and mixing angles, often referred to as the "flavor puzzle", remains one of the most intriguing mysteries in particle physics. The Standard Model accommodates these hierarchies through Yukawa couplings but provides no explanation for their origin or pattern. The clockwork mechanism has emerged as an elegant approach to generate exponential hierarchies without small parameters at the fundamental level, offering a potential solution to the flavor puzzle.

In this chapter, I present a supersymmetric version of the flavor clockwork mechanism. This framework not only addresses the observed hierarchies in the Standard Model fermion spectrum but also makes specific predictions for the flavor structure of supersymmetric particles. The supersymmetric extension serves a dual purpose: it protects the clockwork scale from quadratic sensitivity to higher scales (such as the Planck scale), and it provides a concrete realization of the mechanism that can be tested through searches for flavor-changing neutral current processes.

The supersymmetric clockwork framework presented here not only addresses

the flavor puzzle but also makes specific predictions for flavor violation in the squark sector that can be tested experimentally. While kaon oscillation constraints push superpartner masses into the PeV range, specific patterns of flavor-changing neutral currents could potentially be observed in rare meson decays. This establishes a connection between theoretical approaches to the flavor puzzle and experimental searches for supersymmetry at both high-energy colliders and precision flavor experiments.

The supersymmetric clockwork introduces, for each quark and lepton flavor, a system of superfields that generate exponentially suppressed couplings for the zero modes, which are identified with the Standard Model fermions and their superpartners. A unique feature of this construction is that the flavor structure of soft supersymmetry breaking terms is directly linked to the underlying clockwork mechanism. This leads to a characteristic pattern of flavor violation in the squark sector, with significant mixing between the first and second generations.

The resulting flavor structure has important implications for low-energy observables, particularly kaon oscillations. As demonstrated in the following publication, these constraints require either squarks or gluinos to have masses in the PeV range, highlighting the power of indirect precision tests to probe physics at scales far beyond the direct reach of current colliders.

3.2 Original Publication

Wolfgang Altmannshofer[a], Sri Aditya Gadam[a]

[a]*Department of Physics & Santa Cruz Institute for Particle Physics, University of California, Santa Cruz, CA 95064, USA*

waltmann@ucsc.edu sgadam@ucsc.edu

Abstract. Clockwork models can explain the flavor hierarchies in the Standard Model quark and lepton spectrum. We construct supersymmetric versions of such flavor clockwork models. The zero modes of the clockwork are identified with the fermions and sfermions of the Minimal Supersymmetric Standard Model. In addition to generating a hierarchical fermion spectrum, the clockwork also predicts a specific flavor structure for the soft SUSY breaking sfermion masses. We find sizeable flavor mixing among first and second generation squarks. Constraints from Kaon oscillations require the masses of either squarks or gluinos to be above a scale of $\sim$ 3PeV.

3.2.1 Introduction

Among the many motivations for physics beyond the Standard Model (SM), there is the hierarchical structure of the quark and lepton spectrum that remains unexplained in the SM. In fact, the SM Yukawa couplings span several orders of magnitude, from an $\mathcal{O}(1)$ top quark Yukawa coupling to an electron Yukawa coupling of a few $\times 10^{-6}$. Numerous mechanisms have been invoked in the literature to explain such a hierarchy, including frameworks with spontaneously broken $U(1)$ flavor symmetries [307, 415, 416, 335], localization of fermions in extra dimensions [138, 334, 319, 395], models with large anomalous dimensions [445], and models that explain the hierarchies with loop factors [507, 156] (see [100, 160, 406, 85, 501, 214, 213, 492, 404, 135, 452, 299] for recent attempts based on those ideas).

The clockwork mechanism [325] is another idea that generates exponentially small interactions in theories without small parameters at the fundamental level.

As discussed in [325, 453, 381, 86, 369, 63, 502, 394, 148], a flavor clockwork can be constructed to explain the hierarchical flavor structure of the Yukawa couplings of the SM quarks and leptons. The clockwork mechanism has also useful applications in the context of axion physics [298, 253, 71, 423, 266, 187], inflation [397, 497, 382], and dark sector physics [349, 411, 331, 254, 318, 152]. Additional developments are discussed in [72, 255, 398, 498, 475, 267].

The flavor clockwork mechanism introduces, for each quark and lepton of the SM, a system of fermionic "gears", consisting of N chiral fermions and $N+1$ fermions with opposite chirality. By introducing a specific set of mass terms for the fermions, one finds a single massless mode for each fermion flavor, with the remaining fields combining into N massive Dirac fermions. The massless mode contains a component of the last site of the clockwork that is increasingly exponentially suppressed as the number of gears, N, rises. Any interaction of fields with the last site thereby translates into exponentially suppressed couplings of the massless modes. In the flavor clockwork setup, the massless modes are identified with the fermions of the SM. The gear number N is chosen for each flavor to arrive at appropriately suppressed Yukawa couplings to the Higgs boson. As long as the clockwork mass scale is well above the SM scale of electroweak symmetry breaking, the massive clockwork gear fermions remain unobservable. For a sufficiently small clockwork scale, they might be collider accessible [86].

Despite the absence of any sign of supersymmetric particles at the LHC [217], supersymmetry (SUSY) remains one of the best motivated extensions of the SM. In the context of a flavor clockwork setup, SUSY removes the sensitivity of the electroweak scale to the clockwork scale, stabilizing the Higgs mass against loop corrections from the massive clockwork gears. In a SUSY version of the flavor clockwork, the fermionic gears of the clockwork are promoted to chiral superfields and the clockwork is implemented at the level of the superpotential. Such a setup results in hierarchical Yukawa couplings for the zero modes that are identified with the fermions and sfermions of the minimal supersymmetric standard model (MSSM). Once soft SUSY breaking is included, the clockwork mechanism will not only generate a hierarchical spectrum of quarks and leptons, but will also leave

characteristic imprints on the spectrum of the squarks and sleptons. In turn, the squarks and sleptons can give indirect signatures in low-energy flavor violating processes.

It is well known that Flavor Changing Neutral Current (FCNC) processes, that are forbidden in the SM at tree level, are highly sensitive probes of New Physics (NP). Particularly sensitive processes are meson oscillations that can probe generic flavor violating NP at scales as high as $\Lambda_{\rm NP} \sim 10^5\,\text{TeV}$ [385, 480, 66]. In this paper, we show that in a SUSY flavor clockwork setup, sizable flavor mixing among first and second generation squarks is predicted if SUSY breaking is gravity mediated. We consider constraints from Kaon mixing and derive generic bounds on the masses of squarks and gluinos. We find that the Kaon mixing constraints force either squarks or gluinos to have masses of at least ~ 3 PeV, introducing a considerable hierarchy between the electroweak scale and the scale of SUSY breaking masses.

This paper is organized as follows: In section 3.2.2 we provide the outline of a clockwork flavor model. The model is subsequently supersymmetrized in section 3.2.3, where we detail the predicted flavor structure of the sfermion masses. The constraints on the SUSY breaking masses from Kaon mixing are discussed in section 3.2.4. We conclude in section 5.2.6.

3.2.2 The Flavor Clockwork for SM Fermions

It is instructive to first review the setup of "clockworking" a single fermion, for the mechanism can easily be extended to any number of them. We follow [325]. Consider N left-chiral fermions $\psi_L^{(A)}$ and $N+1$ fermions with opposite chirality, $\psi_R^{(A)}$. In the limit of vanishing fermion masses, a large global chiral symmetry emerges. Each fermion can be associated with an abelian $U(1)$ factor, labeled $U(1)_L^{(A)}$ and $U(1)_R^{(A)}$ for $\psi_L^{(A)}$ and $\psi_R^{(A)}$, respectively. Away from the massless limit, the global chiral symmetry is broken. The degree of symmetry breaking can be tracked by promoting the fermion masses to spurion fields charged under the $U(1)$ factors. The clockwork mechanism is realized if the only symmetry

breaking spurions are masses $m^{(A)}$, with charges $(+1,-1)$ under $U(1)_L^{(A)} \times U(1)_R^{(A)}$ and masses $m_\chi^{(A)}$, with charges $(+1,-1)$ under $U(1)_L^{(A)} \times U(1)_R^{(A+1)}$. Taking for simplicity $m^{(A)} = m$ and $m_\chi^{(A)} = -m\chi$, with a common clockwork mass scale m and a gear ratio $|\chi| > 1$, the relevant part of the fermionic "gear" Lagrangian reads [325]

$$\mathcal{L}_m = -m \sum_{A=1}^{N} \left(\overline{\psi}_L^{(A)} \psi_R^{(A)} - \chi \overline{\psi}_L^{(A)} \psi_R^{(A+1)} + \text{h.c.} \right) . \tag{3.1}$$

This corresponds to a $N \times (N+1)$ mass matrix in clockwork space

$$\boldsymbol{m} = m \begin{pmatrix} 1 & -\chi & 0 & 0 & \cdots & 0 & 0 \\ 0 & 1 & -\chi & 0 & \cdots & 0 & 0 \\ 0 & 0 & 1 & -\chi & \cdots & 0 & 0 \\ \vdots & \vdots & \vdots & \ddots & \ddots & \vdots & \vdots \\ 0 & 0 & 0 & \cdots & 1 & -\chi & 0 \\ 0 & 0 & 0 & \cdots & 0 & 1 & -\chi \end{pmatrix} . \tag{3.2}$$

The above mass matrix leaves a single chiral $U(1)_R$ symmetry unbroken. The residual chiral symmetry is characterized by the existence of a massless mode. This is made more apparent upon observing that the mass matrix annihilates the mode

$$\begin{aligned} \xi_R &\equiv \mathcal{N} \sum_{A=1}^{N+1} \frac{1}{\chi^{A-1}} \psi_R^{(A)} , \\ \mathcal{N}^2 &= \frac{|\chi|^2 - 1}{|\chi|^2 - |\chi|^{-2N}} \simeq 1 + \mathcal{O}\left(|\chi|^{-2}\right) , \end{aligned} \tag{3.3}$$

where $\mathcal{N}$ is a normalization constant. As an eigenstate of the only unbroken part of the chiral symmetry, this is the only massless mode, as a singular value decomposition of the mass matrix confirms. All other mass eigenstates have non-degenerate masses of the order of the clockwork scale m. Due to the unitarity of the diagonalization matrices, the projection of $\psi_R^{(N+1)}$ onto the massless mode ξ_R is $(\mathcal{N}\chi^{-N})^*$.

We now review an example in which the clockwork mechanism leads to exponentially suppressed couplings of the massless mode to another sector. Consider an interaction of the last fermion gear $\psi_R^{(N+1)}$ modeled after the SM Yukawa terms

$$\mathcal{L} \supset -\tilde{Y}\overline{q}_L H \psi_R^{(N+1)} \ , \tag{3.4}$$

where q_L is a left-handed SM quark, and H the SM Higgs doublet. Note that this implies that all the clockwork fermions have to have the quantum numbers of the SM right-handed up quark, $u_R = (3, 1, \frac{2}{3})$. The coupling $\tilde{Y}$ is an $\mathcal{O}(1)$ complex number, representing a proto-Yukawa coupling. Given the projection of $\psi_R^{(N+1)}$ into the massless mode ξ_R, it is apparent that the resulting Yukawa coupling Y of the massless mode is exponentially suppressed by a factor χ^{-N}

$$\mathcal{L} \supset -Y\overline{q}_L H \xi_R = -\left(\frac{\mathcal{N}}{\chi^N}\right)^* \tilde{Y}\overline{q}_L H \xi_R \ . \tag{3.5}$$

In the following, we set the mass of all the massive modes in the clockwork (that have acted as "gears") far higher than the Higgs vacuum expectation value (vev), $v = 246\,\text{GeV}$, by choosing the clockwork scale $m \gg v$. In fact, we will assume that the massive fermions are sufficiently heavy, such that they have a negligible impact on phenomenology. The only observable state is the massless mode which is identified with the SM right-handed up quark, u_R, and which has strongly suppressed interactions as specified in (3.5). A similar construction can be applied to all other SM fermions as well.

Based on the discussion above, it is clear that the flavor structure of the SM Yukawa couplings may be attributed to a clockwork theory that generically gives exponential hierarchies in the couplings of the massless modes of the clockwork. Extending the mechanism to the entire Standard Model fermion content (see e.g. [86]) corresponds to systematically assigning each fermion to the massless mode of its own gear system, with a characteristic clockwork mass scale that we assume to be far above the electroweak scale. In the following, we focus on the quark sector. A completely analogous construction can also be introduced for the charged leptons.

A crucial parameter that determines the couplings of the massless modes is the gear ratio χ, which is generically expected to be an $\mathcal{O}(1)$ number. In the

context of quark Yukawa hierarchies, a natural choice is to relate χ to the sine of the Cabibbo angle, λ, such that $\chi = 1/\lambda \simeq 4$. We consider the simplest possible clockwork extension of the SM flavor sector, with a universal clockwork mass m for all quark gear systems and a universal gear ratio χ

$$m^{(A)}_{q^j_L} = m^{(A)}_{u^j_R} = m^{(A)}_{d^j_R} = m \ , \tag{3.6}$$

$$m\chi^{(A)}_{q^j_L} = m\chi^{(A)}_{u^j_R} = m\chi^{(A)}_{d^j_R} = -m\chi = -\frac{m}{\lambda} \ . \tag{3.7}$$

The number of massive gears will be denoted by $\{N^j_q, N^j_u, N^j_d\}$, where j runs over the flavor indices, $j = 1, 2, 3$. N^j_q is the number of gears of the left-handed quark doublets of flavor j, while N^j_u and N^j_d are the numbers of gears of the right-handed up quark and down quark singlets of flavor j.

These parameters, as well as the choice of proto-Yukawa couplings determine the Yukawa couplings of the SM quarks. Following the same procedure as in the single fermion case discussed above, one finds the SM Yukawa couplings

$$Y^{ij}_x \simeq \tilde{Y}^{ij}_x \ \chi^{-N^i_q - N^j_x} \ , \quad x = u, d \ . \tag{3.8}$$

Here and in the following we work to leading order in an expansion in the gear ratio $1/\chi = \lambda$. Diagonalizing the Yukawa matrices in (3.8) determines the quark masses and the Cabibbo-Kobayashi-Maskawa (CKM) quark mixing matrix

$$\mathrm{diag}(m_u, m_c, m_t) = \frac{v}{\sqrt{2}} V_{L_u} Y_u V^\dagger_{R_u} \ , \tag{3.9}$$

$$\mathrm{diag}(m_d, m_s, m_b) = \frac{v}{\sqrt{2}} V_{L_d} Y_d V^\dagger_{R_d} \ , \tag{3.10}$$

$$V_{\mathrm{CKM}} = V_{L_u} V^\dagger_{L_d} \ . \tag{3.11}$$

For the diagonalization matrices one finds the following scaling with the gear ratio

$$V^{ij}_{L_x} \sim \chi^{-|N^j_q - N^i_q|}, \quad V^{ij}_{R_x} \sim \chi^{-|N^j_x - N^i_x|}, \quad x = u, d \ . \tag{3.12}$$

Due to the suppression of the off-diagonal entries of the diagonalization matrices by powers of the gear ratio, the quark masses are, to a good approximation, given by the diagonal entries in the Yukawa couplings

$$m_u \simeq \frac{v}{\sqrt{2}} |\tilde{Y}^{11}_u| \lambda^{N^1_q + N^1_u} \ , \quad m_d \simeq \frac{v}{\sqrt{2}} |\tilde{Y}^{11}_d| \lambda^{N^1_q + N^1_d} \ , \tag{3.13}$$

$$m_c \simeq \frac{v}{\sqrt{2}}|\tilde{Y}_u^{22}|\lambda^{N_q^2+N_u^2} \ , \quad m_s \simeq \frac{v}{\sqrt{2}}|\tilde{Y}_d^{22}|\lambda^{N_q^2+N_d^2} \ , \tag{3.14}$$

$$m_t \simeq \frac{v}{\sqrt{2}}|\tilde{Y}_u^{33}|\lambda^{N_q^3+N_u^3} \ , \quad m_b \simeq \frac{v}{\sqrt{2}}|\tilde{Y}_d^{33}|\lambda^{N_q^3+N_d^3} \ . \tag{3.15}$$

In the equations above, the quark masses should be evaluated at the clockwork scale. The renormalization group running to high scales can have a significant impact on the quark masses. Therefore, it is convenient to work with ratios of quark masses that are, to a reasonable approximation, renormalization group invariant [100]. Using the quark masses from [516] and evolving them to a common renormalization scale $\mu = v = 246\,\text{GeV}$, taking into account 3 loop QCD running [234], we find

$$\frac{m_u}{m_t} \simeq 7.3 \times 10^{-6} \ , \qquad \frac{m_d}{m_b} \simeq 9.5 \times 10^{-4} \ , \tag{3.16}$$

$$\frac{m_c}{m_t} \simeq 3.7 \times 10^{-3} \ , \qquad \frac{m_s}{m_b} \simeq 1.9 \times 10^{-2} \ , \tag{3.17}$$

$$\frac{m_b}{m_t} \simeq 1.7 \times 10^{-2} \ . \tag{3.18}$$

Since the top quark mass is of the order of the electroweak scale and gear numbers are non-negative, we set

$$N_q^3 = N_u^3 = 0 \ . \tag{3.19}$$

Using $\lambda = 0.2252$ [516], we find that the quark mass ratios give the following constraints on the other gear numbers

$$N_q^1 + N_u^1 = 8 \ , \quad N_q^1 + N_d^1 - N_d^3 = 4 \ , \tag{3.20}$$

$$N_q^2 + N_u^2 = 4 \ , \quad N_q^2 + N_d^2 - N_d^3 = 2 \ , \tag{3.21}$$

$$N_d^3 = 3 \ , \tag{3.22}$$

where we pick the integer gear numbers such as to minimize the deviation of the relevant proto-Yukawa ratios from 1.

In the case of the CKM matrix, it is sufficient to consider the scaling with powers of λ

$$V_{\text{CKM}} \sim \begin{pmatrix} 1 & \lambda^{N_q^1-N_q^2} & \lambda^{N_q^1-N_q^3} \\ \lambda^{N_q^1-N_q^2} & 1 & \lambda^{N_q^2-N_q^3} \\ \lambda^{N_q^1-N_q^3} & \lambda^{N_q^2-N_q^3} & 1 \end{pmatrix} . \tag{3.23}$$

Comparing with the usual Wolfenstein parameterization, gives two additional conditions on the gear numbers of the left-handed quark doublets

$$N_q^1 - N_q^3 = 3 \ , \quad N_q^2 - N_q^3 = 2 \ . \tag{3.24}$$

The complex off-diagonal entries of the $\mathcal{O}(1)$ proto-Yukawa couplings can be adjusted to reproduce the known magnitudes of the CKM matrix elements and the CP-violating CKM phase. Analogous to the quark masses, also the CKM matrix elements should be evaluated at the clockwork scale. However, the scale dependence of the CKM matrix is very mild [158] and can be neglected for our purposes.

The conditions (3.19)-(3.22) combined with (3.24) have the solution

$$N_q = \begin{pmatrix} 3 \\ 2 \\ 0 \end{pmatrix} , \quad N_u = \begin{pmatrix} 5 \\ 2 \\ 0 \end{pmatrix} , \quad N_d = \begin{pmatrix} 4 \\ 3 \\ 3 \end{pmatrix} \ . \tag{3.25}$$

These gear numbers correspond to the following scaling of the Yukawa couplings with the Cabibbo angle

$$Y_u \sim \begin{pmatrix} \lambda^8 & \lambda^5 & \lambda^3 \\ \lambda^7 & \lambda^4 & \lambda^2 \\ \lambda^5 & \lambda^2 & 1 \end{pmatrix} , \quad Y_d \sim \begin{pmatrix} \lambda^7 & \lambda^6 & \lambda^6 \\ \lambda^6 & \lambda^5 & \lambda^5 \\ \lambda^4 & \lambda^3 & \lambda^3 \end{pmatrix} , \tag{3.26}$$

where we do not explicitly show the dependence on the proto-Yukawa couplings. For a similar analysis, one may also follow the discussion in [86] where a slightly different choice of gear numbers has been made (see also [416]). Small changes in gear numbers can be compensated by corresponding changes in the proto-Yukawa couplings and the precise value of the gear ratio χ.

The above discussion serves to highlight the validity and key features of the clockwork mechanism in the context of a setup that explains the SM flavor hierarchies. In the next section, we will construct a supersymmetric version of this setup.

Superfield	Gauge Representations	Multiplicity
$\mathbf{\Phi}_{Q_i}$	$(3, 2, \frac{1}{6})$	$N_q^i + 1$
$\mathbf{\Phi}_{Q_i^c}$	$(\overline{3}, \overline{2}, -\frac{1}{6})$	N_q^i
$\mathbf{\Phi}_{U_i}$	$(3, 1, \frac{2}{3})$	N_u^i
$\mathbf{\Phi}_{U_i^c}$	$(\overline{3}, 1, -\frac{2}{3})$	$N_u^i + 1$
$\mathbf{\Phi}_{D_i}$	$(3, 1, -\frac{1}{3})$	N_d^i
$\mathbf{\Phi}_{D_i^c}$	$(\overline{3}, 1, \frac{1}{3})$	$N_d^i + 1$

Table 3.1: Field content of the supersymmetric flavor clockwork. The multiplicities indicate the vector dimension of the corresponding superfield in clockwork space.

3.2.3 The Supersymmetric Flavor Clockwork

Starting from the flavor clockwork setup discussed above, we promote the clockwork fermions to chiral superfields. The matter field content then consists of gear systems for the three generations of left-handed quark doublet superfields $\mathbf{\Phi}_{Q_i}$, $\mathbf{\Phi}_{Q_i^c}$ the three generations of right-handed up-quark singlet superfields $\mathbf{\Phi}_{U_i^c}$, $\mathbf{\Phi}_{U_i}$, and the three generations of right-handed down-quark singlet superfields $\mathbf{\Phi}_{D_i^c}$, $\mathbf{\Phi}_{D_i}$, where $i = 1, 2, 3$ is the flavor index. The boldface notation indicates that the superfields are vectors in clockwork space, each with an individual multiplicity of fields. The field content with the respective multiplicities is summarized in Table 3.1.

Including the usual two Higgs doublets of the MSSM, H_u and H_d, the relevant part of the superpotential reads

$$W \supset \mathbf{\Phi}_{Q_i} \boldsymbol{m}_{Q_i} \mathbf{\Phi}_{Q_i^c} + \mathbf{\Phi}_{U_i} \boldsymbol{m}_{U_i} \mathbf{\Phi}_{U_i^c} + \mathbf{\Phi}_{D_i} \boldsymbol{m}_{D_i} \mathbf{\Phi}_{D_i^c} + \tilde{Y}_u^{ij} H_u \mathbf{\Phi}_{Q_i} \mathbf{\Delta}_u^{ij} \mathbf{\Phi}_{U_j^c} + \tilde{Y}_d^{ij} H_d \mathbf{\Phi}_{Q_i} \mathbf{\Delta}_d^{ij} \mathbf{\Phi}_{D_j^c} \,, \quad (3.27)$$

where sums over the flavor indices i, j remain implicit. In addition, the superpotential also includes the standard Peccei-Quinn breaking term of the Higgs doublets, $\mu H_u H_d$. The clockwork masses $\boldsymbol{m}_{Q_i}$, $\boldsymbol{m}_{U_i}$, and $\boldsymbol{m}_{D_i}$ are $(N_q^i+1)\times N_q^i$, $N_u^i \times (N_u^i+1)$, and $N_d^i \times (N_d^i+1)$ matrices in clockwork space, and they are multiplied by superfield vectors of corresponding size. Assuming for simplicity that the mass matrices of the clockwork structure are universal, with a common clockwork scale $m = \Lambda_{\rm CW}$ and a common gear ratio $\chi = 1/\lambda$ one has

$$(\boldsymbol{m}_{X_i})_{AB} = m\left(\delta_B^A - \chi\delta_B^{A+1}\right), \quad X = U, D\ , \tag{3.28}$$

$$(\boldsymbol{m}_{Q_i})_{AB} = m\left(\delta_B^A - \chi\delta_{B+1}^{A}\right). \tag{3.29}$$

The $\boldsymbol{\Delta}_u^{ij}$ and $\boldsymbol{\Delta}_d^{ij}$ in the second line of (3.27) are $(N_q^i+1)\times(N_x^j+1)$ matrices in clockwork space with a single non-zero entry for the last sites of each gear system

$$(\boldsymbol{\Delta}_x^{ij})_{AB} = \delta_A^{N_q^i+1}\delta_B^{N_x^j+1}\ , \quad x = u, d\ . \tag{3.30}$$

The corresponding $\tilde{Y}_u$ and $\tilde{Y}_d$ trilinear coefficients are flavor anarchic proto-Yukawa couplings that connect the three flavors of up-quark and down-quark fields at the last site of each gear system.

Next, we introduce soft SUSY breaking terms to provide all superpartners of Standard Model fields with masses above the current bounds from direct searches. We assume that SUSY breaking is gravity mediated to the visible sector by Planck scale suppressed operators. As long as the clockwork scale is sufficiently below the Planck scale $\Lambda_{\rm CW} < M_{\rm Pl}$, the SUSY breaking Lagrangian respects the chiral symmetries of the clockwork structure, and mixing among different flavors is only possible at the last site of each gear system. Therefore, the relevant soft masses for the squarks can be written as

$$\begin{aligned}\mathcal{L}_{\rm soft} \supset\ & \tilde{\mathbf{Q}}_i^\dagger \boldsymbol{\mu}_{Q_i}^2 \tilde{\mathbf{Q}}_i + \tilde{\mathbf{Q}}_i^{c\,\dagger}\boldsymbol{\mu}_{Q_i^c}^2\tilde{\mathbf{Q}}_i^c + (M_Q^2)_{ij}\tilde{\mathbf{Q}}_i^\dagger\boldsymbol{\Delta}_Q^{ij}\tilde{\mathbf{Q}}_j \\ & + \tilde{\mathbf{U}}_i^\dagger\boldsymbol{\mu}_{U_i}^2\tilde{\mathbf{U}}_i + \tilde{\mathbf{U}}_i^{c\,\dagger}\boldsymbol{\mu}_{U_i^c}^2\tilde{\mathbf{U}}_i^c + (M_U^2)_{ij}\tilde{\mathbf{U}}_i^{c\,\dagger}\boldsymbol{\Delta}_U^{ij}\tilde{\mathbf{U}}_j^c \\ & + \tilde{\mathbf{D}}_i^\dagger\boldsymbol{\mu}_{D_i}^2\tilde{\mathbf{D}}_i + \tilde{\mathbf{D}}_i^{c\,\dagger}\boldsymbol{\mu}_{D_i^c}^2\tilde{\mathbf{D}}_i^c + (M_D^2)_{ij}\tilde{\mathbf{D}}_i^{c\,\dagger}\boldsymbol{\Delta}_D^{ij}\tilde{\mathbf{D}}_j^c\ ,\end{aligned} \tag{3.31}$$

where sums over flavor indices i, j are implicit, and $\tilde{\mathbf{Q}}_i$, $\tilde{\mathbf{Q}}_i^c$, $\tilde{\mathbf{U}}_i$, $\tilde{\mathbf{U}}_i^c$, and $\tilde{\mathbf{D}}_i$, $\tilde{\mathbf{D}}_i^c$ are the scalar components of the superfield gear systems. The various soft breaking

masses $\boldsymbol{\mu}^2$ are diagonal matrices in clockwork space. Generically, we expect the non-zero entries to be of the same order that we denote with m_S^2. Similar as in (3.27), the $\boldsymbol{\Delta}_Q^{ij}$, $\boldsymbol{\Delta}_U^{ij}$, and $\boldsymbol{\Delta}_D^{ij}$ are $(N_q^i+1)\times(N_q^j+1)$, $(N_u^i+1)\times(N_u^j+1)$, and $(N_d^i+1)\times(N_d^j+1)$ matrices in clockwork space, respectively, each with a single non-zero entry for the last clockwork site. The soft breaking masses $(M_Q^2)_{ij}$, $(M_U^2)_{ij}$, and $(M_D^2)_{ij}$ are generically expected to be flavor anarchic and also of the order $\sim m_S^2$.

The trilinear A-terms that couple squarks to the Higgs bosons have a structure similar to the proto-Yukawa couplings in the superpotential

$$\mathcal{L}_{\text{soft}} \supset A_u^{ij} H_u \tilde{\mathbf{Q}}_i \boldsymbol{\Delta}_u^{ij} \tilde{\mathbf{U}}_j^c + A_d^{ij} H_d \tilde{\mathbf{Q}}_i \boldsymbol{\Delta}_d^{ij} \tilde{\mathbf{D}}_j^c \ + \text{h.c.} \ . \tag{3.32}$$

Generically, one expects the trilinear terms to be flavor anarchic, and of the same order of the soft masses $A_x^{ij} \sim m_S$, or 1-loop suppressed $A_x^{ij} \sim m_S/16\pi^2$ if their dominant contribution arises from anomaly mediation [324]. The lack of experimental evidence for SUSY particles implies that the SUSY masses have to be significantly above the electroweak scale. In such a case, the trilinear terms have a negligible impact on the low energy flavor observables that we will analyze in the next section. Therefore, we will not consider the trilinear terms in any further detail.

In addition to the soft SUSY breaking terms discussed above, the gaugino masses and the $B\mu$ term can be introduced analogously to the MSSM. Of particular relevance for the discussion of the flavor constraints in section 3.2.4 is the gluino mass $m_{\tilde{g}}$. We will assume that the gluino mass is of the order of the soft scalar masses m_S, keeping in mind that 1-loop suppressed gaugino masses are motivated as well in the context of anomaly mediation [324].

The scenario we consider is then characterized by the following important scales

$$v < m_{\tilde{g}}, m_S \ll \Lambda_{\text{CW}} < M_{\text{Pl}} \ . \tag{3.33}$$

As discussed in appendix 3.2.6, the large number of matter fields in the clockwork setup significantly modifies the running of the gauge couplings above the clockwork scale and leads to a loss of asymptotic freedom. Requiring the absence of Landau

poles below the Planck scale, $M_{\rm Pl}$, implies a lower bound on the clockwork scale a few orders of magnitude below $M_{\rm Pl}$. SUSY stabilizes the electroweak scale against quantum corrections of the order of the clockwork scale or the Planck scale. As SUSY holds to an excellent approximation at the clockwork scale, all superfields $\mathbf{\Phi}$ may be rotated into their mass eigenbases that render the clockwork masses in (3.28) and (3.29) diagonal. This leads to N_q^i, N_u^i, and N_d^i massive modes with masses of the order of the clockwork scale $\Lambda_{\rm CW}$, that are decoupled from phenomenology. The massless modes may consequently be identified with the quarks and squarks of the MSSM $(q_L^i, \tilde{q}_L^i)$, $(u_R^i, \tilde{u}_R^i)$, and $(d_R^i, \tilde{d}_R^i)$. Analogous to the non-SUSY case given in (3.3) we find

$$(q_L^i, \tilde{q}_L^i) \simeq \sum_{A=1}^{N_q^i+1} \frac{1}{\chi^{A-1}} (\mathbf{Q}_i, \tilde{\mathbf{Q}}_i)_A \ , \tag{3.34}$$

$$(u_R^{i\,c}, \tilde{u}_R^{i\,*}) \simeq \sum_{A=1}^{N_u^i+1} \frac{1}{\chi^{A-1}} (\mathbf{U}_i^c, \tilde{\mathbf{U}}_i^c)_A \ , \tag{3.35}$$

$$(d_R^{i\,c}, \tilde{d}_R^{i\,*}) \simeq \sum_{A=1}^{N_d^i+1} \frac{1}{\chi^{A-1}} (\mathbf{D}_i^c, \tilde{\mathbf{D}}_i^c)_A \ , \tag{3.36}$$

where we suppressed normalization factors of order $1 + \mathcal{O}(\chi^{-2})$. The Yukawa couplings of the massless superfields have the exponential structure given in (3.8).

In a supersymmetric context, the gear numbers derived in (3.25) need to be adjusted. As up-type quarks obtain their mass from the Higgs doublet H_u and down-type quarks from the Higgs doublet H_d, part of the hierarchical fermion spectrum could be due to a large ratio of Higgs vevs $\tan\beta = v_u/v_d$. Among the constraints on the gear numbers discussed in section 3.2.2, the constraint in (3.22) gets therefore modified to

$$N_d^3 = 3 - n \ , \tag{3.37}$$

where the integer n is determined by the size of $\tan\beta$ in terms of the gear ratio

$\tan\beta \sim \chi^n$. Viable choices are $n = 0, 1, 2, 3$. The resulting gear numbers are

$$N_q = \begin{pmatrix} 3 \\ 2 \\ 0 \end{pmatrix}, \quad N_u = \begin{pmatrix} 5 \\ 2 \\ 0 \end{pmatrix}, \quad N_d = \begin{pmatrix} 4-n \\ 3-n \\ 3-n \end{pmatrix} . \tag{3.38}$$

The squark components of the massless superfields acquire soft SUSY breaking masses from the terms in (3.31). Since the clockwork mass scale, $\Lambda_{\rm CW}$, is much larger than the soft scalar masses $\sim m_S$, the treatment of the soft masses as a perturbation on the clockwork structures provides an excellent approximation of the squark mass matrices. We find for the left-handed and right-handed squark soft masses of the MSSM

$$(\hat{m}^2_{\tilde{q}_L})_{ij} \simeq (\boldsymbol{\mu}^2_{Q_i})_{11}\delta_{ij} + (M^2_Q)_{ij}\chi^{-N^i_q - N^j_q} , \tag{3.39}$$

$$(\hat{m}^2_{\tilde{u}_R})_{ij} \simeq (\boldsymbol{\mu}^2_{U_i})_{11}\delta_{ij} + (M^2_U)^*_{ji}\chi^{-N^i_u - N^j_u} , \tag{3.40}$$

$$(\hat{m}^2_{\tilde{d}_R})_{ij} \simeq (\boldsymbol{\mu}^2_{D_i})_{11}\delta_{ij} + (M^2_D)^*_{ji}\chi^{-N^i_d - N^j_d} . \tag{3.41}$$

These mass matrices are obtained upon discarding terms that are higher order in $m_S^2/\Lambda^2_{\rm CW}$ and in the gear ratio $1/\chi$. The leading flavor diagonal squark masses are provided by the soft SUSY breaking terms of the first clockwork gears $(\boldsymbol{\mu}^2_{Q_i})_{11}$, $(\boldsymbol{\mu}^2_{U_i})_{11}$, and $(\boldsymbol{\mu}^2_{D_i})_{11}$. These masses are all of order m_S^2 and not suppressed by the gear ratio. It is important to note that these masses are flavor diagonal but not necessarily flavor universal. The flavor violating masses originate from the M^2_Q, M^2_U, and M^2_D terms and are suppressed by powers of the gear ratio. The generic scaling with the sine of the Cabibbo angle is given by

$$\hat{m}^2_{\tilde{q}_L} \sim m_S^2 \begin{pmatrix} 1 & \lambda^{N^1_q + N^2_q} & \lambda^{N^1_q + N^3_q} \\ \lambda^{N^1_q + N^2_q} & 1 & \lambda^{N^2_q + N^3_q} \\ \lambda^{N^1_q + N^3_q} & \lambda^{N^2_q + N^3_q} & 1 \end{pmatrix}, \tag{3.42}$$

$$\hat{m}^2_{\tilde{x}_R} \sim m_S^2 \begin{pmatrix} 1 & \lambda^{N^1_x + N^2_x} & \lambda^{N^1_x + N^3_x} \\ \lambda^{N^1_x + N^2_x} & 1 & \lambda^{N^2_x + N^3_x} \\ \lambda^{N^1_x + N^3_x} & \lambda^{N^2_x + N^3_x} & 1 \end{pmatrix}, \tag{3.43}$$

where $x = u, d$. At first sight, this flavor structure of the squark masses seems to indicate strongly suppressed flavor mixing, in particular between the first and second generation of squarks. However, to make the connection to phenomenology, it is important to express the squark masses in (3.42) and (3.43) in the super-CKM basis. Performing the flavor rotations (3.12) that diagonalize the quark Yukawa couplings also on the squarks gives the following squark mass matrices

$$m^2_{\tilde{x}_L} = V_{L_x} \hat{m}^2_{\tilde{q}_L} V^\dagger_{L_x}, \quad x = u, d \ , \tag{3.44}$$

$$m^2_{\tilde{x}_R} = V_{R_x} \hat{m}^2_{\tilde{x}_R} V^\dagger_{R_x}, \quad x = u, d \ , \tag{3.45}$$

where the un-hatted $m^2_{\tilde{x}_R}$ and $m^2_{\tilde{x}_L}$ are the squark mass matrices in the super-CKM basis. As mentioned above, the diagonal entries of $\hat{m}^2_{\tilde{x}_R}$ and $\hat{m}^2_{\tilde{q}_L}$ are not universal and the rotations therefore tend to increase the off-diagonal entries. This is particularly relevant for the $1 \leftrightarrow 2$ mixing entries. We find

$$m^2_{\tilde{x}_L} \sim m^2_S \begin{pmatrix} 1 & \lambda^{|N^1_q - N^2_q|} & \lambda^{|N^1_q - N^3_q|} \\ \lambda^{|N^1_q - N^2_q|} & 1 & \lambda^{|N^2_q - N^3_q|} \\ \lambda^{|N^1_q - N^3_q|} & \lambda^{|N^2_q - N^3_q|} & 1 \end{pmatrix}, \tag{3.46}$$

$$m^2_{\tilde{x}_R} \sim m^2_S \begin{pmatrix} 1 & \lambda^{|N^1_x - N^2_x|} & \lambda^{|N^1_x - N^3_x|} \\ \lambda^{|N^1_x - N^2_x|} & 1 & \lambda^{|N^2_x - N^3_x|} \\ \lambda^{|N^1_x - N^3_x|} & \lambda^{|N^2_x - N^3_x|} & 1 \end{pmatrix}, \tag{3.47}$$

where $x = u, d$. Note that the mass matrices of the right-handed up and down squarks, $m^2_{\tilde{u}_R}$ and $m^2_{\tilde{d}_R}$, are independent from each other. In contrast, the mass matrices for the left-handed squarks are related due to $SU(2)_L$ symmetry

$$m^2_{\tilde{u}_L} = V_{\rm CKM} \, m^2_{\tilde{d}_L} V^\dagger_{\rm CKM} \ . \tag{3.48}$$

Using the gear numbers in (3.38), the squark masses in the super-CKM basis have the following explicit scaling with the Cabibbo angle, independently of the value

for $\tan\beta$

$$\frac{m^2_{\tilde{d}_L}}{m^2_S} \sim \begin{pmatrix} 1 & \lambda & \lambda^3 \\ \lambda & 1 & \lambda^2 \\ \lambda^3 & \lambda^2 & 1 \end{pmatrix} , \tag{3.49}$$

$$\frac{m^2_{\tilde{u}_R}}{m^2_S} \sim \begin{pmatrix} 1 & \lambda^3 & \lambda^5 \\ \lambda^3 & 1 & \lambda^2 \\ \lambda^5 & \lambda^2 & 1 \end{pmatrix} , \quad \frac{m^2_{\tilde{d}_R}}{m^2_S} \sim \begin{pmatrix} 1 & \lambda & \lambda \\ \lambda & 1 & 1 \\ \lambda & 1 & 1 \end{pmatrix} . \tag{3.50}$$

The flavor diagonal entries are all of the same order, but not universal. The off-diagonal entries can be complex and are generically expected to have $\mathcal{O}(1)$ CP-violating phases. We note in particular sizeable entries of $\mathcal{O}(\lambda)$ that lead to mixing of the first and second generation of down type squarks. This is reminiscent of the situation in the simplest supersymmetric Froggatt-Nielsen flavor models with a single $U(1)$ flavor symmetry [416].

It could be interesting to explore variations of our setup that lead to hierarchical sfermion masses as in [448], or to a sfermion spectrum with inverted hierarchy as in [214, 213].

3.2.4 Constraints from Meson Mixing

In the presence of flavor violating squark masses, many low-energy flavor observables receive SUSY contributions [310, 93]. Particularly sensitive probes of flavor violating squarks are Kaon oscillations that are potentially sensitive to squarks at the PeV scale [109, 386].

The observables of interest are Δm_K, the frequency of $K^0 - \bar{K}^0$ oscillations, and ϵ_K, that measures indirect CP-violation $K^0 - \bar{K}^0$ oscillations. The computation of meson oscillation observables is commonly cast into an OPE framework, providing an effective Hamiltonian consisting of dimension 6 operators O_k and their corresponding Wilson coefficients C_k

$$\mathcal{H}_{\text{eff}} = \sum_{k=1}^{5} C_k O_k + \sum_{k=1}^{3} \tilde{C}_k \tilde{O}_k + \text{h.c.} . \tag{3.51}$$

Based on this effective Hamiltonian, the observables can be computed as

$$\Delta m_K = 2\,\mathrm{Re}\,\langle K^0|\,\mathcal{H}_{\rm eff}\,|\bar{K}^0\rangle\,, \tag{3.52}$$

$$|\epsilon_K| = \frac{\kappa_\epsilon}{\sqrt{2}\Delta m_K}\mathrm{Im}\,\langle K^0|\,\mathcal{H}_{\rm eff}\,|\bar{K}^0\rangle\,, \tag{3.53}$$

where $\kappa_\epsilon \simeq 0.94 \pm 0.02$ [207] encapsulates long-distance contributions to the CP violating parameter.

The dominant SUSY contributions to the Wilson coefficients are coming from gluino-squark loops and are proportional to the mixing between the first and second generation of down-type quarks. Additional chargino-squark and neutralino-squark loop contributions have been considered for example in [94, 256]. They can be relevant in regions of parameter space where gluino contributions are accidentally small. This is not the case in our scenario.

The relevant entries in the squark mass matrices (3.50) and (3.49) that enter the gluino contributions are suppressed by the sine of the Cabibbo angle. It is thus justified to work in the mass insertion approximation, expanding the SUSY contributions to first order in the left-left and right-right mass insertions

$$(\delta^d_{12})_{LL} = \frac{(m^2_{\tilde{d}_L})_{12}}{m_S^2} \sim \lambda, \quad (\delta^d_{12})_{RR} = \frac{(m^2_{\tilde{d}_R})_{12}}{m_S^2} \sim \lambda. \tag{3.54}$$

Additional left-right mixing mass insertions are proportional to the trilinear soft A-terms introduced in (3.32). They are suppressed by the electroweak scale $(\delta^d_{ij})_{LR} \propto v/m_S$ and can be safely neglected. In that case, the only relevant operators in the effective Hamiltonian are

$$O_1 = (\bar{d}^\alpha_L \gamma_\mu s^\alpha_L)(\bar{d}^\beta_L \gamma^\mu s^\beta_L)\,, \tag{3.55}$$

$$\tilde{O}_1 = (\bar{d}^\alpha_R \gamma_\mu s^\alpha_R)(\bar{d}^\beta_R \gamma^\mu s^\beta_R)\,, \tag{3.56}$$

$$O_4 = (\bar{d}^\alpha_R s^\alpha_L)(\bar{d}^\beta_L s^\beta_R)\,, \tag{3.57}$$

$$O_5 = (\bar{d}^\alpha_R s^\beta_L)(\bar{d}^\beta_L s^\alpha_R)\,, \tag{3.58}$$

where $\alpha, \beta = 1, \ldots, 3$ are color indices. In the mass insertion approximation, the Wilson coefficients depend on the gluino mass $m_{\tilde{g}}$ and the common squark mass m_S. They read [310, 238, 93]

$$C_1 = \frac{1}{216}\frac{\alpha_s^2}{m_S^2}(\delta^d_{12})^2_{LL} f_1(m^2_{\tilde{g}}/m^2_S)\,, \tag{3.59}$$

$$\tilde{C}_1 = \frac{1}{216}\frac{\alpha_s^2}{m_S^2}(\delta^d_{12})^2_{RR} f_1(m_{\tilde{g}}^2/m_S^2) \ , \tag{3.60}$$

$$C_4 = -\frac{23}{180}\frac{\alpha_s^2}{m_S^2}(\delta^d_{12})_{LL}(\delta^d_{12})_{RR} f_4(m_{\tilde{g}}^2/m_S^2) \ , \tag{3.61}$$

$$C_5 = \frac{7}{540}\frac{\alpha_s^2}{m_S^2}(\delta^d_{12})_{LL}(\delta^d_{12})_{RR} f_5(m_{\tilde{g}}^2/m_S^2) \ . \tag{3.62}$$

The loop functions are normalized such that $f_i(1) = 1$, and the explicit expressions are

$$f_1(x) = \frac{2(11+144x+27x^2-2x^3)}{(1-x)^4} + \frac{12x(13+17x)}{(1-x)^5}\log x \ , \tag{3.63}$$

$$f_4(x) = \frac{10(2-99x-54x^2+7x^3)}{23(1-x)^4} - \frac{60x(5+19x)}{23(1-x)^5}\log x \ , \tag{3.64}$$

$$f_5(x) = \frac{10(10+117x+18x^2-x^3)}{7(1-x)^4} + \frac{60x(11+13x)}{7(1-x)^5}\log x \ . \tag{3.65}$$

The operator matrix elements $\langle O_i \rangle = \langle K^0 | \, O_i \, | \bar{K}^0 \rangle$, relevant to evaluate the observables Δm_K and ϵ_K in (3.52) and (3.53), can be written as

$$\langle O_1 \rangle = \langle \tilde{O}_1 \rangle = \frac{1}{3} B_1 m_K f_K^2 \ , \tag{3.66}$$

$$\langle O_4 \rangle = \frac{1}{4} B_4 m_K f_K^2 \frac{m_K^2}{(m_d+m_s)^2} \ , \tag{3.67}$$

$$\langle O_5 \rangle = \frac{1}{12} B_5 m_K f_K^2 \frac{m_K^2}{(m_d+m_s)^2} \ , \tag{3.68}$$

where $f_K = 155.7\,\text{MeV}$ [130] is the Kaon decay constant. For the so-called bag parameters B_i we use the lattice determinations from [223] $B_1 = 0.506 \pm 0.017$, $B_4 = 0.78 \pm 0.05$, and $B_5 = 0.49 \pm 0.04$. Note that these parameters are renormalization scheme and scale dependent and the given values correspond to the $\overline{\text{MS}}$ scheme at a low hadronic scale of $\mu_{\text{low}} = 3\,\text{GeV}$. The quark masses in the matrix elements (3.67) and (3.68) have to be evaluated in the same scheme and at the same scale. We use $m_s(\mu_{\text{low}}) \simeq 86\,\text{MeV}$ and $m_d(\mu_{\text{low}}) \simeq 4.3\,\text{MeV}$ [516, 234]. Note the chiral enhancement of the matrix elements $\langle O_4 \rangle$ and $\langle O_5 \rangle$ by the factor $m_K^2/(m_d+m_s)^2 \simeq 30$.

In contrast to the hadronic matrix elements, the Wilson coefficients discussed above are defined at a high renormalization scale that corresponds to the masses

of the SUSY particles $\mu_{\rm high} \sim m_S, m_{\tilde{g}}$. In particular, the strong coupling constant in the Wilson coefficients is evaluated at that scale. The Wilson coefficients are evolved to the low scale $\mu_{\rm low}$ by solving their renormalization group equations [241, 210, 209]. At the low scale they are combined with the hadronic matrix elements to determine the observables Δm_K and ϵ_K. As we consider the leading order SUSY contributions to the Wilson coefficients, 1-loop running is appropriate. The low scale Wilson coefficients are thus given by

$$C_1(\mu_{\rm low}) = \eta_4^{6/25}\eta_5^{6/23}\eta_6^{2/7} C_1(\mu_{\rm high}) \ , \tag{3.69}$$

$$\tilde{C}_1(\mu_{\rm low}) = \eta_4^{6/25}\eta_5^{6/23}\eta_6^{2/7} \tilde{C}_1(\mu_{\rm high}) \ , \tag{3.70}$$

$$\begin{aligned} C_4(\mu_{\rm low}) = {} & \eta_4^{-24/25}\eta_5^{-24/23}\eta_6^{-8/7} C_4(\mu_{\rm high}) \\ & + \frac{1-\eta_4^{27/25}\eta_5^{27/23}\eta_6^{9/7}}{3\eta_4^{24/25}\eta_5^{24/23}\eta_6^{8/7}} C_5(\mu_{\rm high}) \ , \end{aligned} \tag{3.71}$$

$$C_5(\mu_{\rm low}) = \eta_4^{3/25}\eta_5^{3/23}\eta_6^{1/7} C_5(\mu_{\rm high}) \ , \tag{3.72}$$

where the η_i factors are ratios of the strong coupling constant evaluated at different scales in a 4, 5, or 6 flavor scheme as appropriate

$$\eta_6 = \frac{\alpha_s^{(6)}(\mu_{\rm high})}{\alpha_s^{(6)}(\mu_t)}, \ \eta_5 = \frac{\alpha_s^{(5)}(\mu_t)}{\alpha_s^{(5)}(\mu_b)}, \ \eta_4 = \frac{\alpha_s^{(4)}(\mu_b)}{\alpha_s^{(4)}(\mu_{\rm low})}. \tag{3.73}$$

We use the numerical values $\eta_4 \simeq 0.89$ and $\eta_5 \simeq 0.48$ [234]. We decide to evaluate η_6 at the larger of the squark mass and gluino mass $\mu_{\rm high} = \max(m_{\tilde{g}}, m_S)$.

In Figure 3.1, we show the SUSY contributions to ϵ_K (left plot) and to Δm_K (right plot) as function of the gluino mass $m_{\tilde{g}}$ and the generic squark mass m_S. The solid black contours in the left plot indicate the size of the contribution $\epsilon_K^{\rm SUSY}$ relative to the uncertainty of the SM prediction [198]

$$\epsilon_K^{\rm SM} = (2.16 \pm 0.18) \times 10^{-3} \ , \tag{3.74}$$

which is in excellent agreement with the very precise experimental value [516]

$$\epsilon_K^{\rm exp} = (2.228 \pm 0.011) \times 10^{-3} \ . \tag{3.75}$$

SUSY contributions significantly larger than the SM theory uncertainty are therefore excluded. The dark (light) red region in the left plot of Figure 3.1, corresponds to a SUSY contribution larger than $2\times$ ($1.5\times$) the SM uncertainty.

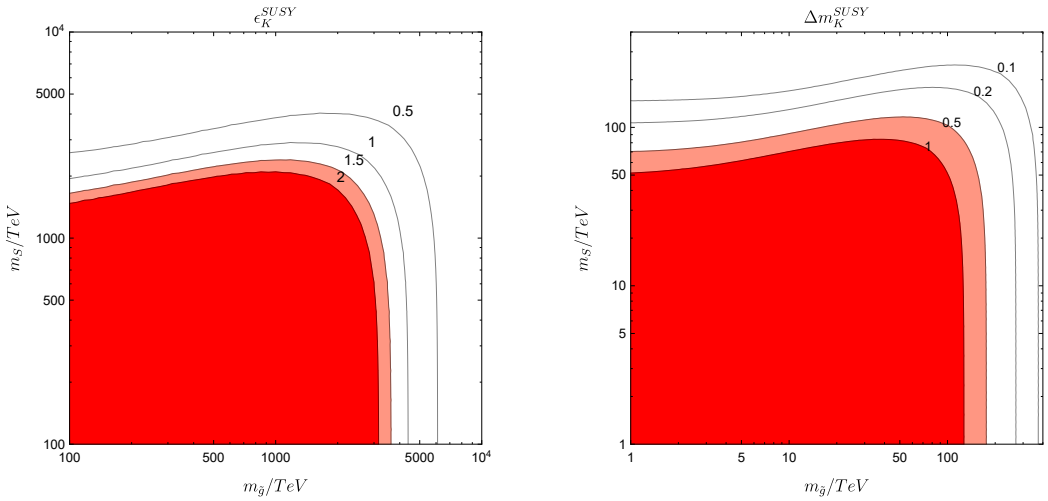

Figure 3.1: Constraints on the squark and gluino masses from Kaon oscillations. In the red regions, the SUSY contributions to ϵ_K (left) and Δm_K (right) exceed acceptable values. The solid black contours indicate the size of $\epsilon_K^{\rm SUSY}$ relative to the SM uncertainty of ϵ_K and the size of $\Delta m_K^{\rm SUSY}$ relative to the experimental central value of Δm_K, respectively.

The solid contours in the right plot of Figure 3.1 indicate the size of $\Delta m_K^{\rm SUSY}$ relative to the measured value [516]

$$\Delta m_K^{\rm exp} = (3.484 \pm 0.006) \times 10^{-15}\ \text{GeV}\ . \tag{3.76}$$

The SM prediction of Δm_K is subject to large hadronic uncertainties. Perturbative calculations of the short-distance piece find values close to the experimental value with $\sim 40\%$ uncertainty [196]. First lattice calculations that include both short-distance and long-distance parts have similar precision [236, 153, 503]. In such a situation, it is a meaningful approach to bound the size of the SUSY contributions to Δm_K by the experimental value itself. In the right plot of Figure 3.1, the dark (light) red region corresponds to a $\Delta m_K^{\rm SUSY}$ that saturates the experimental value (corresponds to 50% of the experimental value).

For definiteness we use the following values of the mass insertions in the plots

$$\text{Re}\big[(\delta^d_{12})^2_{LL}\big] = \text{Im}\big[(\delta^d_{12})^2_{LL}\big] = \text{Re}\big[(\delta^d_{12})^2_{RR}\big] =$$

$$= \mathrm{Im}\big[(\delta^d_{12})^2_{RR}\big] = -\mathrm{Re}\big[(\delta^d_{12})_{LL}(\delta^d_{12})_{RR}\big] = \\ = -\mathrm{Im}\big[(\delta^d_{12})_{LL}(\delta^d_{12})_{RR}\big] = \lambda^2 \ . \quad (3.77)$$

Order one changes in the mass insertions lead to order one changes in the excluded regions in the squark and gluino masses. Note that the new physics effect to Kaon mixing is dominated by the contribution from the Wilson coefficient $C_4 \propto (\delta^d_{12})_{LL}(\delta^d_{12})_{RR}$, because C_4 contains the largest numerical pre-factor, see (3.61), and comes with a chirally enhanced matrix element $\langle O_4 \rangle$, see (3.67). The explicit choice of signs in the above mass insertions corresponds to a positive SUSY contribution to the Kaon mixing matrix element $M^K_{12} = \langle K^0 | \mathcal{H}_{\text{eff}} | \bar{K}_0 \rangle$. Different sign choices do not qualitatively change the results shown in Figure 3.1.

We see that ϵ_K severely constrains the masses of the SUSY particles. Either squarks or gluinos have to be heavier than a few PeV in the considered SUSY flavor clockwork model. The constraint from Δm_K is significantly weaker, leading to lower bounds on the squark or gluino masses of around 100 TeV.

3.2.5 Discussion and Conclusions

In this paper, we constructed a supersymmetric version of a flavor model based on the clockwork mechanism. For each SM fermion, a gear system is introduced that leads to an exponential suppression of its Yukawa couplings with the exponent determined by the number of gear fermions. All massive gear fermions have a mass of the order of the clockwork scale Λ_{CW} and decouple from phenomenology. SUSY stabilizes the electroweak scale against quantum corrections proportional to Λ_{CW} (and the Planck scale).

The flavor clockwork leaves a characteristic imprint on the masses of the fermions' superpartners. Assuming gravity mediated SUSY breaking, we find that the flavor clockwork predicts sizable flavor changing entries in the squark mass matrices. In particular, mixing between the first and second generation of squarks is predicted to be of the order of the Cabibbo angle.

The large flavor mixing of squarks leads to large 1-loop contributions to Kaon oscillations. In the absence of accidental cancellations and assuming generic $\mathcal{O}(1)$

CP-violating phases, we find that squarks or gluinos have to have masses of at least a few PeV to avoid the stringent constraints from the Kaon mixing observable ϵ_K.

For PeV scale SUSY particles, the new physics effects in other neutral meson systems is strongly suppressed. First, B_s, B_d, and D^0 meson oscillations are generically less sensitive to new physics compared to Kaon oscillations. Second, in the considered SUSY model, the relevant mass insertions in (3.49) and (3.50) are suppressed by additional powers of the Cabibbo angle λ. Taking into account only the dominant contribution from the Wilson coefficient C_4, and neglecting $\mathcal{O}(1)$ ratios of hadronic matrix elements, we find the following approximate scaling relations for the B_s and B_d mixing matrix elements

$$\frac{(M_{12}^{B_s})_{\rm SUSY}}{(M_{12}^{B_s})_{\rm SM}} \sim \frac{(M_{12}^{B_d})_{\rm SUSY}}{(M_{12}^{B_d})_{\rm SM}} \sim \lambda^6 \frac{m_B^2}{m_K^2}\frac{m_s^2}{m_b^2}\frac{\epsilon_K^{\rm SUSY}}{\epsilon_K^{\rm SM}} \lesssim 5\times 10^{-7}\ , \tag{3.78}$$

far below any foreseeable sensitivities. Similarly in D^0 mixing we expect new physics effects that are several orders of magnitude below the current sensitivities.

The mass of the SM-like Higgs boson of $m_h \simeq 125.5\,\text{GeV}$ is easily achieved in a scenario with squarks at the PeV scale without the need of large stop mixing [326]. The preferred value for $\tan\beta$ is on the low side, $\tan\beta \sim \mathcal{O}(1)$ or $\mathcal{O}(\chi)$.

On the downside, very heavy squarks and gluinos correspond to a severe fine tuning of the electroweak scale of the order of $v^2/m_S^2 \sim 10^{-8}$. Interestingly, in the mini-split SUSY scenario with gaugino masses, a 1-loop factor below the scalar masses [139, 137] is compatible with the experimental constraints on the SUSY flavor clockwork. The gauginos might be collider accessible.

3.2.5.1 acknowledgments

The research of W.A. is supported by the U.S. Department of Energy grant number DE-SC0010107.

Appendix

3.2.6 Runnning of Gauge Couplings

The presence of the clockwork gear systems significantly alters the running of the gauge couplings above the clockwork scale. In fact, due to the large number of additional matter fields in the clockwork setup, asymptotic freedom is lost and the gauge couplings develop Landau poles above the clockwork scale. For example, the 1-loop renormalization group equation of the strong gauge coupling in the presence of the quark gear systems reads

$$\frac{d\alpha_s}{d\log\mu} = 2\left(\beta_0 + \sum_i \left(2N_q^i + N_u^i + N_d^i\right)\right)\frac{\alpha_s^2}{4\pi} \,, \tag{3.79}$$

with the well known $SU(3)_c$ 1-loop beta function coefficient of the MSSM $\beta_0 = -3$, and the sum runs over the three generations $i = 1, \ldots, 3$. Using the gear numbers from (3.38), we find a large and positive beta function coefficient

$$\beta_0 + \sum_i \left(2N_q^i + N_u^i + N_d^i\right) = 24 - 3n \,, \tag{3.80}$$

for $n \in \{0, 1, 2, 3\}$, determined by the magnitude of $\tan\beta$. The corresponding location of the Landau pole,

$$\Lambda_{\text{LP}} = \Lambda_{\text{CW}} \exp\left[\frac{2\pi}{(24-3n)\alpha_s(\Lambda_{\text{CW}})}\right] \,, \tag{3.81}$$

is approximately 3-4 orders of magnitude above the clockwork scale and depends weakly on the choice of n or the value $\tan\beta$. Requiring that the strong gauge coupling does not develop a Landau pole below the Planck scale, $\Lambda_{\text{LP}} < M_{\text{Pl}} \sim 10^{19}\,\text{GeV}$, places a lower bound on the clockwork scale of around $\Lambda_{\text{CW}} \gtrsim 10^{16}\,\text{GeV}$.

A qualitatively similar behavior is expected for the $SU(2)_L$ and $U(1)_Y$ gauge couplings. However, their running depends also on the details of the clockwork systems of the charged leptons and neutrinos. A quantitative discussion is therefore beyond the scope of this work.

3.3 Chapter Conclusion

This chapter has developed a supersymmetric implementation of the clockwork mechanism that simultaneously addresses the flavor puzzle and predicts specific patterns of flavor violation in the supersymmetric sector. This work contributes to the thesis by demonstrating how theoretical approaches to the flavor hierarchies can lead to testable predictions in low-energy flavor observables.

It's worth noting that while the kaon mixing constraints in our supersymmetric clockwork model push superpartner masses to the PeV scale, this introduces tension with the naturalness motivation for supersymmetry. With such high-scale SUSY breaking, the fine-tuning of the electroweak scale is significant, approximately v^2/m^2 10. However, this scenario remains viable in the context of 'split supersymmetry' frameworks, where the hierarchy problem is addressed differently. In these approaches, scalar superpartners can have masses far above the TeV scale, while gauginos might remain lighter due to additional symmetry protections. Alternative mechanisms like flavor-blind mediation schemes could potentially allow for lower superpartner masses while still satisfying flavor constraints, though these would modify the direct connection between the clockwork structure and flavor violation that is a key feature of our model. The tension between flavor constraints and naturalness underscores the importance of considering multiple theoretical approaches to supersymmetry breaking when addressing the flavor puzzle.

That kaon mixing constraints push the scale of superpartners to the PeV range highlights the power of precision flavor measurements to probe physics at scales far beyond the direct reach of current colliders. This reinforces a key theme of this dissertation: that rare processes and precision measurements can provide some of our most powerful windows into physics at extremely high energy scales.

Chapter 4

Probing New Physics with $\mu^+\mu^- \to bs$ at a Muon Collider

4.1 Introduction to the Chapter

High-energy muon colliders have emerged as promising candidates for the next generation of particle physics facilities, with the potential to probe energy scales far beyond those accessible at current colliders. Their clean experimental environment and high center-of-mass energies make them particularly suited for precision measurements and searches for new physics. In this chapter, I explore how a future high-energy muon collider could directly probe the same four-fermion contact interactions that might be responsible for the observed anomalies in rare B meson decays.

The process $\mu^+\mu^- \to bs$ offers a unique window into potential new physics affecting the $b \to s$ transition. Unlike rare B decays, which are limited by hadronic uncertainties and the indirect nature of the probes, this direct production process becomes increasingly sensitive to new physics as the center-of-mass energy increases. This complementary approach could provide crucial insights into the nature of the current B anomalies and potentially discover new physics even if it lies at scales of tens or hundreds of TeV.

This study bridges two important aspects of the flavor physics program: the

investigation of rare B decay anomalies at dedicated flavor facilities and the direct probing of flavor-changing interactions at high-energy colliders. By demonstrating how the same operators potentially responsible for B decay anomalies can be directly accessed at a muon collider, this work highlights the complementarity between intensity and energy frontier approaches to flavor physics. This synergy exemplifies how a comprehensive flavor program requires multiple experimental approaches to fully understand the nature of potential new physics in the flavor sector.

In the following publication, I present a comprehensive analysis of the new physics sensitivity of bottom-strange production at a high-energy muon collider. I consider the full set of four-fermion contact interactions that can contribute to this process at dimension 6 and discuss how measurements of both the total cross-section and the forward-backward asymmetry of the b-jet can provide detailed information about the underlying chirality structure of any new physics that might be present.

The results demonstrate that a muon collider operating at a center-of-mass energy of 10 TeV could probe new physics scales approaching 100 TeV through this channel. This highlights the extraordinary potential of future lepton colliders as precision tools for exploring physics beyond the Standard Model, complementing the traditional approach of direct searches at hadron colliders.

4.2 Original Publication

Wolfgang Altmannshofer[a], Sri Aditya Gadam[a], Stefano Profumo[a]

[a]*Department of Physics & Santa Cruz Institute for Particle Physics, University of California, Santa Cruz, CA 95064, USA*

waltmann@ucsc.edu sgadam@ucsc.edu profumo@ucsc.edu

Abstract. We show that bottom-strange production at a high-energy muon collider, $\mu^+\mu^- \to bs$, is a sensitive probe of new physics. We consider the full set of four-fermion contact interactions that contribute to this process at dimension 6, and discuss the complementarity of a muon collider and of the study of rare B meson decays that also probe said new physics. If a signal were to be found at a muon collider, the forward-backward asymmetry of the b-jet provides diagnostics about the underlying chirality structure of the new physics couplings. In the absence of a signal at a center of mass energy of 10 TeV, $\mu^+\mu^- \to bs$ can indirectly probe new physics at scales close to 100 TeV. We also discuss the impact that beam polarization has on the muon collider sensitivity performance.

4.2.1 Introduction

Rare decays of bottom quark (b) hadrons are widely acknowledged as important probes of Beyond the Standard Model (BSM) physics [177, 92]. Several experimental results on rare b decays show poor agreement with the corresponding Standard Model (SM) predictions. The LHCb collaboration reports deviations in the angular distribution of the $B \to K^*\mu^+\mu^-$ decay (the "P_5' anomaly") and in the branching ratios of the $B_s \to \phi\mu^+\mu^-$, $B \to K^*\mu^+\mu^-$, and $B \to K\mu^+\mu^-$ decays. Until recently, these hints for new physics were supported by LHCb results on R_K and R_{K^*} that showed evidence for lepton flavor universality violation in rare B meson decays. Global fits of rare b decay data had found a remarkably consistent explanation of these "B anomalies" in terms of new physics [315, 116, 77, 380, 239, 341].

However, the latest update from LHCb on R_K and R_{K^*} is in excellent agreement with the SM predictions [40, 38], implying that the origin of the remaining $b \to s\mu\mu$ anomalies, be it SM or BSM physics, is to a good approximation universal for muons and electrons. If the anomalies are due to new physics, global fits point to the lepton flavor universal 4-fermion contact interaction $(\bar{s}\gamma_\alpha P_L b)(\bar{\ell}\gamma^\alpha \ell)$. As is well known, new physics in this contact interaction can, in principle, be mimicked by non-perturbative QCD effects. While recent calculations indicate that hadronic effects are under control [343, 341], a SM origin of the anomalies cannot be excluded. In this context, it is highly motivated to consider additional probes of this type of 4-fermion contact interaction.

The B anomalies hint at a new physics scale $\Lambda_{\rm NP} \sim 35$ TeV for $\mathcal{O}(1)$ couplings. It is thus conceivable that if new physics is responsible for the rare B decay anomalies, it is beyond the direct reach of current colliders. The description in terms of contact interactions might remain valid up to energies of 10's of TeV. Even in that case, there are model-independent signatures that can be predicted at colliders.

For example, at proton-proton colliders, one can access the parton level $bs \to \mu^+\mu^-$ process and expect enhanced di-muon production at large di-muon invariant mass [332]. However, the expected sensitivity at the high-luminosity LHC will be insufficient to test a heavy new physics origin of the rare B anomalies in a model-independent fashion.

In a preliminary study, published as a Snowmass whitepaper [103], we showed that non-standard $\mu^+\mu^- \to bs$ production could be observed with high significance at a 10 TeV muon collider if the B anomalies are due to heavy new physics. Furthermore, the forward-backward asymmetry of the b-jet provides diagnostics of the chirality structure of the new physics couplings. The high sensitivity of the muon collider stems from the fact that the non-standard $\mu^+\mu^- \to bs$ cross section increases with the center of mass energy, while the relevant background cross sections (mainly misidentified di-jets) decrease. For recent related studies see e.g. [377, 376, 140, 460, 147, 494].

In this paper, we extend the analysis of [103] and provide a detailed discussion

of the prospects to probe new physics using $\mu^+\mu^- \to bs$ at a muon collider. In section 4.2.2, we introduce the theoretical framework and outline the operators we include in our analysis. In contrast to [103], we include the full set of 4-fermion contact interactions that can contribute to $\mu^+\mu^- \to bs$ at leading order. In section 4.2.3, we review the status of the global rare b decay fit after the recent LHCb update of R_K and R_{K^*}. We identify two relevant scenarios: (i) new physics is lepton flavor universal and it addresses the remaining $b \to s\mu\mu$ anomalies; (ii) new physics is muon-specific, and thus strongly constrained. In both cases, we also discuss the expected sensitivity of rare b decays after the high-luminosity phase of the LHC. In section 4.2.4, we discuss the differential $\mu^+\mu^- \to bs$ cross-section, taking into account the full set of 4-fermion contact interactions and including the effect of muon beam polarization. In section 4.2.5, we discuss all relevant sources of backgrounds, including the irreducible SM background as well as di-jet production where one of the jets is mis-tagged. Finally, in section 4.2.6, we provide the sensitivity projections for a future muon collider. Assuming the presence of new physics, we discuss how precisely a muon collider could identify a lepton-universal new physics effect. In the absence of new physics, we estimate the constraining power of a muon collider. We also compare the muon collider sensitivity to the sensitivity from rare b decays. We conclude in section 5.2.6. In appendices 4.2.8 and 4.2.9, we give details about the renormalization group running of the Wilson coefficients and our global rare b decay fit.

4.2.2 Theoretical Framework

We employ the standard effective Hamiltonian framework that parametrizes the BSM contributions to the $b \to s\ell\ell$ decays at the scale of the B mesons, considering all relevant dimension 6 operators along with their Wilson coefficients:

$$\begin{aligned}\mathcal{H}_{\text{eff}} = \mathcal{H}_{\text{eff}}^{\text{SM}} - \frac{4G_F}{\sqrt{2}} V_{tb}V_{ts}^* \frac{e^2}{16\pi^2} \\ \times \Big(\Delta C_9^\ell O_9^\ell + \Delta C_{10}^\ell O_{10}^\ell + C_9'^\ell O_9'^\ell + C_{10}'^\ell O_{10}'^\ell \\ + C_S^\ell O_S^\ell + C_P^\ell O_P^\ell + C_S'^\ell O_S'^\ell + C_P'^\ell O_P'^\ell \Big) \,, \end{aligned} \tag{4.1}$$

where ℓ runs over the three lepton flavors e, μ, τ. This effective Hamiltonian retains the standard normalization factors, including the CKM factors that are typical of the SM contributions to this process. The operators can be expressed as 4-fermion contact structures and are

$$O_9^\ell = (\overline{s}\gamma^\alpha P_L b)(\overline{\ell}\gamma_\alpha \ell) \ , \tag{4.2}$$

$$O_{10}^\ell = (\overline{s}\gamma^\alpha P_L b)(\overline{\ell}\gamma_\alpha \gamma_5 \ell) \ , \tag{4.3}$$

$$O_S^\ell = (\overline{s}P_R b)(\overline{\ell}\ell) \ , \tag{4.4}$$

$$O_P^\ell = (\overline{s}P_R b)(\overline{\ell}\gamma_5 \ell) \ . \tag{4.5}$$

The remaining operators, O', can be obtained from the operators O with the interchange $\{L \leftrightarrow R\}$.

The SM Hamiltonian, $\mathcal{H}_{\rm eff}^{\rm SM}$, contains the operators O_9^ℓ and O_{10}^ℓ with lepton flavor universal Wilson coefficients $C_9^{\rm SM} \simeq 4.2$ and $C_{10}^{\rm SM} \simeq -4.1$. The corresponding new physics Wilson coefficients can in principle be lepton flavor specific and we denote them as ΔC_9^ℓ and ΔC_{10}^ℓ. All the other operators are negligible in the SM.

We assume that the new physics that sources the effective Hamiltonian in (4.1) is sufficiently heavy compared to the center of mass energy of a muon collider, such that the effective framework remains applicable. We consider this a conservative assumption: If the new physics is lighter, it can be produced on-shell at the muon collider and it would be generically easier to detect [377, 376, 140, 460, 147].

At the high center of mass energy of a muon collider, the $SU(2)_L \times U(1)_Y$ gauge symmetry of the SM needs to be taken into account. This can be done by using the Standard Model Effective Field Theory (SMEFT) [337] to parameterize new physics at energies above the electroweak scale. As there are no $bs\ell\ell$ 4-fermion operators with tensor structures in SMEFT, we omitted them in the effective Hamiltonian (4.1) to be consistent. Moreover, the scalar and pseudoscalar operators are related in SMEFT such that [87]

$$C_S^\ell = -C_P^\ell \ , \qquad C_S'^\ell = C_P'^\ell \ . \tag{4.6}$$

We will impose these relations throughout. One can expect generic corrections to these relations of order $v^2/\Lambda_{\rm NP}^2$, where $v \simeq 246\,\text{GeV}$ is the vacuum expectation

value of the Higgs and $\Lambda_{\rm NP}$ the new physics scale. As we will see, for $\mathcal{O}(1)$ new physics couplings, this ratio is of $\mathcal{O}(10^{-5})$, and in that case, the corrections are completely negligible.

The remaining operators in the effective Hamiltonian (4.1) are unconstrained in SMEFT and the corresponding Wilson coefficients can be treated as independent parameters. Instead of using SMEFT notation, we prefer to adopt the low-energy notation of (4.1) to facilitate the comparison between the muon collider and rare B decays.

For a precise sensitivity comparison, one should take into account the renormalization group running between the center of mass energy of a muon collider, $\mu \sim \sqrt{s}$, and the relevant energy scale for B meson decays, typically chosen to be the b mass, $\mu \sim m_b$. While these scales differ by more than 3 orders of magnitude, the impact of running is modest and usually does not exceed 10%. Details are given in appendix 4.2.8.

4.2.3 Status and Prospects of Rare B Decay Fits

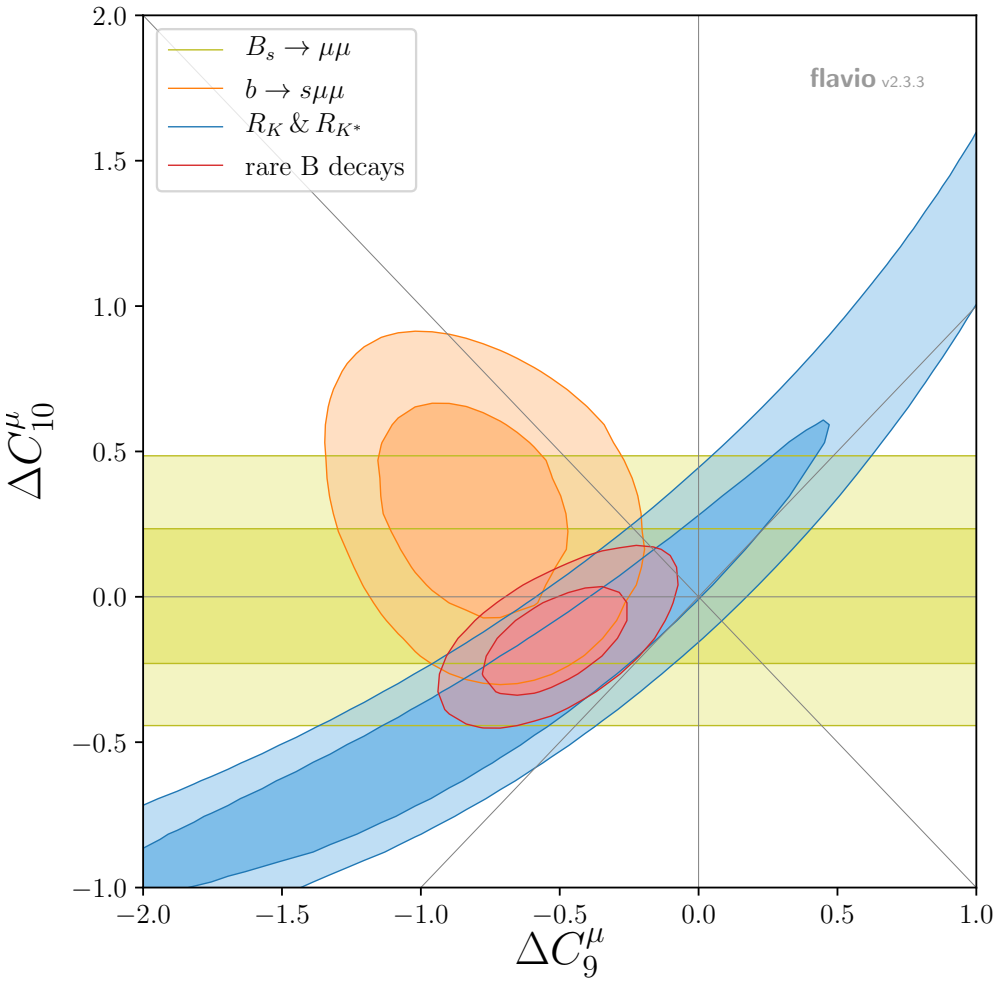

Figure 4.1: The global rare B decay fit in the plane of muon specific new physics contributions to C_9 and C_{10}, after the recent updates of $B_s \to \mu^+\mu^-$ [3] and R_K, R_{K^*} [40, 38]. The fit includes the $B_s \to \mu^+\mu^-$ branching ratio (yellow), R_K, R_{K^*} and other LFU tests (blue), and $B \to K\mu^+\mu^-$, $B \to K^*\mu^+\mu^-$, $B_s \to \phi\mu^+\mu^-$, $\Lambda_b \to \Lambda\mu^+\mu^-$ branching ratios and angular observables (orange). The result of the global fit is shown in red.

At a muon collider, we are interested in 4-fermion operators with $\ell = \mu$, while B meson decays can, in principle, be used to probe all lepton flavors $\ell = e, \mu, \tau$. Until recently, rare B decays have provided intriguing hints for new physics contributions to the muon-specific Wilson coefficients ΔC_9^{μ} and ΔC_{10}^{μ}

(see e.g. [315, 116, 77, 380, 239]). Those hints were based on a number of experimental results, in particular the anomalously low rates of the $B \to K\mu\mu$, $B \to K^*\mu\mu$, and $B_s \to \phi\mu\mu$ decays [18, 23, 34], the anomalous angular distribution of $B \to K^*\mu\mu$ [29, 32] and the hints for lepton universality violation [25, 35]. However, the most recent results by LHCb on the lepton flavor universality ratios R_K and R_{K^*} [40, 38] are in excellent agreement with the SM predictions and strongly constrain new physics in muon-specific Wilson coefficients.

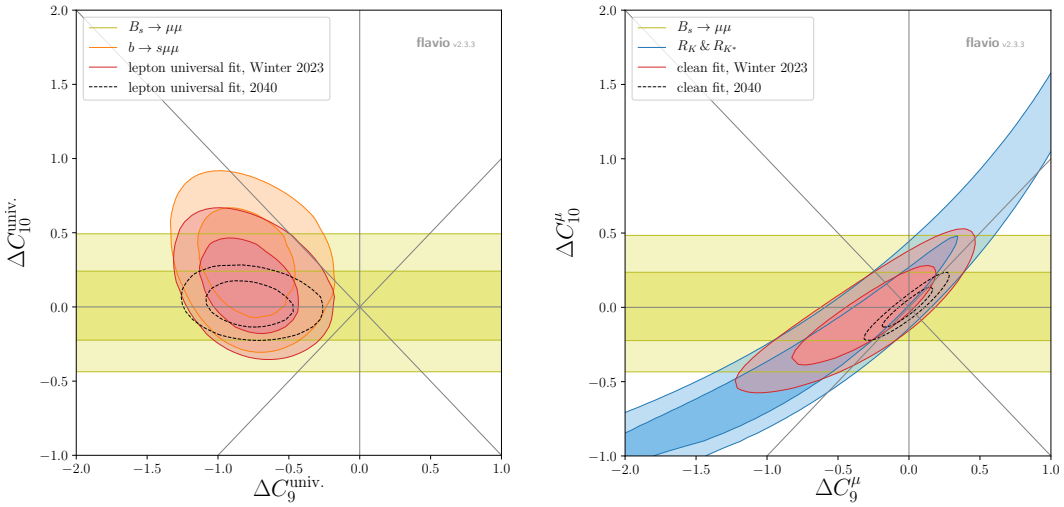

Figure 4.2: Top: Rare B decay fit in the plane of lepton universal new physics contributions to C_9 and C_{10}. Bottom: Rare B decay fit in the plane of muon-specific new physics contributions to C_9 and C_{10}, including only theoretically clean observables.

The situation is summarized in figure 4.1 which shows the various constraints on the muon specific ΔC_9^μ and ΔC_{10}^μ (see also [240, 333, 80, 76, 509, 81] for related studies). Details on how this figure was obtained are given in appendix 4.2.9. As in [116], the observables are grouped into three categories: lepton flavor universality tests (blue), the $B_s \to \mu^+\mu^-$ branching ratio (yellow), and the semileptonic $b \to s\mu\mu$ branching ratios and angular observables (orange). The combination is shown in red. Compared to the situation two years ago [116], there is a tension among the different categories. Both the $B_s \to \mu^+\mu^-$ branching ratio and the lepton flavor universality tests R_K and R_{K^*} are compatible with the SM predictions ($\Delta C_9^\mu = \Delta C_{10}^\mu = 0$), while the $b \to s\mu\mu$ observables do show a preference for a

non-standard ΔC_9^μ.

The tension in the fit can be resolved in two ways: (i) assuming that the new physics effect is lepton flavor universal; (ii) assuming that the SM predictions for the $b \to s\mu\mu$ observables are affected by unexpectedly large hadronic effects, rendering the corresponding region unreliable.

In case (i), the constraints from the LFU tests, R_K and R_{K^*} in particular, do not apply, and one is left with the overlap of the $B_s \to \mu^+\mu^-$ region and the $b \to s\mu^+\mu^-$ region. This situation is shown in the upper plot of figure 4.2. Approximating the likelihood in the vicinity of the best-fit point by a multivariate Gaussian, we find

$$\Delta C_9^{\text{univ.}} = -0.81 \pm 0.22 \ , \quad \Delta C_{10}^{\text{univ.}} = +0.12 \pm 0.20 \ , \tag{4.7}$$

with an error correlation of $\rho = -30\%$. This corresponds to a $\sim 2.8\sigma$ preference for new physics, mainly in $\Delta C_9^{\text{univ.}}$. Such a lepton-universal shift in C_9 can, in principle, be mimicked by a hadronic effect in the rare B decays. Therefore it is highly motivated to test this possibility at a muon collider.

In case (ii), one focuses on the theoretically clean lepton flavor universality tests and the $B_s \to \mu^+\mu^-$ branching ratio. As shown in the lower plot of figure 4.2, this results in a best-fit region that is fully compatible with the SM expectation. A multivariate Gaussian approximation gives

$$\Delta C_9^{\mu} = -0.28 \pm 0.33 \ , \quad \Delta C_{10}^{\mu} = -0.07 \pm 0.22 \ , \tag{4.8}$$

with a larger positive error correlation of $\rho = +86\%$. The best fit agrees with the SM at 0.8σ.

For comparison with the sensitivity of a muon collider, we also consider the sensitivity projections of rare B decays after the high-luminosity phase of the LHC. The uncertainties of the current measurements of the $B_s \to \mu^+\mu^-$ branching ratio are still statistically dominated, and one can expect significant improvements from ATLAS, CMS, and LHCb [7, 36, 3]. We assume that the measured $B_s \to \mu^+\mu^-$ branching ratio will coincide with the SM prediction and use an experimental uncertainty of $\pm 0.10 \times 10^{-9}$, a factor 3 reduction in uncertainty compared to the

current world average [125], commensurate with an order of magnitude increase in statistics. Concerning the CKM input for the corresponding theory prediction, one can expect that the CKM matrix element $|V_{cb}|$ will be known with percent level precision from Belle II [68]. For our projection, we conservatively assume that the uncertainty on $|V_{cb}|$ will be half the one quoted currently by the PDG [513] $|V_{cb}| = (40.8 \pm 1.4) \times 10^{-3} \to |V_{cb}| = (40.8 \pm 0.7) \times 10^{-3}$.

Future LHCb measurements of R_K and R_{K^*} are expected to reach uncertainties at the percent level [172]. We assume that the measured future central values of R_K and R_{K^*} will coincide with the SM prediction of 1.0 with uncertainties that are a factor of 5 better than those quoted in the most recent analysis [40, 38]. This corresponds approximately to the expected uncertainties quoted in [27].

The constraining power of the $b \to s\mu\mu$ branching ratios and angular observables is already limited by theory uncertainties. To be conservative, we assume no significant improvement in those observables.

The corresponding projected 1σ and 2σ contours are shown in the plots of figure 4.2 by the black dashed contours. Gaussian approximations give in case (i)

$$\Delta C_9^{\text{univ.}} = -0.81 \pm 0.20 \ , \quad \Delta C_{10}^{\text{univ.}} = 0.02 \pm 0.10 \ , \tag{4.9}$$

with an error correlation of $\rho = -18\%$. In case (ii), we find

$$\Delta C_9^{\mu} = 0.00 \pm 0.12 \ , \quad \Delta C_{10}^{\mu} = 0.00 \pm 0.09 \ , \tag{4.10}$$

with a large positive error correlation of $\rho = +92\%$.

In section 4.2.6 below, we consider two scenarios:

On the one hand, we will use the best-fit point from (4.7) as a new physics benchmark for lepton universal Wilson coefficients. We will discuss how well a high-energy muon collider can probe such a scenario and compare it to the precision of a future B decay fit (4.9). We note that in contrast to the $b \to s\mu\mu$ observables, bottom-strange production at a muon collider is not significantly affected by long-distance hadronic uncertainties;

On the other hand, we will assume the absence of new physics and compare the muon collider sensitivity to muon-specific Wilson coefficients to the current and expected sensitivity from rare B decays (4.8) and (4.10).

4.2.4 Bottom-Strange Production at a Muon Collider

In addition to a Higgs pole run at a center of mass energy of $\sqrt{s} = 125\,\text{GeV}$, a future muon collider is proposed to run at several high energies, including $\sqrt{s} = 3\,\text{TeV}$, $\sqrt{s} = 10\,\text{TeV}$, and even $\sqrt{s} = 30\,\text{TeV}$ [73, 175, 64]. Under the assumption that the scale of new physics is sufficiently larger than the center of mass energy, the cross-section for bottom-strange production at a muon collider, $\mu^+\mu^- \to b\bar{s}$ or $\bar{b}s$, can be computed model independently in the effective formalism provided by the Hamiltonian (4.1). To compute the cross-section, we used `FeynCalc` [439, 478, 479] and took into account generic polarization fractions of the muon beams.

We find that the differential cross-sections can be expressed as

$$\frac{d\sigma(\mu^+\mu^- \to b\bar{s})}{dz} = \frac{3}{16}\sigma(\mu^+\mu^- \to bs) \times \left(\frac{4}{3}F_S + (1-F_S)\big(1+z^2\big) + \frac{8}{3}zA_{\text{FB}}\right) , \quad (4.11)$$

$$\frac{d\sigma(\mu^+\mu^- \to \bar{b}s)}{dz} = \frac{3}{16}\sigma(\mu^+\mu^- \to bs) \times \left(\frac{4}{3}F_S + (1-F_S)\big(1+z^2\big) - \frac{8}{3}zA_{\text{FB}}\right) , \quad (4.12)$$

where $z = \cos\theta$ with θ the angle between the μ^- beam and the b or $\bar{b}$, respectively. In the equations above, we have expressed the differential cross-sections in terms of the total cross-section

$$\sigma(\mu^+\mu^- \to bs) = 2\sigma(\mu^+\mu^- \to b\bar{s}) = 2\sigma(\mu^+\mu^- \to \bar{b}s) = \frac{G_F^2\alpha^2}{8\pi^3}|V_{tb}V_{ts}^*|^2 s\left(\frac{3}{4}a_0 + a_2\right) , \quad (4.13)$$

as well as the forward-backward asymmetry of the bottom quark, A_{FB}, and the fraction of the cross-section that originates from scalar or pseudoscalar operators, F_S,

$$A_{\text{FB}} = \frac{3a_1}{3a_0 + 4a_2} , \quad F_S = \frac{3a_0}{3a_0 + 4a_2} . \quad (4.14)$$

The coefficients a_0, a_1, and a_2 are given by the following combinations of Wilson coefficients

$$a_0 = (1 + P_+P_-)\Big(|C_S|^2 + |C_P|^2 + |C'_S|^2 + |C'_P|^2\Big) + 2(P_- + P_+)\Big(\mathfrak{Re}(C_S C_P^*) + \mathfrak{Re}(C'_S C'^*_P)\Big) \ , \quad (4.15)$$

$$a_1 = (P_+ - P_-)\Big(|\Delta C_9|^2 + |\Delta C_{10}|^2 - |C'_9|^2 - |C'_{10}|^2\Big) - 2(1 - P_+P_-)\Big(\mathfrak{Re}(\Delta C_9 \Delta C_{10}^*) - \mathfrak{Re}(C'_9 C'^*_{10})\Big) \ , \quad (4.16)$$

$$a_2 = (1 - P_+P_-)\Big(|\Delta C_9|^2 + |\Delta C_{10}|^2 + |C'_9|^2 + |C'_{10}|^2\Big) + 2(P_- - P_+)\Big(\mathfrak{Re}(\Delta C_9 \Delta C_{10}^*) + \mathfrak{Re}(C'_9 C'^*_{10})\Big) \ . \quad (4.17)$$

where for better readability, we dropped the lepton superscript "μ" on the Wilson coefficients, c.f. eq. (4.1). The beam polarizations $P_\pm \in [-1, 1]$ specify the fraction of polarized μ^+ and μ^-, respectively, with $P_\pm = +1(-1)$ indicating purely right-handed (left-handed) beams. The unpolarized limit is restored by setting $P_\pm = 0$.

In the absence of beam polarization, the total cross-section simplifies to

$$\sigma(\mu^+\mu^- \to bs) = = \frac{G_F^2 \alpha^2}{8\pi^3} |V_{tb} V_{ts}^*|^2 s \Big[|\Delta C_9|^2 + |\Delta C_{10}|^2 + |C'_9|^2 + |C'_{10}|^2 + \frac{3}{4}\Big(|C_S|^2 + |C_P|^2 + |C'_S|^2 + |C'_P|^2\Big)\Big] \ . \quad (4.18)$$

As expected from dimensional analysis, the signal cross section grows linearly with the center of mass energy squared, s. Standard Model background processes (see the discussion in section 4.2.5), are expected to fall with the center of mass energy. At sufficiently high center of mass energies, a muon collider will thus be able to detect a new physics signal in the benchmark scenario (4.7). If a new physics signal is established, measurements of the forward-backward asymmetry, $A_{\rm FB}$ provide further information about the relative size of $C_9^{(\prime)}$ and $C_{10}^{(\prime)}$ Wilson coefficients. Note that the forward-backward asymmetry enters the differential $\mu^+\mu^- \to b\bar{s}$ and $\mu^+\mu^- \to b\bar{s}$ cross sections with opposite sign, c.f. equations (4.11) and (4.12). A measurement of $A_{\rm FB}$ thus requires charge tagging of the b jet.

Both the cross-section and the forward-backward asymmetry are affected by the degree of muon beam polarization. The muons are produced from pion decay, and the outgoing muon is fully polarized in the center-of-mass frame of a decaying pion. In the lab frame, on the other hand, the polarization depends on the decay angle and pion energy and is typically around 20% [128]. Higher polarization can be achieved if muons from forward pion decays are selected. This comes at the expense of luminosity. For example, a polarization of $\sim 50\%$ might be achieved for a decrease in luminosity by a factor of ~ 4 [128].

As can be seen from the equations for the cross-section and the forward-backward asymmetry above, the beam polarization does have an impact. In the numerical analysis discussed below, we will consider as representative cases unpolarized muon beams, as well as muon beams with +50% polarization.

4.2.5 Background Processes

Various background processes contribute to a $\mu^+\mu^- \to bs$ signal at a muon collider. On the one hand, there is an irreducible SM background that is suppressed by the Glashow–Iliopoulos–Maiani (GIM) mechanism. On the other hand, there are reducible backgrounds from di-jet production $\mu^+\mu^- \to jj$ where one of the jets is incorrectly flavor tagged, as well as backgrounds from processes with missing energy, $\mu^+\mu^- \to bs + \not{E}$. We detail the various types of backgrounds in the following. Example Feynman diagrams are shown in figures 4.3, 4.4, and 4.5.

4.2.5.1 SM loop contribution

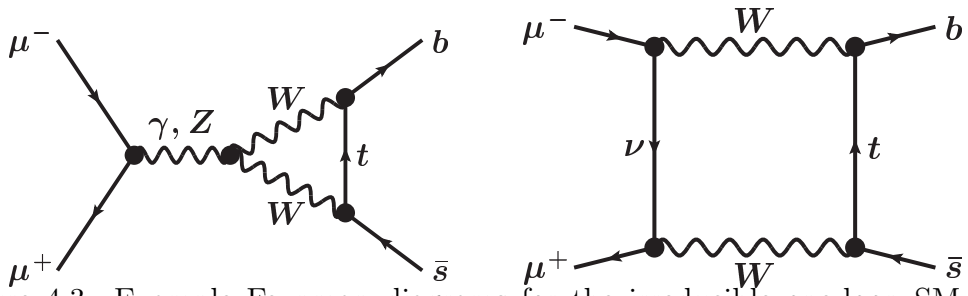

Figure 4.3: Example Feynman diagrams for the irreducible one-loop SM background $\mu^+\mu^- \to bs$.

The irreducible SM contribution to the $\mu^+\mu^- \to bs$ cross-section arises at the one-loop level and is, as mentioned above, GIM suppressed. Example diagrams are shown in figure 4.3. At a high-energy muon collider, this SM loop contribution cannot be described by a contact interaction but requires a calculation with dynamical top quarks, W bosons, and Z bosons. We have calculated this cross section for an arbitrary center of mass energy $\sqrt{s}$ using `FeynArts` [347] and `FormCalc` [346]. For a large $\sqrt{s} \gg m_t, m_W, m_Z$, we find that the cross-section falls with $1/s$, or more precisely

$$\sigma_{\text{bg}}^{\text{loop}} \propto \frac{G_F^2 m_t^4 \alpha^2}{128\pi^3} |V_{tb} V_{ts}^*|^2 \frac{1}{s} \,. \tag{4.19}$$

This turns out to be completely negligible at a multi-TeV muon collider.

4.2.5.2 Mistagged di-jet events

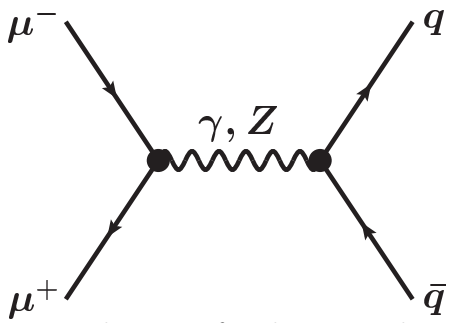

Figure 4.4: Feynman diagram for di-jet production, $\mu^+\mu^- \to q\bar{q}$.

A much more important source of background stems from mistagged di-jet events from the diagram shown in figure 4.4. We consider the production of b jets, $\mu^+\mu^- \to b\bar{b}$, in which one b-jet is misidentified as a light jet, as well as $\mu^+\mu^- \to c\bar{c}$ and $\mu^+\mu^- \to q\bar{q}$ events with light quarks $q = u, d, s$, where one of the charm or light quark jets is identified as a b-jet. We analytically calculated the corresponding di-jet cross sections at tree level. We assume that top tagging at a muon collider is sufficiently accurate such that $\mu^+\mu^- \to t\bar{t}$ events do not give a relevant background. The corresponding background cross section from di-jets

that we consider is therefore

$$\sigma_{\text{bg}}^{\text{jj}} = \sum_{q=u,d,s,c,b} 2\epsilon_q(1-\epsilon_q)\ \sigma(\mu^+\mu^- \to q\bar{q})\ , \tag{4.20}$$

where ϵ_b is the b-tag efficiency and $\epsilon_{u,d,s,c}$ the probabilities that a charm or light quark jet is misidentified as a b-jet. For the numerical analysis we follow [376] and adopt the values: $\epsilon_b = 70\%$, $\epsilon_c = 10\%$, and $\epsilon_u = \epsilon_d = \epsilon_s = 1\%$. These values are comparable to those that are currently achieved by the ATLAS and CMS experiments at the LHC for jets with transverse momentum up to a few hundred GeV [482, 2]. The performance of traditional flavor taggers decreases significantly for a jet p_T in the multi-TeV regime. However, novel tagging techniques [456] should improve the performance for multi-TeV jets to the level quoted above.

4.2.5.3 Di-jet events from vector boson fusion

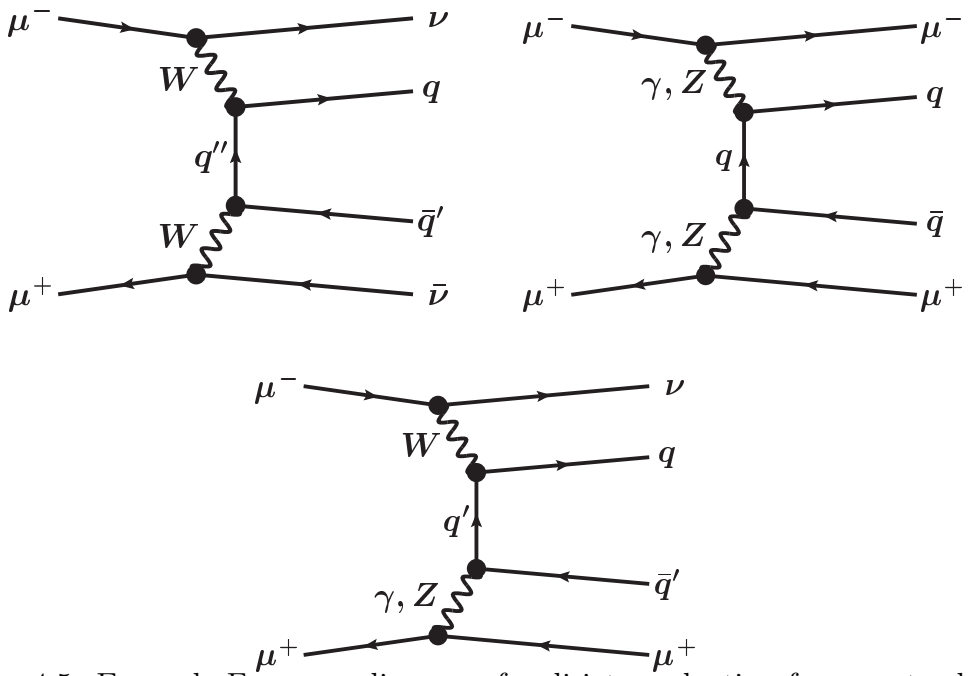

Figure 4.5: Example Feynman diagrams for di-jet production from vector boson fusion $\mu^+\mu^- \to q\bar{q}'\nu\bar{\nu}$, $\mu^+\mu^- \to q\bar{q}\mu^+\mu^-$, and $\mu^+\mu^- \to q\bar{q}'\mu\nu$.

Finally, additional backgrounds come from di-jet production through vector boson fusion in association with forward muons or neutrinos that remain undetected. The relevant processes are $\mu^+\mu^- \to b\bar{b}\nu\bar{\nu}$, $\mu^+\mu^- \to c\bar{c}\nu\bar{\nu}$, or $\mu^+\mu^- \to$

$q\bar{q}\nu\bar{\nu}$ with mistagged quarks, $\mu^+\mu^- \to b\bar{s}\nu\bar{\nu}$, as well as $\mu^+\mu^- \to q\bar{q}'\mu^+\mu^-$ and $\mu^+\mu^- \to q\bar{q}'\mu\nu$ with appropriate quark flavors. Example diagrams can be found in figure 4.5. These processes are potentially relevant as the vector boson fusion cross section grows with the center of mass energy [251]. This form of background can be largely removed by cuts on the di-jet invariant mass. For $\mu^+\mu^- \to bs$ signal events, one expects $m_{jj} \simeq \sqrt{s}$, while for vector boson fusion events, one expects a significantly reduced di-jet invariant mass, $m_{jj} < \sqrt{s}$, due to the forward muons or neutrinos carrying away energy. A di-jet invariant mass resolution of $\sim 2\%$ for 5 TeV di-jets has been achieved at ATLAS [4]. We assume that detectors at a future muon collider will perform at least as well. We determine the cross sections of the vector boson fusion background, $\sigma_{\text{bg}}^{\text{VBF}}$, using `MadGraph5` [120] to simulate the 4 body final states $\mu^+\mu^- \to q\bar{q}'\nu\bar{\nu}$, $\mu^+\mu^- \to q\bar{q}'\mu\nu$, and $\mu^+\mu^- \to q\bar{q}'\mu^+\mu^-$ with all relevant quark flavors. We employ a cut on the di-jet invariant mass of $m_{jj}/\sqrt{s} = 1 \pm 0.04$. Such a cut retains $\simeq 95\%$ of the signal but reduces this background by $5-6$ orders of magnitude, to a subdominant level.

A more precise calculation of this background could be done by making use of lepton PDFs [351, 352, 469, 312]. This is left for future work.

4.2.5.4 Comparison of signal and background

In figure 4.6, we show as a function of the center of mass energy $\sqrt{s}$ the cross sections of the new physics $\mu^+\mu^- \to bs$ signal, σ_{NP} (red), and the background processes mentioned above, namely the irreducible SM one-loop contribution, $\sigma_{\text{bg}}^{\text{loop}}$ (blue), mistagged di-jets, σ_{bg}^{jj} (green), and di-jets from vector boson fusion, $\sigma_{\text{bg}}^{\text{VBF}}$ (orange). The shown VBF cross-section only includes the $\mu^+\mu^- \to q\bar{q}'\nu\bar{\nu}$ processes. The $\mu^+\mu^- \to q\bar{q}'\mu\nu$ and $\mu^+\mu^- \to q\bar{q}'\mu^+\mu^-$ cross sections are somewhat larger, but might be reduced by vetoing muons in the event. The muons from VBF production are very forward and are therefore typically outside the coverage of the detector (the detector described in [64] has a rapidity coverage out to $\eta_{\text{max}} = 2.44$). An efficient muon veto may be possible with a dedicated forward muon detector [468]. As the dominant background is from di-jet events, we consider it justified to neglect the VBF production with muons to simplify our

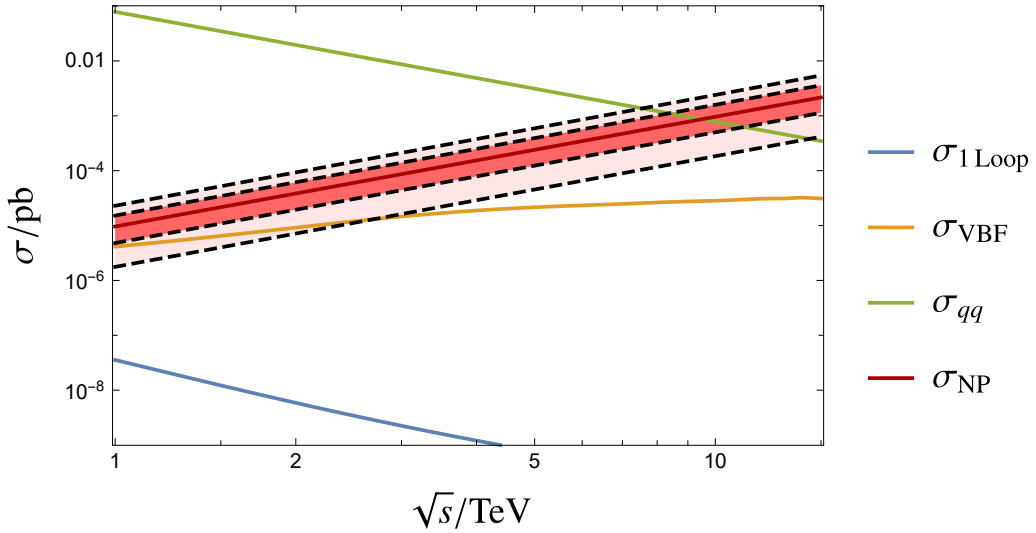

Figure 4.6: The cross sections of the $\mu^+\mu^- \to bs$ signal and background processes at a muon collider with a center of mass energy $\sqrt{s}$. The shown cross sections take into account flavor tagging efficiencies and mistag rates as discussed in the text. The signal cross section corresponds to the benchmark point (4.7) with 1σ and 2σ uncertainties. The muon beams are assumed to be unpolarized.

analysis.

For the signal cross-section, we assume a new physics benchmark as in (4.7), with the red shaded regions indicating the 1σ and 2σ uncertainties. All shown cross-sections take into account the flavor tagging efficiencies and mistag rates. The muon beams are assumed to be unpolarized. Qualitatively similar results are obtained for polarized muon beams.

At a low center of mass energy, the mistagged di-jet background dominates the signal by orders of magnitude. Among the di-jet backgrounds, the $b\bar{b}$ final state contributes the most, followed by $c\bar{c}$ and light quarks. The SM loop background and the background from vector boson fusion (with m_{jj} cut) are subdominant and we will neglect them in the following. As anticipated, the signal cross-section increases with s, while the most important background cross-section falls approximately like $1/s$. Signal and background become comparable for a center of mass energy of around 10 TeV. This suggests that a 10 TeV muon collider should be able to observe a non-standard $\mu^+\mu^- \to bs$ production with high significance.

4.2.6 Sensitivity Projections

Based on the discussion in the previous section, we investigate the sensitivity of a multi-TeV muon collider to the contact interactions in (4.1). Proposed runs of a muon collider include a center of mass energy of $\sqrt{s} = 6$ TeV with an integrated luminosity of $\mathcal{L} = 4\,\text{ab}^{-1}$ and $\sqrt{s} = 10\,\text{TeV}$ with $\mathcal{L} = 10\,\text{ab}^{-1}$ [175].

4.2.6.1 Lepton flavor universal new physics benchmark

First, we discuss the sensitivity to the new physics benchmark point (4.7), which corresponds to lepton flavor universal new physics. As discussed in section 4.2.9, this new physics benchmark is unconstrained by the lepton flavor universality ratios R_K and R_{K^*} and motivated by the anomalously low branching ratios of $b \to s\mu\mu$ decays and the angular distribution of $B \to K^*\mu\mu$. We stress again that these hints for new physics rely on the modeling of hadronic effects in rare b decays and might be due to underestimated theory uncertainties. A completely independent cross-check at a muon collider would therefore be more than welcome.

	$6\,\text{TeV},\ 4\,\text{ab}^{-1}$	$10\,\text{TeV},\ 1\,\text{ab}^{-1}$	$10\,\text{TeV},\ 10\,\text{ab}^{-1}$
N_{tot}	10050 ± 220	$1,740 \pm 50$	$17,400 \pm 220$
N_{bg}	8670 ± 220	780 ± 42	$7,800 \pm 200$
N_{sig}	1380 ± 310	960 ± 68	$9,600 \pm 300$

Table 4.1: Expected $\mu^+\mu^- \to bs$ event numbers at different configurations of a muon collider with unpolarized muon beams.

With the chosen benchmark point, we obtain the expected $\mu^+\mu^- \to bs$ event numbers for unpolarized muon beams summarized in table 4.1. The numbers include the flavor tagging efficiencies and mistag rates discussed above. Explicitly,

this means

$$N_{\text{bg}} = \mathcal{L} \times \sum_{q=u,d,s,c,b} 2\epsilon_q(1-\epsilon_q)\ \sigma(\mu^+\mu^- \to q\bar{q})\ , \tag{4.21}$$

$$N_{\text{tot}} = N_{\text{bg}} + \mathcal{L} \times \epsilon_b(1-\epsilon_s)\ \sigma(\mu^+\mu^- \to bs)\ . \tag{4.22}$$

The quoted uncertainties on the total event numbers, N_{tot}, and the background event numbers, N_{bg}, include the statistical as well as a 2% systematic uncertainty added in quadrature. In all cases, the total number of events is significantly above the background prediction. The number of signal events is determined from $N_{\text{sig}} = N_{\text{tot}} - N_{\text{bg}}$, with the errors added in quadrature. Based on these numbers, we expect that the signal cross section can be measured with a precision of $\sim 22\%$ at 6 TeV with $4\,\text{ab}^{-1}$, $\sim 7\%$ at 10 TeV with $1\,\text{ab}^{-1}$, and $\sim 3\%$ at 10 TeV with $10\,\text{ab}^{-1}$.[1]

For a beam polarization of $P_- = -P_+ = 50\%$, we analogously find the event numbers in table 4.2. Both background and signal event numbers are slightly smaller in this case. This results in a comparable expected precision on the signal cross-section.

	6 TeV, $4\,\text{ab}^{-1}$	10 TeV, $1\,\text{ab}^{-1}$	10 TeV, $10\,\text{ab}^{-1}$
N_{tot}	7890 ± 180	$1,490 \pm 50$	$14,580 \pm 190$
N_{bg}	6610 ± 180	600 ± 40	$5,947 \pm 160$
N_{sig}	1280 ± 250	890 ± 60	8905 ± 250

Table 4.2: Expected $\mu^+\mu^- \to bs$ event numbers at different configurations of a muon collider with a beam polarization of $P_- = -P_+ = 50\%$.

[1] Note that the expected precision is significantly better compared to the preliminary results we reported in the whitepaper [103]. This is due to the change of the signal benchmark point (4.7) motivated by the new R_K, R_{K^*} results [40, 38].

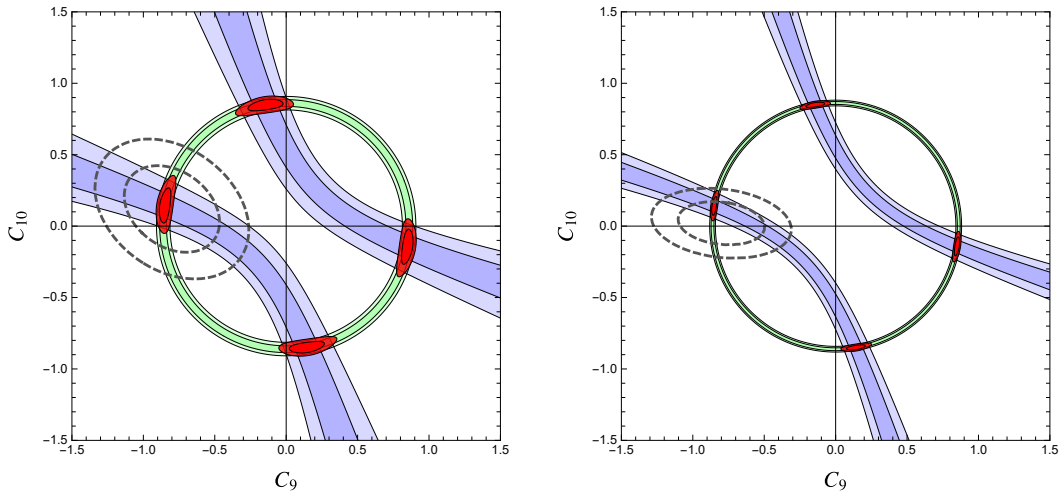

Figure 4.7: Sensitivity of a 10 TeV muon collider with unpolarized beams in the $\Delta C_9^{\text{univ.}}$ vs. $\Delta C_{10}^{\text{univ.}}$ plane, assuming the new physics benchmark point in (4.7). Shown in green (blue) is the region that can be determined by a measurement of the $\mu^+\mu^- \to bs$ cross section (the forward-backward asymmetry). The combination is in red. The left (right) plot assumes an integrated luminosity of 1 ab^{-1} (10 ab^{-1}). The dashed black lines are the current best-fit region from rare B decays (4.7) (left plot) or the expected region after the HL-LHC and Belle II (4.9) (right plot).

The 1σ and 2σ constraints in the $C_9 - C_{10}$ plane from the expected measurement of the $\mu^+\mu^- \to bs$ cross-section are shown in green in figures 4.7 and 4.8.

The forward-backward asymmetry introduced in (4.11) and (4.12) provides complementary information about the new physics. As mentioned in section 4.2.4, a measurement of the forward-backward asymmetry requires charge tagging in addition to flavor tagging. We estimate the expected precision of a A_{FB} measurement by splitting the events into forward and backward categories. A better precision could likely be obtained by performing an unbinned maximum likelihood fit to the angular distributions in (4.11) and (4.12). This is, however, beyond the scope of this work. Denoting the charge tagging efficiency by $\epsilon_\pm$, and implicitly including flavor tagging efficiencies, the expected number of observed forward and backward signal events is given by

$$N_{\text{sig, obs}}^{\text{F},b\bar{s}} \;=\; \epsilon_\pm \, N_{\text{sig}}^{\text{F},b\bar{s}} + (1-\epsilon_\pm)\, N_{\text{sig}}^{\text{F},s\bar{b}} \;, \tag{4.23}$$

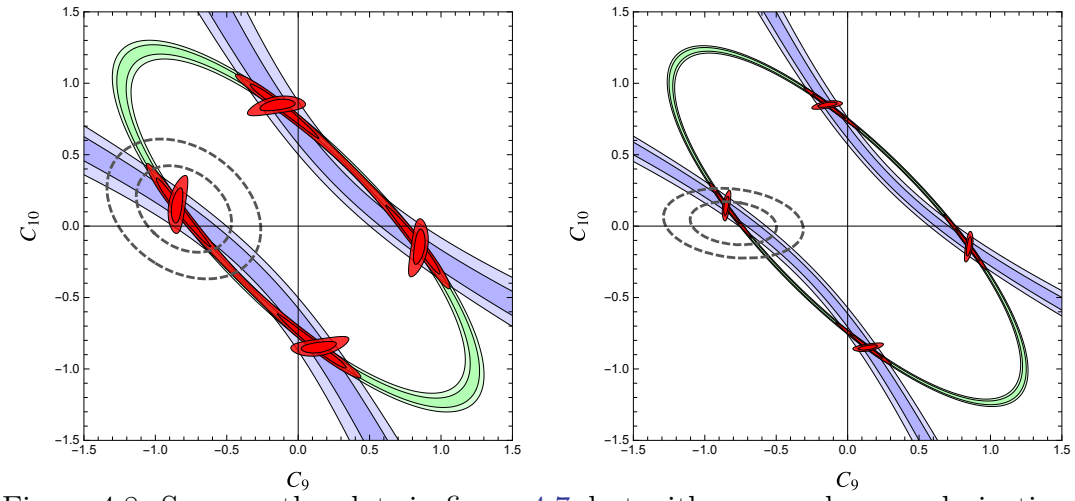

Figure 4.8: Same as the plots in figure 4.7, but with a muon beam polarization of $P_- = -P_+ = 50\%$. The combination of the unpolarized best-fit regions are overlaid on the polarized regions, highlighting the complementarity of the polarized and unpolarized beams.

$$N^{\mathrm{B},b\bar{s}}_{\mathrm{sig,\,obs}} = \epsilon_\pm\, N^{\mathrm{B},b\bar{s}}_{\mathrm{sig}} + (1-\epsilon_\pm)\, N^{\mathrm{B},s\bar{b}}_{\mathrm{sig}}\ , \tag{4.24}$$

$$N^{\mathrm{F},s\bar{b}}_{\mathrm{sig,\,obs}} = \epsilon_\pm\, N^{\mathrm{F},s\bar{b}}_{\mathrm{sig}} + (1-\epsilon_\pm)\, N^{\mathrm{F},b\bar{s}}_{\mathrm{sig}}\ , \tag{4.25}$$

$$N^{\mathrm{B},s\bar{b}}_{\mathrm{sig,\,obs}} = \epsilon_\pm\, N^{\mathrm{B},s\bar{b}}_{\mathrm{sig}} + (1-\epsilon_\pm)\, N^{\mathrm{B},b\bar{s}}_{\mathrm{sig}}\ , \tag{4.26}$$

and analogously for background events from flavor mistags. The observed total forward-backward asymmetry, $A^{\mathrm{obs}}_{\mathrm{FB}}$, is then given by

$$A^{\mathrm{obs}}_{\mathrm{FB}} = \frac{N^{\mathrm{F}}_{\mathrm{obs}} - N^{\mathrm{B}}_{\mathrm{obs}}}{N^{\mathrm{F}}_{\mathrm{obs}} + N^{\mathrm{B}}_{\mathrm{obs}}}\ , \tag{4.27}$$

where the observed event numbers are the sum of signal and background and take into account charge tagging and flavor tagging

$$N^{\mathrm{F}}_{\mathrm{obs}} = N^{\mathrm{F},b\bar{s}}_{\mathrm{sig,\,obs}} + N^{\mathrm{B},\bar{b}s}_{\mathrm{sig,\,obs}} + N^{\mathrm{F},b\bar{s}}_{\mathrm{bg,\,obs}} + N^{\mathrm{B},\bar{b}s}_{\mathrm{bg,\,obs}}\ , \tag{4.28}$$

$$N^{\mathrm{B}}_{\mathrm{obs}} = N^{\mathrm{B},b\bar{s}}_{\mathrm{sig,\,obs}} + N^{\mathrm{F},\bar{b}s}_{\mathrm{sig,\,obs}} + N^{\mathrm{B},b\bar{s}}_{\mathrm{bg,\,obs}} + N^{\mathrm{F},\bar{b}s}_{\mathrm{bg,\,obs}}\ . \tag{4.29}$$

Alternatively, $A^{\mathrm{obs}}_{\mathrm{FB}}$ can be expressed as the following combination of the truth level signal forward-backward asymmetry, A_{FB} as given in (4.14), and the truth level background forward-backward asymmetry, $A^{\mathrm{bg}}_{\mathrm{FB}}$,

$$A^{\mathrm{obs}}_{\mathrm{FB}} = (2\epsilon_\pm - 1)\Big(\frac{N_{\mathrm{sig}}}{N_{\mathrm{tot}}} A_{\mathrm{FB}} + \frac{N_{\mathrm{bg}}}{N_{\mathrm{tot}}} A^{\mathrm{bg}}_{\mathrm{FB}}\Big)\ , \tag{4.30}$$

Assuming unpolarized muon beams, the signal forward-backward asymmetry of the chosen benchmark point (4.7) is $A_{\rm FB} \simeq 0.24$, while for the background we find $A_{\rm FB}^{\rm bg} \simeq 0.62$. For polarized beams these values change to $A_{\rm FB} \simeq -0.48$ and $A_{\rm FB}^{\rm bg} \simeq 0.59$.

We assume that the b-jet charge tagging performance of a future muon collider will be comparable to that achieved at LEP, $\epsilon_\pm = 70\%$ [54]. We are not aware of any dedicated studies in the literature that establish charge tagging efficiencies at a high-energy muon collider. Performing such a study is beyond the scope of our work, and we use the LEP efficiency of 70% as a benchmark. Modern analysis techniques might improve the efficiency, while other effects like the beam background might degrade it.

The imperfect charge tagging washes out the observed forward-backward asymmetry by a factor of $(2\epsilon_\pm - 1) = 0.4$, as shown in (4.30).

The uncertainty on the observed forward-backward asymmetry can be estimated from (4.27). Treating the number of forward and backward events as independent, we find

$$\delta A_{\rm FB}^{\rm obs} = \frac{2}{N_{\rm tot}^2}\sqrt{(N_{\rm obs}^{\rm F})^2(\delta N_{\rm obs}^{\rm B})^2 + (N_{\rm obs}^{\rm B})^2(\delta N_{\rm obs}^{\rm F})^2}\ . \tag{4.31}$$

We expect that this slightly overestimates the uncertainty. In the determination of the $\delta N_{\rm obs}^{\rm F}$ and $\delta N_{\rm obs}^{\rm B}$, we take into account the statistical as well as a 2% systematic uncertainty.

We find expected measurements of the total forward-backward asymmetry $A_{\rm FB}^{\rm obs} = (22.7 \pm 1.7)\%$ at 6 TeV with 4 ab^{-1}, $A_{\rm FB}^{\rm obs} = (16.4 \pm 2.9)\%$ at 10 TeV with 1 ab^{-1}, and $A_{\rm FB}^{\rm obs} = (16.4 \pm 1.6)\%$ at 10 TeV with 10 ab^{-1}.

The forward-backward asymmetry is highly complementary to the cross-section and leads to orthogonal constraints in the $C_9 - C_{10}$ plane, presented in the blue regions in figures 4.7 and 4.8.

The combination of cross-section and forward-backward asymmetry is shown in red. For comparison, the dashed black contours in the plots on the left-hand side show the 1σ and 2σ best-fit region of the current rare B decay fit from (4.7). The dashed black contours in the plots on the right-hand side correspond to the

1σ and 2σ region of the projection (4.9).

We also checked how a reduced charge tagging efficiency impacts our findings. For a charge tagging of 65%, the region selected by $A_{\rm FB}$ with 1 ab^{-1} is comparable to the one by the current B decay fit. Once the charge tagging drops below ∼60%, two of the four best-fit regions start to merge at the 2σ level. Below ∼55%, very little information can be extracted from the forward-backward asymmetry with an integrated luminosity of 1 ab^{-1}. In fact, for a charge tagging of 55%, the observed $A_{\rm FB}$ is one order of magnitude smaller than the raw one, c.f. equation (4.30), and measuring the $A_{\rm FB}$ would be challenging even with 10 ab^{-1}.

The plots illustrate that a 10 TeV muon collider could establish a new physics signal with remarkable precision. Interestingly, a muon collider would select regions in the new physics parameter space with a four-fold degeneracy. Combining the information from the muon collider with the information from rare B decays allows one to uniquely identify the new physics. The best-fit new physics region determined by a 10 TeV muon collider with unpolarized beams and 1 ab^{-1} of data that is compatible with the rare B decay data is

$$\Delta C_9^{\rm univ.} = -0.81 \pm 0.03 \ , \quad \Delta C_{10}^{\rm univ.} = 0.12 \pm 0.08 \ , \tag{4.32}$$

with an error correlation of $\rho = +40\%$. For 10 ab^{-1}, this further improves to

$$\Delta C_9^{\rm univ.} = -0.81 \pm 0.01 \ , \quad \Delta C_{10}^{\rm univ.} = 0.12 \pm 0.04 \ . \tag{4.33}$$

with an error correlation of $\rho = +53\%$. Going to even higher luminosity has little impact as the precision starts to be limited by systematic uncertainties. We note that the expected muon collider results are much more precise than the expected precision from rare B decays alone (4.9).

The sensitivity of a muon collider could be improved even further if multiple runs with different beam polarizations were an option. As shown in the plots of figure 4.8, beam polarization does shape the best-fit regions that are selected in the new physics parameter space. As the various operators in (4.1) correspond to different linear combinations of muon chiralities, changing the polarizations of the muon beams also changes the sensitivity to different types of operators and would allow one to narrow down the parameter space further.

4.2.6.2 Constraints on muon-specific new physics

In the absence of new physics, a high-energy muon collider can constrain the size of the Wilson coefficients in Eq. (4.1). Switching on one Wilson coefficient at a time and demanding that the number of $\mu^+\mu^- \to bs$ signal events does not exceed the 2σ uncertainty of the background, we find for unpolarized muon beams

$$|C_{\text{vector}}| < \begin{cases} 0.46 & @\ 6\ \text{TeV}\ , \quad 4\ \text{ab}^{-1} \\ 0.22 & @\ 10\ \text{TeV}\ , \quad 1\ \text{ab}^{-1} \\ 0.17 & @\ 10\ \text{TeV}\ , \quad 10\ \text{ab}^{-1} \end{cases} , \tag{4.34}$$

for the vector Wilson coefficients $C_{\text{vector}} = \Delta C_9^\mu$, ΔC_{10}^μ, $C_9^{\prime\mu}$, or $C_{10}^{\prime\mu}$, and

$$|C_{\text{scalar}}| < \begin{cases} 0.53 & @\ 6\ \text{TeV}\ , \quad 4\ \text{ab}^{-1} \\ 0.26 & @\ 10\ \text{TeV}\ , \quad 1\ \text{ab}^{-1} \\ 0.19 & @\ 10\ \text{TeV}\ , \quad 10\ \text{ab}^{-1} \end{cases} , \tag{4.35}$$

for the scalar Wilson coefficients $C_{\text{scalar}} = C_S^\mu$, C_P^μ, $C_S^{\prime\mu}$, or $C_P^{\prime\mu}$. Here we give the values for the Wilson coefficients at a renormalization scale that corresponds to the center of mass energy of the collider $\mu = \sqrt{s}$.

Already with 1 ab^{-1} at a center of mass energy of 10 TeV, the constraint would be approximately as strong as the current one from R_K and R_{K^*} (4.8).

The constraint on the Wilson coefficients can also be translated into a sensitivity to a high new physics scale. Assuming $\mathcal{O}(1)$ flavor violating new physics couplings, one has for each Wilson coefficient C

$$\Lambda_{\text{NP}}^C = \left(\frac{4G_F}{\sqrt{2}} |V_{tb} V_{ts}^*| \frac{\alpha}{4\pi} |C| \right)^{-\frac{1}{2}} , \tag{4.36}$$

such that

$$\Lambda_{\text{NP}}^{\text{vector}} > \begin{cases} 53\ \text{TeV} & @\ 6\ \text{TeV}\ , \quad 4\ \text{ab}^{-1} \\ 76\ \text{TeV} & @\ 10\ \text{TeV}\ , \quad 1\ \text{ab}^{-1} \\ 86\ \text{TeV} & @\ 10\ \text{TeV}\ , \quad 10\ \text{ab}^{-1} \end{cases} , \tag{4.37}$$

$$\Lambda_{\rm NP}^{\rm scalar} \;>\; \begin{cases} 49 \text{ TeV} & @\ 6 \text{ TeV}\,, \quad 4 \text{ ab}^{-1} \\ 70 \text{ TeV} & @\ 10 \text{ TeV}\,, \quad 1 \text{ ab}^{-1} \\ 82 \text{ TeV} & @\ 10 \text{ TeV}\,, \quad 10 \text{ ab}^{-1} \end{cases} . \tag{4.38}$$

These results show that a muon collider has indirect sensitivity to new physics scales far above its center of mass energy and also above the scale of $\Lambda_{\rm NP}^{|C|=1} \simeq 35$ TeV, which is the generic scale associated with rare B decays.

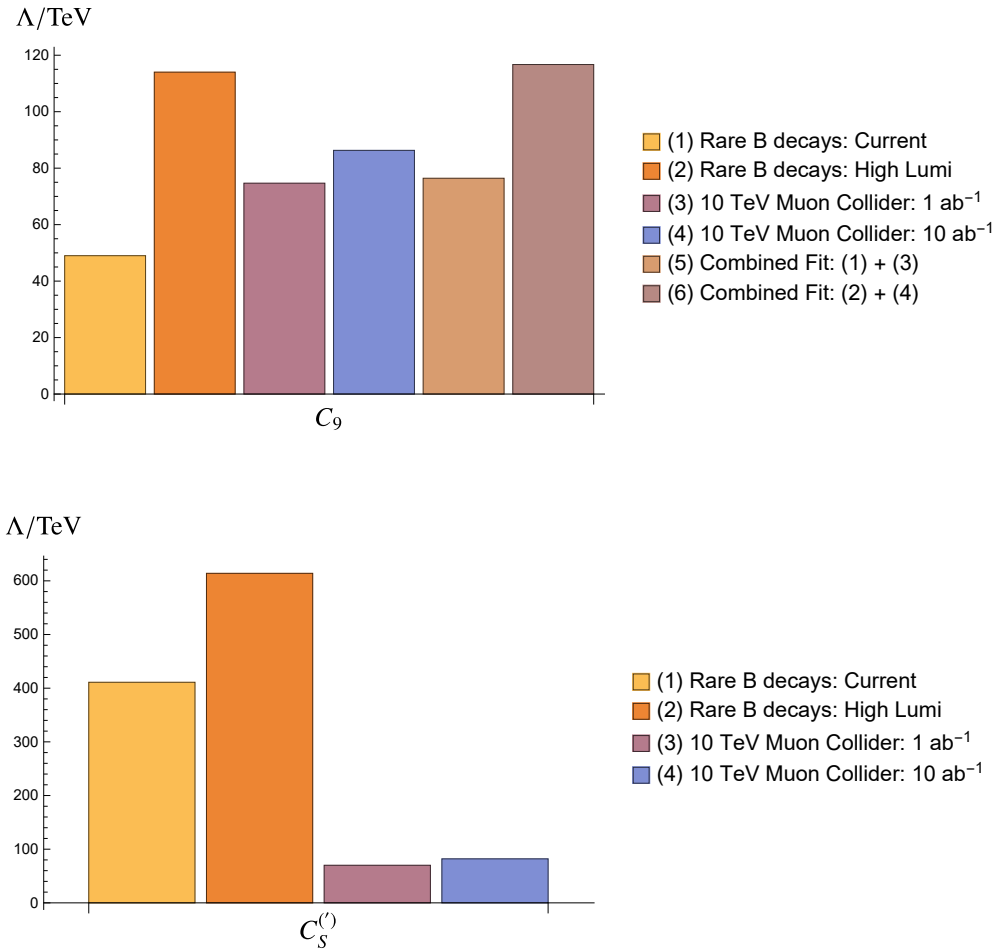

Figure 4.9: The new physics scales that can be probed by a muon collider and by B decay data from LHCb, both current and future projections. The histogram on the top corresponds to the Wilson coefficient ΔC_9^μ, the one on the bottom to $C_S^{(\prime)\,\mu}$. Other vector and scalar coefficients follow identical trends.

In figure 4.9 we compare the scales that can be probed by a muon collider

to those probed by current and expected future rare B decay data as well as combinations thereof, for the ΔC_9^μ coefficient in the left panel, and for $C_S^{(\prime)\,\mu}$ in the right panel. As in (4.34) and (4.35), we assume dominance of a single Wilson coefficient. We observe that for vector mediators the sensitivity to new physics of a 10 TeV muon collider surpasses the current LHCb sensitivity to the associated rare B decays, but lags behind our projections for LHCb runs at high luminosity; vice-versa, for scalar mediators, we find that current constraints from LHCb from rare B decays are anticipated to outperform a future 10 TeV collider. This is due to the fact that scalar mediators lift the helicity suppression of the $B_s \to \mu^+\mu^-$ decay, which is known to be a particularly sensitive probe of scalar new physics [113]. The two histograms to the right in the left panel illustrate that, while beneficial, combining the results of the LHC and a muon collider would only marginally strengthen the constraints from the best-performing collider.

Note that throughout our analysis, we have not made use of strange quark tagging. Therefore, in principle, the constrained cross sections do not correspond to $\sigma(\mu^+\mu^- \to bs)$ alone, but to the combination $\sigma(\mu^+\mu^- \to bs) + \sigma(\mu^+\mu^- \to bd)$. Our results hold under the plausible assumption that the new physics flavor violating couplings are larger for $b \to s$ than for $b \to d$ (resembling the SM flavor hierarchies). If that is not the case, the bounds on the Wilson coefficients in (4.34) and (4.35) can be interpreted as bounds on the square sum of $b \to s$ and $b \to d$ Wilson coefficients

$$|C| \to \sqrt{|C^{b\to s}|^2 + |C^{b\to d}|^2}\ . \tag{4.39}$$

It is interesting to contrast the results from sections 4.2.6.1 and 4.2.6.2. In the presence of a sizeable new physics signal (i.e. the scenario discussed in section 4.2.6.1, with main results in figure 4.7), a future muon collider would be able to measure the new physics with much higher precision than LHCb. In the absence of new physics (i.e. the scenario discussed in section 4.2.6.2, with main results in figure 4.9), or for very small new physics signals, expected rare B decay results from the high-luminosity runs of the LHC are more powerful in constraining new physics. In fact, in the context of the rare B decays, the new physics can interfere with the corresponding SM amplitudes, and one is linearly sensitive to small

new physics. At a muon collider on the other hand, the new physics amplitude does not interfere with the backgrounds from mistags, and one is therefore only quadratically sensitive to a small new physics amplitude.

4.2.7 Conclusions

While the recent changes in the experimental status of the $R_{K^{(*)}}$ observables indicate lepton flavor universal physics, a few anomalies in rare B decays persist. These anomalies, along with the overarching goal to search for new physics, provide a strong motivation to probe $bs\mu\mu$ interactions, while minimizing the impact of hadronic uncertainties in predicting the corresponding observable processes. With the highly complementary information that a muon collider analysis would provide, bounds on heavy new physics contributing to $b \to s\mu\mu$ decays are made far more robust in various scenarios, bolstered by the relatively clean environment of muon beams.

Here, we first reviewed the status of the global b decays fit, in light of recent updates on R_K and R_{K^*}, and identified two possible scenarios: on the one hand some new physics could be *lepton-flavor universal*, while addressing the $b \to s\mu\mu$ anomalies; on the other hand, some different new physics could instead be *muon-specific*, thus violating lepton flavor universality; in either scenario, we focused on the expected sensitivity from rare b decays from the high-luminosity phase of the LHC, and then proceeded to evaluate the possible role of a future muon collider.

We computed in detail the differential cross-section for bottom-strange quark production from muon-muon collisions, including the possible effect of muon beam polarization; we then discussed and computed the irreducible Standard Model background, as well as the expected background from mis-tagged di-jet events. We then proceeded to evaluate the potential and sensitivity projections for a multi-TeV muon collider at different luminosity, center of mass energy, and beam polarization. We showed the resulting sensitivity on the plane defined by deviations of the relevant Wilson coefficients from the flavor-universal case, as well as on the potential for constraints on muon-specific new physics. Broadly, we find

that a multi-TeV muon collider would be highly complementary to the LHC, and would vastly exceed the current (but not necessarily the expected high-luminosity) LHC performance in constraining new physics in b decays.

Acknowledgments

The research of WA, SAG, and SP is supported by the U.S. Department of Energy grant number DE-SC0010107. We thank Patrick Meade and Vladimir Shiltsev for useful discussions on muon collider performance.

Appendix

4.2.8 Renormalization Group Evolution

For a precise sensitivity comparison of the rare B decays and a muon collider, one should take into account the renormalization group running between the relevant scales. At a muon collider, the natural scale choice for the Wilson coefficients is the center of mass energy $\mu \sim \sqrt{s}$. On the other hand, the Wilson coefficients probed by B decays are typically renormalized at a low energy scale, of the order of the b mass, $\mu \sim m_b$. These scales differ by more than three orders of magnitude, and RGE running may be relevant.

We assume that the 4 fermion contact interactions in the effective Hamiltonian (4.1) are the only non-zero Wilson coefficients at the scale of the muon collider. Above the electroweak scale, it is convenient to use the SMEFT operator basis from [337]. Our Wilson coefficients can be translated as follows [2]

$$[C_{\ell q}^{(1)}]_{2223} + [C_{\ell q}^{(3)}]_{2223} = \Delta C_9^\mu - \Delta C_{10}^\mu \,, \tag{4.40}$$

$$[C_{qe}]_{2322} = \Delta C_9^\mu + \Delta C_{10}^\mu \,, \tag{4.41}$$

[2]Note that both the SMEFT coefficients $C_{\ell q}^{(1)}$ and $C_{\ell q}^{(3)}$ map onto the same combination $C_9 - C_{10}$, and the translation into the SMEFT operators is thus not unique. Interestingly, choosing an arbitrary linear combination of $C_{\ell q}^{(1)}$ and $C_{\ell q}^{(3)}$ has no impact on the final result. We find that the difference in SMEFT RGE running of $C_{\ell q}^{(1)}$ and $C_{\ell q}^{(3)}$ is exactly compensated by threshold corrections at the electroweak scale, and at leading log accuracy, we find a unique relation between the Wilson coefficients at the collider scale and the b scale.

$$[C_{\ell d}]_{2223} = C_9'^{\mu} - C_{10}'^{\mu} \,, \tag{4.42}$$

$$[C_{ed}]_{2223} = C_9'^{\mu} + C_{10}'^{\mu} \,, \tag{4.43}$$

$$[C_{\ell edq}]^*_{2232} = 2C_S^{\mu} \,, \tag{4.44}$$

$$[C_{\ell edq}]_{2223} = 2C_S'^{\mu} \,, \tag{4.45}$$

and analogously for the Wilson coefficients with electrons and taus.

We run the Wilson coefficients from $\mu \sim \sqrt{s}$ to the electroweak scale $\mu \sim m_Z$, with the mass of the Z boson $m_Z \simeq 91.2$ GeV, taking into account the impact of the gauge couplings and the top Yukawa coupling [392, 88]. After decoupling particles of electroweak mass, the Wilson coefficients are evolved further to the b scale using 1-loop QED and QCD running [391, 390]. We find

$$\begin{aligned}\Delta C_9^{\mu}(m_b) \simeq{}& \Delta C_9^{\mu}(\sqrt{s})\left[1 - \frac{n_\ell \alpha}{3\pi}\log\left(\frac{s}{m_b^2}\right) - \frac{\alpha}{16\pi s_W^2}\left(\frac{1}{c_W^2} + 2 + \frac{m_t^2}{2m_W^2}\right)\log\left(\frac{s}{m_Z^2}\right)\right] \\ &+ \Delta C_{10}^{\mu}(\sqrt{s})\left[\frac{\alpha}{2\pi}\log\left(\frac{s}{m_b^2}\right) + \frac{\alpha}{16\pi s_W^2}\left(\frac{1}{c_W^2} + 2\right)\left(1 - 4s_W^2\right)\log\left(\frac{s}{m_Z^2}\right)\right],\end{aligned} \tag{4.46}$$

$$\begin{aligned}\Delta C_{10}^{\mu}(m_b) \simeq{}& \Delta C_{10}^{\mu}(\sqrt{s})\left[1 - \frac{\alpha}{16\pi s_W^2}\left(\frac{1}{c_W^2} + 2 + \frac{m_t^2}{2m_W^2}\right)\log\left(\frac{s}{m_Z^2}\right)\right] \\ &+ \Delta C_9^{\mu}(\sqrt{s})\left[\frac{\alpha}{2\pi}\log\left(\frac{s}{m_b^2}\right) + \frac{\alpha}{16\pi s_W^2}\left(\frac{1}{c_W^2} + 2\right)\left(1 - 4s_W^2\right)\log\left(\frac{s}{m_Z^2}\right)\right],\end{aligned} \tag{4.47}$$

$$\begin{aligned}C_9'^{\mu}(m_b) \simeq{}& C_9'^{\mu}(\sqrt{s})\left[1 - \frac{n_\ell \alpha}{3\pi}\log\left(\frac{s}{m_b^2}\right) - \frac{\alpha}{8\pi c_W^2}\log\left(\frac{s}{m_Z^2}\right)\right] \\ &- C_{10}'^{\mu}(\sqrt{s})\left[\frac{\alpha}{2\pi}\log\left(\frac{s}{m_b^2}\right) - \frac{\alpha}{8\pi c_W^2}\left(1 - 4s_W^2\right)\log\left(\frac{s}{m_Z^2}\right)\right],\end{aligned} \tag{4.48}$$

$$\begin{aligned}C_{10}'^{\mu}(m_b) \simeq{}& C_{10}'^{\mu}(\sqrt{s})\left[1 - \frac{\alpha}{8\pi c_W^2}\log\left(\frac{s}{m_Z^2}\right)\right] \\ &- C_9'^{\mu}(\sqrt{s})\left[\frac{\alpha}{2\pi}\log\left(\frac{s}{m_b^2}\right) - \frac{\alpha}{8\pi c_W^2}\left(1 - 4s_W^2\right)\log\left(\frac{s}{m_Z^2}\right)\right],\end{aligned} \tag{4.49}$$

$$C_S^\mu(m_b) \simeq C_S^\mu(\sqrt{s}) \left(\frac{\alpha_s(m_b)}{\alpha_s(m_Z)}\right)^{\frac{12}{23}} \left(\frac{\alpha_s(m_Z)}{\alpha_s(\sqrt{s})}\right)^{\frac{4}{7}} \times \left[1 + \frac{5\alpha}{6\pi}\log\left(\frac{s}{m_b^2}\right) + \frac{\alpha}{3\pi}\left(\frac{1}{c_W^2} - \frac{5}{2}\right)\log\left(\frac{s}{m_Z^2}\right)\right], \tag{4.50}$$

$$C_S'^\mu(m_b) \simeq C_S'^\mu(\sqrt{s}) \left(\frac{\alpha_s(m_b)}{\alpha_s(m_Z)}\right)^{\frac{12}{23}} \left(\frac{\alpha_s(m_Z)}{\alpha_s(\sqrt{s})}\right)^{\frac{4}{7}} \times \left[1 + \frac{5\alpha}{6\pi}\log\left(\frac{s}{m_b^2}\right) + \frac{\alpha}{3\pi}\left(\frac{1}{c_W^2} - \frac{5}{2} - \frac{3m_t^2}{32 s_W^2 m_W^2}\right)\log\left(\frac{s}{m_Z^2}\right)\right]. \tag{4.51}$$

Where $n_\ell = 1$ in the scenario with muon-specific Wilson coefficients and $n_\ell = 3$ in the scenario with lepton universal coefficients. In these expressions, s_W and c_W are the sine and cosine of the weak mixing angle, α is the fine structure constant, and α_s is the strong coupling constant. Note that only the scalar coefficients $C_S = -C_P$ and $C_S' = C_P'$ experience QCD running. In the above expressions, we re-summed the QCD logarithms but used a leading logarithmic approximation for the (much smaller) electroweak RGE corrections.

In the lepton universal scenario, running to the low scale preserves universality, and the expressions above also hold analogously for the electron and tau coefficients. In the muon-specific scenario, the RGE running induces operators with electrons and taus. This is, in principle, relevant in the context of the rare B decays, as the LFU ratios $R_{K^{(*)}}$ are to a good approximation sensitive to the differences of the muon and electron Wilson coefficients $C_i^\mu - C_i^e$. In this case, the non-zero electron coefficients at the b scale are

$$\Delta C_9^e(m_b) \simeq -\Delta C_9^\mu(\sqrt{s})\frac{\alpha}{3\pi}\log\left(\frac{s}{m_b^2}\right), \tag{4.52}$$

$$C_9'^e(m_b) \simeq -C_9'^\mu(\sqrt{s})\frac{\alpha}{3\pi}\log\left(\frac{s}{m_b^2}\right). \tag{4.53}$$

In practice, we find that the RGE running has a small impact. The shifts between the Wilson coefficients $C_{9,10}^{(\prime)}$ at the low scale $\mu \simeq m_b \simeq 4.2$ GeV and the high scale $\mu \simeq \sqrt{s} = 10$ TeV are typically around 5-10%. We do include the running of $C_{9,10}^{(\prime)}$ in the leading log approximation in our numerical analysis for

completeness. In the case of the scalar coefficients $C_{S,P}^{(\prime)}$, we take into account the small electroweak running and the QCD running, which is an $\mathcal{O}(1)$ effect. We note that tools that can perform the running numerically are, in principle, available [67, 308, 284].

4.2.9 Updated Rare B Decay Fit

In this appendix, we briefly describe our rare B decay fit that incorporates the recent LHCb results of R_K and R_{K^*} [40, 38] (see also [240, 333, 80, 76, 509, 81] for other recent discussions).

We perform our own global fit using `flavio` [493] (version 2.3.3) and include the following set of experimental results

- branching ratio measurements of $B_s \to \mu^+\mu^-$ from CDF [46], ATLAS [7], and LHCb [36];
- branching ratios measurements of $B \to K\mu^+\mu^-$, $B \to K^*\mu^+\mu^-$, and $B_s \to \phi\mu^+\mu^-$ from CDF [440], Belle [235], CMS [402], and LHCb [18, 23, 34];
- angular observables of the decays $B \to K^*\mu^+\mu^-$ and $B_s \to \phi\mu^+\mu^-$ from CDF [440], ATLAS [5], CMS [483], and LHCb [29, 32, 33];
- branching ratios and angular observables of $\Lambda_b \to \Lambda\mu^+\mu^-$ from CDF [440] and LHCb [20, 26];
- lepton flavor universality tests in rare B meson decays from Belle [505, 235] and LHCb [37].

To reduce hadronic uncertainties on the semi-leptonic branching ratios and angular observables, we only take into account q^2 bins below 6 GeV^2, as well as broad bins above the narrow charmonium resonances that span the entire available kinematic range. To be conservative, we do not use `flavio`'s default values for the CKM matrix elements, but instead use the PDG values [513] $|V_{cb}| = (40.8 \pm 1.4) \times 10^{-3}$ and $|V_{ub}| = (3.82 \pm 0.20) \times 10^{-3}$, which are a conservative average of inclusive and exclusive determinations with inflated uncertainties.

In addition to the observables listed above, we implement the recent CMS results on the $B_s \to \mu^+\mu^-$ decay from [3], as well as the latest LHCb results on R_K and R_{K^*} [40, 38] which were not yet included in version 2.3.3 of `flavio` (but have been added in the latest update). These results have a significant impact on the fit. In figure 4.1 in the main text, we show the result of our fit in the standard plane of muon specific C_9 and C_{10} Wilson coefficients.

4.3 Chapter Conclusion

In this chapter, I have shown that a high-energy muon collider could provide a powerful and complementary approach to studying the same underlying new physics that might be responsible for current anomalies in rare B decays. This work advances the central argument of the dissertation by establishing a direct connection between precision flavor measurements and high-energy collider physics. The finding that measurements of both cross-section and forward-backward asymmetry can disentangle different chirality structures of new physics demonstrates how targeted observables can maximize the physics reach of future facilities. The exceptional sensitivity to new physics scales approaching 100 TeV further underscores how flavor physics can probe energy scales far beyond direct production capabilities, a recurring theme throughout this thesis.

Chapter 5

New Strategies for New Physics Search with $\Lambda_b \to \Lambda \nu \bar{\nu}$ Decays

5.1 Introduction to the Chapter

Rare decays based on the $b \to s\nu\bar{\nu}$ transition offer exceptionally clean probes of new physics due to their minimal sensitivity to hadronic uncertainties. Unlike their charged-lepton counterparts, these di-neutrino modes are not affected by non-local hadronic effects, making them theoretically pristine windows into potential physics beyond the Standard Model. The recent evidence for the $B^+ \to K^+\nu\bar{\nu}$ decay reported by Belle II, with a branching ratio significantly above the Standard Model prediction, further highlights the importance of these processes in our quest to understand the fundamental laws of nature.

In this chapter, I explore a novel approach to probing new physics through the rare decay $\Lambda_b \to \Lambda\nu\bar{\nu}$. This decay, which will be accessible at future Z-pole machines like FCC-ee and CEPC, offers unique advantages compared to mesonic decays. Most notably, Λ_b baryons produced in Z decays are longitudinally polarized, introducing a new observable; the zero crossing of the forward-backward asymmetry $A_{FB}^{\uparrow}$ in the angle between the outgoing Λ momentum and the Λ_b spin provides complementary sensitivity to the chirality structure of potential new physics interactions.

The study of $\Lambda_b \to \Lambda\nu\bar{\nu}$ decay extends the flavor physics program into the heavy baryon sector, complementing studies of rare mesonic decays. By utilizing the longitudinal polarization of Λ_b baryons at Z-factories, this work shows how baryon decays offer unique observables that probe the chirality structure of new physics interactions. This approach connects to other components of the flavor program, including rare $V \to K^{(*)}\nu\bar{\nu}$ decays at Belle II and $\Lambda_b \to \Lambda\ell^+\ell^-$ measurements at LHCb, providing a more complete picture of potential new physics affecting flavor-changing neutral currents.

The following publication presents a comprehensive study of the $\Lambda_b \to \Lambda\nu\bar{\nu}$ decay of longitudinally polarized Λ_b baryons. It provides state-of-the-art Standard Model predictions for the branching ratio and the forward-backward asymmetry, and explores their sensitivity to new physics. Interestingly, the zero crossing of the forward-backward asymmetry is found to be independent of new physics, offering a robust test of form factor calculations.

This work demonstrates that precision measurements of rare heavy baryon decays at future e^+e^- colliders can provide powerful and complementary constraints on new physics models, further enriching our toolkit for exploring physics beyond the Standard Model.

5.2 Original Publication

Wolfgang Altmannshofer[a], Sri Aditya Gadam[a], Kevin Toner[a]

[a]*Department of Physics & Santa Cruz Institute for Particle Physics, University of California, Santa Cruz, CA 95064, USA*

waltmann@ucsc.edu sgadam@ucsc.edu ktoner@ucsc.edu

Abstract. We examine the new physics sensitivity of the rare decay $\Lambda_b \to \Lambda\nu\bar{\nu}$ which can be accessible at future Z-pole machines like FCC-ee and CEPC. We find that the longitudinal polarization of Λ_b baryons produced in Z decays introduces a novel observable, the forward-backward asymmetry $A_{\rm FB}^{\uparrow}$ in the angle between the outgoing Λ momentum and the Λ_b spin. We provide Standard Model predictions for the $\Lambda_b \to \Lambda\nu\bar{\nu}$ branching ratio and $A_{\rm FB}^{\uparrow}$, and show that future precision measurements of these observables are complementary and probe new physics scales comparable to other $b \to s\nu\bar{\nu}$ and $b \to s\ell^+\ell^-$ processes. We also show that the zero crossing of the forward-backward asymmetry offers a robust test of form factor calculations independent of new physics.

5.2.1 Introduction

Rare b decays are highly suppressed in the Standard Model and therefore exceptionally sensitive to new physics at very high energy scales. They garner much effort and attention from the theoretical and experimental communities alike [177, 92].

Precise experimental measurements and accurate SM predictions are essential to fully harness the potential of rare b decays as probes of new physics. Experimental results from LHCb, ATLAS, and CMS exist for a multitude of rare semi-leptonic B meson decays including $B \to K\mu^+\mu^-$, $B \to K^*\mu^+\mu^-$ and $B_s \to \phi\mu^+\mu^-$. Measured observables include differential branching ratios [18, 23, 34], angular distributions [22, 483, 5, 29, 32, 33, 44, 41, 43, 356], and lepton flavor universality ratios [37, 40, 16, 357, 45]. To maximize the potential of rare decay

observables in probing new physics, global fits incorporating all relevant rare b decay data are frequently performed, for recent results see [116, 481, 240, 333, 76, 509, 104, 339, 379, 190]. Intriguingly, there are several measured branching ratios and angular observables that do not agree well with SM predictions and that fairly consistently point to new physics. The interpretation of the observed deviations in terms of new physics relies critically on the robust control of hadronic effects in $b \to s\ell^+\ell^-$ decays, parameterized by local and non-local form factors [372, 195, 371, 154, 340, 341, 342, 78].

In this context, the rare decays based on the $b \to s\nu\bar{\nu}$ transition emerge as an interesting complementary probe of new physics [95, 205, 200, 162, 170, 461]. The di-neutrino modes are theoretically cleaner than their charged-lepton counterparts, as they are not affected by the non-local hadronic effects (e.g. the charm loops). All hadronic physics in the exclusive $b \to s\nu\bar{\nu}$ decays is encapsulated by local form factors. The $b \to s\nu\bar{\nu}$ modes play a dual role in probing new physics: they test heavy new physics through model-independent four-fermion contact interactions (potentially linked to $b \to s\ell^+\ell^-$ transitions via $SU(2)_L$ symmetry) and provide a window into light dark sectors, as decays like $b \to sX$—where X is a neutral, invisibly decaying, or long-lived light particle—mimic the missing-energy signature of di-neutrino processes.

On the experimental side, BaBar and Belle established upper limits on the $B \to K\nu\bar{\nu}$ and $B \to K^*\nu\bar{\nu}$ branching ratios a factor of few above the SM predictions [277, 424, 413, 336], while Belle II recently found first evidence for $B^+ \to K^+\nu\bar{\nu}$ [65]. The measured branching ratio is $\sim 2.7\sigma$ above the SM expectation, which sparked renewed interest in the $b \to s\nu\bar{\nu}$ decays as probes of new physics [163, 82, 301, 291, 359, 166, 272, 96, 433, 306, 366, 232, 311, 373, 358, 186, 429, 208, 83, 115, 375]. Belle II is expected to measure the $B^+ \to K^+\nu\bar{\nu}$ and $B^0 \to K^{*0}\nu\bar{\nu}$ branching ratios with $\sim 10\%$ precision [91]. Future e^+e^- machines running on the Z-pole like FCC-ee and CEPC [48, 167, 289, 419] have the potential to further improve this precision and have the unique capability to observe the $B_s \to \phi\nu\bar{\nu}$ and $\Lambda_b \to \Lambda\nu\bar{\nu}$ decays [418, 124]. Combining the insights from the full range of di-neutrino modes—including pseudoscalar-to-pseudoscalar tran-

sitions ($B \to K\nu\bar{\nu}$), pseudoscalar-to-vector transitions ($B \to K^*\nu\bar{\nu}$, $B_s \to \phi\nu\bar{\nu}$), and fermion-to-fermion transitions ($\Lambda_b \to \Lambda\nu\bar{\nu}$)—offers a powerful approach to probing new physics.

The decays of the Λ_b baryon are particularly interesting, as the Λ_b can be polarized and thus provide novel observables that are not accessible in the meson decays. Here, we will be especially interested in the fact that Λ_b baryons that are produced in Z decays are longitudinally polarized [425, 297, 211, 52, 62]. The goal of our work is to provide a comprehensive study of the decay $\Lambda_b \to \Lambda\nu\bar{\nu}$ of longitudinally polarized Λ_b baryons (see [231, 79, 491, 365, 270, 124], for related work on $\Lambda_b \to \Lambda\nu\bar{\nu}$ decays). The kinematics of the decay is characterized by the energy of the Λ and the angle between its momentum and the spin of the Λ_b. We find that the corresponding angular decay distribution depends on a novel observable, a forward-backward asymmetry $A_{\rm FB}^{\uparrow}$, that is proportional to the longitudinal polarization of the Λ_b. We work out state-of-the-art SM predictions for the integrated branching ratio, $\mathrm{BR}(\Lambda_b \to \Lambda\nu\bar{\nu})$, and the forward-backward asymmetry, $A_{\rm FB}^{\uparrow}$, and explore their sensitivity to new physics, in particular to the new physics' chirality structure. See [364] for similar ideas in the context of the $\Lambda_b \to \Lambda\gamma$ decay.

The corresponding decays with charged leptons in the final state, $\Lambda_b \to \Lambda\ell^+\ell^-$, have been observed at LHCb [20, 26] and are extensively discussed in the literature [281, 185, 443, 282, 176, 465, 179, 178]. It would be interesting to extend our work, and to study the decays of longitudinally polarized $\Lambda_b \to \Lambda\ell^+\ell^-$, at future Z-pole machines. Note that in our paper, we focus on the decay $\Lambda_b \to \Lambda\nu\bar{\nu}$, where Λ refers to the weakly decaying Λ baryon ground state. An analogous analysis could also be performed for the $\Lambda_b \to \Lambda(1520)\nu\bar{\nu}$ decay or other higher excited Λ baryon states. See [435, 189, 436, 122] for the relevant transition form factors, and [278, 269, 123, 420, 164, 24, 31, 39, 42] for related work on $\Lambda_b \to \Lambda(1520)\ell^+\ell^-$ decays.

This paper is organized as follows: In section 5.2.2, we introduce the effective Hamiltonian that describes the $b \to s\nu\bar{\nu}$ decay in the SM and in models with heavy new physics and define the relevant $\Lambda_b \to \Lambda$ form factors. We discuss in detail the

uncertainties from the short distance SM contributions and the CKM input. In section 5.2.3, we present our results for the differential $\Lambda_b \to \Lambda\nu\bar{\nu}$ branching ratio in the presence of longitudinal Λ_b polarization and introduce the forward-backward asymmetry $A_{\rm FB}^{\uparrow}$. We give SM predictions for the branching ratio and the forward-backward asymmetry and discuss qualitatively the impact of new physics on the observables. In section 5.2.4 we determine the new physics sensitivity of precision measurements of the $\Lambda_b \to \Lambda\nu\bar{\nu}$ observables. Finally, in section 5.2.5, we discuss the imprint of the forward-backward asymmetry on the Λ energy distribution in the lab frame. This distribution might provide an alternative method to test new physics with $\Lambda_b \to \Lambda\nu\bar{\nu}$. We conclude in section 5.2.6. Details about our implementation of the $\Lambda_b \to \Lambda$ form factors are collected in appendix 5.2.7.

5.2.2 Effective Hamiltonian and Hadronic Matrix Elements

The effective Hamiltonian that underlies the description of the $\Lambda_b \to \Lambda\nu\bar{\nu}$ decay is

$$\mathcal{H}_{\rm eff} = -\frac{4G_F}{\sqrt{2}}\frac{\alpha}{4\pi}V_{ts}^*V_{tb}\Big(C_L O_L + C_R O_R\Big) \;+\; \text{h.c.}\,, \tag{5.1}$$

with the four-fermion operators

$$O_L = (\bar{s}\gamma^\mu P_L b)(\bar{\nu}\gamma_\mu(1-\gamma_5)\nu)\,, \qquad O_R = (\bar{s}\gamma^\mu P_R b)(\bar{\nu}\gamma_\mu(1-\gamma_5)\nu)\,. \tag{5.2}$$

In the SM, the Wilson coefficients are $C_L^{\rm SM} = -X(x_t)/s_W^2$ where $s_W = \sin\theta_W$ is the sine of the weak mixing angle, and $C_R^{\rm SM} \simeq 0$. The loop function $X(x_t)$ depends on the ratio of the top quark $\overline{\rm MS}$ mass and the W mass $x_t = m_t^2(m_t)/m_W^2$. Its most recent determination can be found in [197, 199]. The uncertainties in the W mass and the sine of the weak mixing angle s_W can be neglected when evaluating the SM Wilson coefficient, but the uncertainty in the top mass is not entirely negligible.

To obtain a value for $C_L^{\rm SM}$, we re-scale the $X(x_t)$ function given in [199] to take into account the latest experimental results on the top mass. We translate the top quark pole mass from cross-section measurements quoted by the PDG, $m_t = (172.5 \pm 0.7)\,\text{GeV}$ [513], into the top quark $\overline{\rm MS}$ mass at 3-loop QCD accuracy

using `RunDec` [362] and find $m_t(m_t) = 162.92 \pm 0.72\,\text{GeV}$. Using $m_W = 80.377\,\text{GeV}$ and $s_W^2 = 0.2314$ [513] we arrive at

$$C_L^{\text{SM}} = -6.322 \pm 0.031\Big|_{m_t} \pm 0.074\Big|_{\text{QCD}} \pm 0.009\Big|_{\text{EW}} , \tag{5.3}$$

where the three uncertainties are due to the top mass, higher-order QCD corrections, and higher-order EW corrections, respectively. The value of the electromagnetic coupling α that enters the effective Hamiltonian is the running α at the electroweak scale, $\alpha^{-1} \simeq 127.95$ with negligible uncertainty.

We determine the relevant CKM matrix elements that enter the effective Hamiltonian from input given by the PDG. In particular, we use [513]

$$|V_{cb}| = (40.8 \pm 1.4) \times 10^{-3} , \quad |V_{ub}| = (3.82 \pm 0.20) \times 10^{-3} , \quad \gamma = 65.9^\circ \pm 3.5^\circ . \tag{5.4}$$

The values for $|V_{cb}|$ and $|V_{ub}|$ are conservative averages of determinations using inclusive and exclusive tree-level B decays. For the sine of the Cabibbo angle, we use $\lambda \simeq 0.225$ [513], neglecting its tiny uncertainty. This results in

$$|V_{ts}^* V_{tb}|^2 = \left(1.609 \pm 0.109\Big|_{V_{cb}} \pm 0.001\Big|_{V_{ub}} \pm 0.004\Big|_{\gamma}\right) \times 10^{-3} , \tag{5.5}$$

with the uncertainty entirely dominated by $|V_{cb}|$.

The hadronic matrix elements relevant for the $\Lambda_b \to \Lambda \nu \bar{\nu}$ decay can be parameterized by form factors in the following way [300, 282, 178]

$$\begin{aligned}\langle \Lambda | \bar{s} \gamma^\mu b | \Lambda_b \rangle = \bar{u}_\Lambda \Bigg[& f_t^V(q^2)(m_{\Lambda_b} - m_\Lambda)\frac{q^\mu}{q^2} + f_\perp^V(q^2)\left(\gamma^\mu - \frac{2(m_\Lambda P^\mu + m_{\Lambda_b} p^\mu)}{(m_{\Lambda_b} + m_\Lambda)^2 - q^2}\right) \\ & + f_0^V(q^2)\frac{m_{\Lambda_b} + m_\Lambda}{(m_{\Lambda_b} + m_\Lambda)^2 - q^2}\left(P^\mu + p^\mu - (m_{\Lambda_b}^2 - m_\Lambda^2)\frac{q^\mu}{q^2}\right)\Bigg] u_{\Lambda_b} , \end{aligned} \tag{5.6}$$

$$\begin{aligned}\langle \Lambda | \bar{s} \gamma^\mu \gamma_5 b | \Lambda_b \rangle = -\bar{u}_\Lambda \gamma_5 \Bigg[& f_t^A(q^2)(m_{\Lambda_b} + m_\Lambda)\frac{q^\mu}{q^2} + f_\perp^A(q^2)\left(\gamma^\mu + \frac{2(m_\Lambda P^\mu - m_{\Lambda_b} p^\mu)}{(m_{\Lambda_b} - m_\Lambda)^2 - q^2}\right) \\ & + f_0^A(q^2)\frac{m_{\Lambda_b} - m_\Lambda}{(m_{\Lambda_b} - m_\Lambda)^2 - q^2}\left(P^\mu + p^\mu - (m_{\Lambda_b}^2 - m_\Lambda^2)\frac{q^\mu}{q^2}\right)\Bigg] u_{\Lambda_b} , \end{aligned} \tag{5.7}$$

where P and p are the momenta of the Λ_b and Λ, respectively, and m_{Λ_b} and m_Λ are their masses. The form factors $f_{t,0,\perp}^{V,A}$ are functions of $q^2 = (P - p)^2$,

the di-neutrino invariant mass squared. For our numerical analysis, we use the $\Lambda_b \to \Lambda$ form factors from [282] (see also [178]). More details are provided in appendix 5.2.7.

5.2.3 Differential Branching Ratio in the SM and Beyond

With the effective Hamiltonian introduced in the previous section, we can determine the differential branching ratio of the $\Lambda_b \to \Lambda \nu \bar{\nu}$ decay. For the decay of a polarized Λ_b, the kinematics of the visible decay products depends on two independent variables. One convenient choice is E_Λ, the energy of the Λ in the Λ_b restframe, and θ_Λ, the angle between the Λ momentum and the spin quantization axis of the Λ_b in its restframe. Alternatively, one may want to use the di-neutrino invariant mass squared q^2 and the angle θ_Λ, with q^2 given in terms of the Λ energy by

$$q^2 = m_{\Lambda_b}^2 + m_\Lambda^2 - 2 m_{\Lambda_b} E_\Lambda \ . \tag{5.8}$$

We find that the double differential branching ratio has a very simple dependence on $\cos\theta_\Lambda$ that can be written as

$$\frac{d\mathrm{BR}(\Lambda_b \to \Lambda \nu \bar{\nu})}{dE_\Lambda d\cos\theta_\Lambda} = \frac{d\mathrm{BR}(\Lambda_b \to \Lambda \nu \bar{\nu})}{dE_\Lambda} \left(\frac{1}{2} + A_{\mathrm{FB}}^{\uparrow} \cos\theta_\Lambda \right) \ . \tag{5.9}$$

The differential branching ratio as a function of the Λ energy is given by

$$\begin{aligned} \frac{d\mathrm{BR}(\Lambda_b \to \Lambda \nu \bar{\nu})}{dE_\Lambda} = \tau_{\Lambda_b} \frac{\alpha^2 G_F^2}{32\pi^5} m_{\Lambda_b}^5 |V_{ts}^* V_{tb}|^2 \frac{E_\Lambda^2}{m_{\Lambda_b}^3} \sqrt{1 - \frac{m_\Lambda^2}{E_\Lambda^2}} \\ \times \left(\left| C_L + C_R \right|^2 \mathcal{F}_V + \left| C_L - C_R \right|^2 \mathcal{F}_A \right) \ , \end{aligned} \tag{5.10}$$

where we summed over all three neutrino flavors, assuming that the Wilson coefficients are neutrino flavor conserving and neutrino flavor universal, as is the case in the SM. The numerical value for the Λ_b lifetime that enters the branching ratio is $\tau_{\Lambda_b} = (0.970 \pm 0.009) \times \tau_{B^0} = (1.473 \pm 0.014) \times 10^{-12}\,\mathrm{s}$ [513].

The quantity $A_{\mathrm{FB}}^{\uparrow}$ is a forward-backward asymmetry of the Λ with respect to the spin quantization axis of the Λ_b. We find

$$A_{\mathrm{FB}}^{\uparrow} = \frac{\mathcal{P}_{\Lambda_b} \left(\left| C_R \right|^2 - \left| C_L \right|^2 \right) \mathcal{F}_{VA}}{\left| C_L + C_R \right|^2 \mathcal{F}_V + \left| C_L - C_R \right|^2 \mathcal{F}_A} \ . \tag{5.11}$$

To simplify notation in the above expressions for the branching ratio and the forward-backward asymmetry, we have introduced the following quadratic functions of the $\Lambda_b \to \Lambda$ form factors

$$\mathcal{F}_V = \left(1 - \frac{m_\Lambda}{E_\Lambda}\right)\left((1+x_\Lambda)^2\left(f_0^V(q^2)\right)^2 + \frac{2q^2}{m_{\Lambda_b}^2}\left(f_\perp^V(q^2)\right)^2\right) , \tag{5.12}$$

$$\mathcal{F}_A = \left(1 + \frac{m_\Lambda}{E_\Lambda}\right)\left((1-x_\Lambda)^2\left(f_0^A(q^2)\right)^2 + \frac{2q^2}{m_{\Lambda_b}^2}\left(f_\perp^A(q^2)\right)^2\right) , \tag{5.13}$$

$$\mathcal{F}_{VA} = \sqrt{1 - \frac{m_\Lambda^2}{E_\Lambda^2}}\left(\left(1-x_\Lambda^2\right) f_0^V(q^2) f_0^A(q^2) - \frac{2q^2}{m_{\Lambda_b}^2} f_\perp^V(q^2) f_\perp^A(q^2)\right) . \tag{5.14}$$

All form factors in the above expressions depend on the di-neutrino invariant mass squared q^2 as introduced already in (5.8). For later convenience, we have introduced the ratio of Λ mass and Λ_b mass $x_\Lambda = m_\Lambda / m_{\Lambda_b}$.

The quantity $\mathcal{P}_{\Lambda_b}$ that enters the forward-backward asymmetry is the polarization asymmetry of the Λ_b, i.e. it corresponds to the difference of Λ_b baryons with spin-up and spin-down

$$\mathcal{P}_{\Lambda_b} = \frac{N_{\Lambda_b}^\uparrow - N_{\Lambda_b}^\downarrow}{N_{\Lambda_b}^\uparrow + N_{\Lambda_b}^\downarrow} . \tag{5.15}$$

The natural choice for the spin quantization axis is the direction of the Λ_b momentum in the lab frame. In that case, $\mathcal{P}_{\Lambda_b}$ corresponds to the longitudinal polarization fraction of the Λ_b. On the Z pole, this polarization can be measured using semi-leptonic Λ_b decays [425, 437, 188, 285]. Measurements at LEP found

$$\mathcal{P}_{\Lambda_b} = \begin{cases} -0.23^{+0.24+0.08}_{-0.20-0.07} , & \text{ALEPH [211]} , \\ -0.49^{+0.32}_{-0.30} \pm 0.17 , & \text{DELPHI [62]} , \\ -0.56^{+0.20}_{-0.13} \pm 0.09 , & \text{OPAL [52]} , \end{cases} \tag{5.16}$$

where the first uncertainty is due to statistics and the second due to systematics. A naive weighted average of the LEP measurements that neglects possible correlations gives

$$\mathcal{P}_{\Lambda_b} = -0.40 \pm 0.14 . \tag{5.17}$$

We expect that a future Z pole machine should be able to measure $\mathcal{P}_{\Lambda_b}$ with percent level accuracy. In fact, the statistical uncertainty at FCC-ee or CEPC

should be negligible, while systematic uncertainties from e.g. the lepton energy and missing energy resolution should be improved significantly compared to LEP.[1]

5.2.3.1 Standard Model Predictions

Before discussing the new physics sensitivity of the $\Lambda_b \to \Lambda\nu\bar{\nu}$ decay, we provide the SM predictions for the branching ratio and the forward-backward asymmetry.

The SM expression for the integrated branching ratio can be found from (5.10), setting the right-handed Wilson coefficient to zero

$$\mathrm{BR}(\Lambda_b \to \Lambda\nu\bar{\nu})_{\mathrm{SM}} = \tau_{\Lambda_b} \frac{\alpha^2 G_F^2}{32\pi^5} m_{\Lambda_b}^5 |V_{ts}^* V_{tb}|^2 \left|C_L^{\mathrm{SM}}\right|^2 \int_{E_\Lambda^{\min}}^{E_\Lambda^{\max}} \frac{dE_\Lambda E_\Lambda^2}{m_{\Lambda_b}^3} \sqrt{1 - \frac{m_\Lambda^2}{E_\Lambda^2}} \left(\mathcal{F}_V + \mathcal{F}_A\right) , \tag{5.18}$$

where $\mathcal{F}_V$ and $\mathcal{F}_A$ were already introduced in eqs. (5.12) and (5.13), and the integration boundaries are given by

$$E_\Lambda^{\min} = m_\Lambda \ , \qquad E_\Lambda^{\max} = \frac{m_{\Lambda_b}}{2}\left(1 + x_\Lambda^2\right) \ . \tag{5.19}$$

We stress that the branching ratio is independent of the Λ_b polarization $\mathcal{P}_{\Lambda_b}$.

Using the numerical input discussed previously, we arrive at the following numerical SM prediction for the integrated branching ratio

$$\mathrm{BR}(\Lambda_b \to \Lambda\nu\bar{\nu})_{\mathrm{SM}} = (7.71 \pm 1.06) \times 10^{-6} \ , \tag{5.20}$$

which has an uncertainty of approximately 14%. In figure 5.1, we show a pie chart of the various sources of uncertainty that enter our SM prediction. The bulk of the uncertainty is shared by the form factors and the CKM input, with the form factors being dominant. The other sources of uncertainty are subdominant

$$\begin{aligned} \delta\mathrm{BR}(\Lambda_b \to \Lambda\nu\bar{\nu})_{\mathrm{SM}} \times 10^6 = \pm 0.90\Big|_{\mathrm{ff}} \pm 0.53\Big|_{\mathrm{CKM}} \pm 0.18\Big|_{\mathrm{QCD}} \\ \pm 0.08\Big|_{m_t} \pm 0.07\Big|_{\tau_{\Lambda_b}} \pm 0.02\Big|_{\mathrm{EW}} = \pm 1.06 \ , \end{aligned} \tag{5.21}$$

where we added all uncertainties in quadrature.

[1] Note that even in the challenging environment of the LHC, measurements of the (transversal) Λ_b polarization with an uncertainty of few percent have been performed [484, 30]

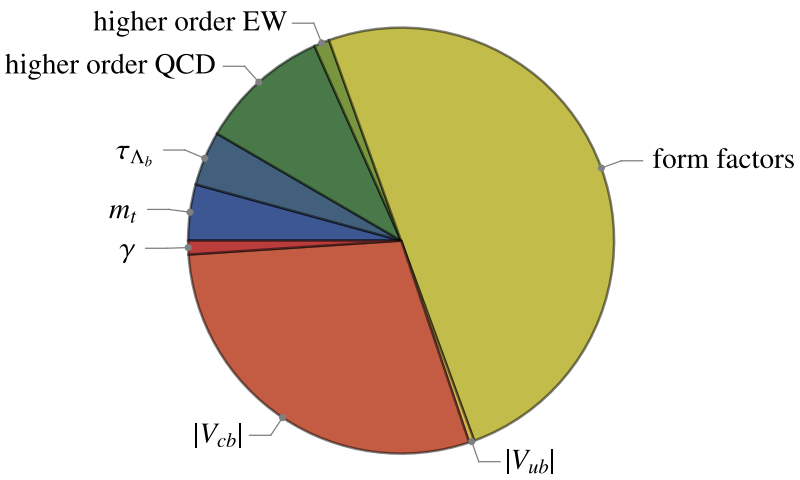

Figure 5.1: Pie chart that shows the most relevant sources of uncertainty entering the SM prediction of the $\Lambda_b \to \Lambda \nu \bar{\nu}$ branching ratio.

In figure 5.2, we show the differential branching ratio (5.10) in the SM as a function of the Λ energy E_Λ (left panel) and the di-neutrino invariant mass squared (right panel). Also these spectra are independent of the Λ_b polarization $\mathcal{P}_{\Lambda_b}$. The uncertainty increases for small q^2 or large E_Λ, respectively, as the uncertainties in the form factors increases in that kinematic regime.

The forward-backward asymmetry in the SM is given by

$$(A_{\rm FB}^{\uparrow})_{\rm SM} = \frac{-\mathcal{P}_{\Lambda_b} \mathcal{F}_{VA}}{\mathcal{F}_V + \mathcal{F}_A} \,. \tag{5.22}$$

Besides $\mathcal{P}_{\Lambda_b}$, the only other source of uncertainty are the form factors contained in the functions $\mathcal{F}_V$, $\mathcal{F}_A$, and $\mathcal{F}_{VA}$ in eqs. (5.12), (5.13), and (5.14). In figure 5.3, we show $(A_{\rm FB}^{\uparrow})_{\rm SM}$ as a function of the Λ energy E_Λ (left panel) and the di-neutrino invariant mass squared (right panel). For concreteness we set the Λ_b polarization to the central value given in eq. (5.17). The shown uncertainty is from the form factors only. The forward-backward asymmetry vanishes at the kinematic endpoint $E_\Lambda^{\rm min} = m_\Lambda$, or correspondingly $q^2_{\rm max} = (m_{\Lambda_b} - m_\Lambda)^2$. We find that the forward-backward asymmetry has a zero crossing in the SM, which is determined by the relative size of the form factors $f_0^{V,A}$ and $f_\perp^{V,A}$, cf. equation (5.14), by the

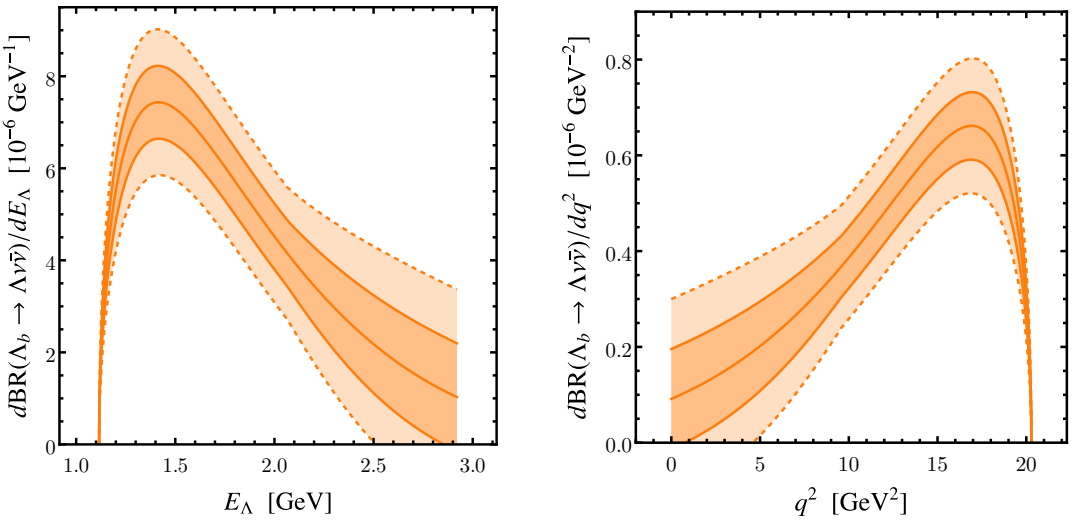

Figure 5.2: The differential branching ratio of $\Lambda_b \to \Lambda\nu\bar{\nu}$ in the SM as a function of the Λ energy in the Λ_b rest frame E_Λ (left) and the di-neutrino invariant mass squared q^2 (right). The relevant phase space boundaries of the decay are $m_\Lambda < E_\Lambda < \frac{m_{\Lambda_b}}{2}(1+m_\Lambda^2/m_{\Lambda_b}^2)$ and $0 < q^2 < (m_{\Lambda_b} - m_\Lambda)^2$. The colored bands correspond to the 1σ and 2σ uncertainties.

implicit relation

$$q^2 = \frac{m_{\Lambda_b}^2}{2}\left(1 - x_\Lambda^2\right)\frac{f_0^V(q^2) f_0^A(q^2)}{f_\perp^V(q^2) f_\perp^A(q^2)} \,. \tag{5.23}$$

The corresponding numerical zero crossing values for the Λ energy and the di-neutrino invariant mass are

$$(E_\Lambda)_0^{\mathrm{SM}} = (1.80 \pm 0.11)\ \mathrm{GeV}\,, \quad (q^2)_0^{\mathrm{SM}} = (12.6 \pm 1.2)\ \mathrm{GeV}^2\,. \tag{5.24}$$

The uncertainties in these values are entirely due to the form factors.

Integrating over the whole range of Λ energies we find in the SM

$$\langle A_{\mathrm{FB}}^{\uparrow}\rangle_{\mathrm{SM}} = -\mathcal{P}_{\Lambda_b} \times \frac{\int_{E_\Lambda^{\mathrm{min}}}^{E_\Lambda^{\mathrm{max}}} dE_\Lambda E_\Lambda^2 \sqrt{1 - \frac{m_\Lambda^2}{E_\Lambda^2}}\ \mathcal{F}_{VA}}{\int_{E_\Lambda^{\mathrm{min}}}^{E_\Lambda^{\mathrm{max}}} dE_\Lambda E_\Lambda^2 \sqrt{1 - \frac{m_\Lambda^2}{E_\Lambda^2}}\ \left(\mathcal{F}_V + \mathcal{F}_A\right)} = -\mathcal{P}_{\Lambda_b} \times \left(2.7 \pm 3.4\right) \times 10^{-2}\,. \tag{5.25}$$

The SM prediction of the integrated asymmetry is fairly small, with the uncertainty entirely due to the form factors. If we instead split the integration region into two parts at the zero crossing of the forward-backward asymmetry, we find

$$\langle A_{\mathrm{FB}}^{\uparrow}\rangle_{\mathrm{SM}}^{\mathrm{low}} \;=\; -\mathcal{P}_{\Lambda_b} \times \left(13.2 \pm 4.2\right) \times 10^{-2}\,, \quad 0 < q^2 < 12.6\,\mathrm{GeV}^2\,, \tag{5.26}$$

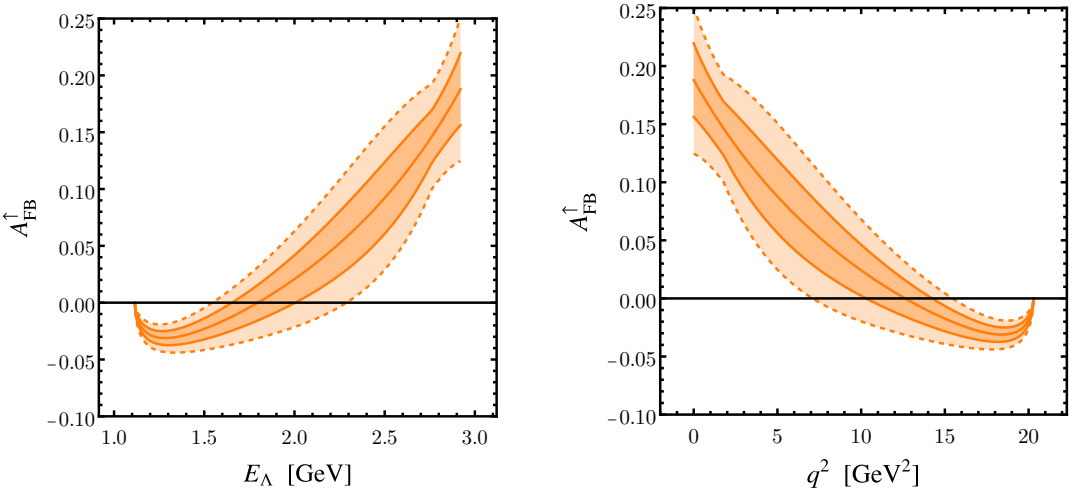

Figure 5.3: The forward-backward asymmetry in $\Lambda_b \to \Lambda\nu\bar{\nu}$ in the SM as a function of the Λ energy in the Λ_b rest frame E_Λ (left) and the di-neutrino invariant mass squared q^2 (right). The relevant phase space boundaries of the decay are $m_\Lambda < E_\Lambda < \frac{m_{\Lambda_b}}{2}(1 + m_\Lambda^2/m_{\Lambda_b}^2)$ and $0 < q^2 < (m_{\Lambda_b} - m_\Lambda)^2$. The colored bands correspond to the 1σ and 2σ uncertainties. Only uncertainties due to the form factors are shown. The Λ_b polarization is set to its central experimental value $\mathcal{P}_{\Lambda_b} = -0.40$.

$$\langle A_{\rm FB}^{\uparrow}\rangle_{\rm SM}^{\rm high} \;=\; -\mathcal{P}_{\Lambda_b} \times \big(-5.3 \pm 1.4\big) \times 10^{-2}\,, \quad 12.6\,{\rm GeV}^2 < q^2 < q^2_{\rm max} \tag{5.27}$$

where "low" and "high" refer to the q^2 regions $0 < q^2 < 12.6\,{\rm GeV}^2$ and $12.6\,{\rm GeV}^2 < q^2 < q^2_{\rm max}$, respectively. We find that the uncertainties of the forward-backward asymmetries in the low and high q^2 regions are correlated, with a correlation coefficient of $\rho \simeq +52\%$.

Analogously, we can also obtain SM predictions for the branching ratio in the two different q^2 regions

$$\begin{aligned} {\rm BR}(\Lambda_b \to \Lambda\nu\bar{\nu})_{\rm SM}^{\rm low} &= (3.32 \pm 0.99) \times 10^{-6}\,, \quad 0 < q^2 < 12.6\,{\rm GeV}^2\,, & (5.28)\\ {\rm BR}(\Lambda_b \to \Lambda\nu\bar{\nu})_{\rm SM}^{\rm high} &= (4.39 \pm 0.47) \times 10^{-6}\,, \quad 12.6\,{\rm GeV}^2 < q^2 < q^2_{\rm max} & (5.29)\end{aligned}$$

with an error correlation of $\rho \simeq +40\%$. The prediction is less precise at low q^2, because of the larger form factor uncertainties in this kinematic regime.

As we will see below, splitting the phase space into the two q^2 regions below

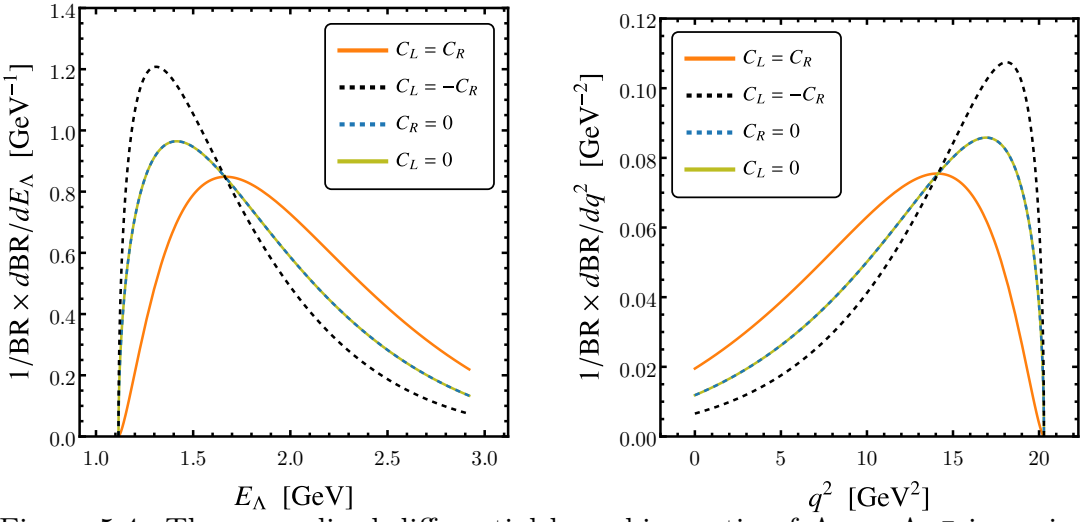

Figure 5.4: The normalized differential branching ratio of $\Lambda_b \to \Lambda\nu\bar{\nu}$ in various new physics scenarios as a function of the Λ energy in the Λ_b rest frame E_Λ (left) and the di-neutrino invariant mass squared q^2 (right). The scenario with $C_R = 0$ coincides with the SM prediction.

and above the zero crossing of the forward-backward asymmetry enhances the sensitivity to new physics.

5.2.3.2 Impact of Heavy New Physics

In this paper we focus on the impact of heavy new physics on the $\Lambda_b \to \Lambda\nu\bar{\nu}$ decay. A study of light new physics will be presented elsewhere. Heavy new physics is parameterized by modifications of the two Wilson coefficients C_L and C_R in the effective Hamiltonian, see equation (5.1). Heavy new physics can change the values of the branching ratio and the forward-backward asymmetry, as well as their kinematic distributions.

In the plots of figure 5.4, we show the normalized differential branching ratio as a function of the Λ energy (left) and of q^2 (right) in four different new physics scenarios. Scenarios with only left-handed currents ($C_R = 0$, dashed blue) or only right-handed currents ($C_L = 0$, yellow) result in the same kinematic distributions that coincide the SM prediction. Scenarios with vector currents ($C_L = C_R$, orange) give a slightly harder E_Λ spectrum, while the E_Λ spectrum for axial-vector currents

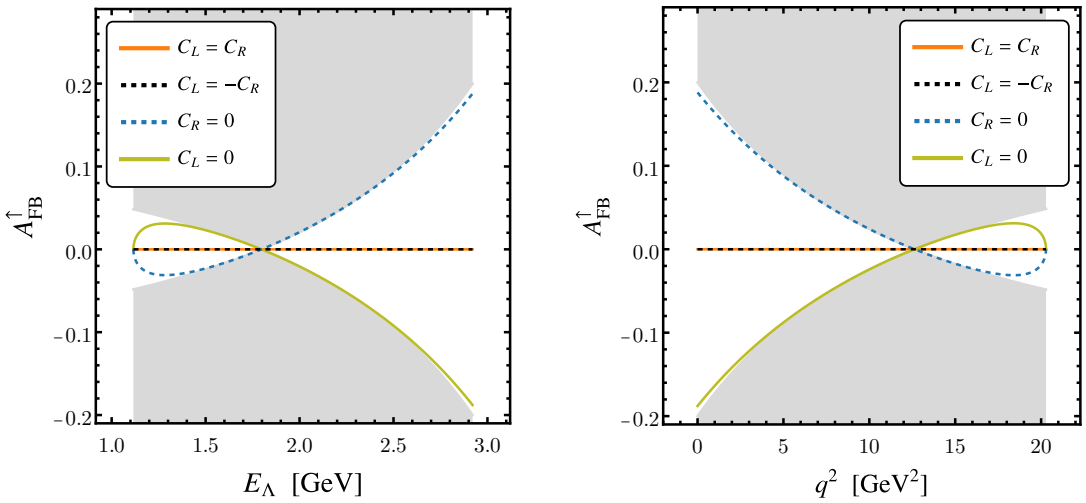

Figure 5.5: The forward-backward asymmetry in $\Lambda_b \to \Lambda \nu \bar{\nu}$ in various new physics scenarios as a function of the Λ energy in the Λ_b rest frame E_Λ (left) and the di-neutrino invariant mass squared q^2 (right). The Λ_b polarization is set to its central experimental value $\mathcal{P}_{\Lambda_b} = -0.40$. The scenario with $C_R = 0$ coincides with the SM prediction.

($C_L = -C_R$, dashed black) is slightly softer.

The new physics effects on the forward-backward asymmetry are highly complementary. The plots of figure 5.5 show the forward-backward asymmetry as a function of the Λ energy (left) and of q^2 (right) in the same four new physics scenarios. The forward-backward asymmetry maximally distinguishes the two chiral scenarios $C_R = 0$ and $C_L = 0$. The forward-backward asymmetry vanishes for both the vector and axial-vector scenarios. The gray regions in the plots is theoretically inaccessible. In fact, the maximum value of the forward-backward asymmetry that can in principle be reached is given by

$$\left|A_{\rm FB}^{\uparrow}\right| < \left|\frac{\mathcal{P}_{\Lambda_b}\mathcal{F}_{VA}}{2\sqrt{\mathcal{F}_V\mathcal{F}_A}}\right| , \tag{5.30}$$

which defines the boundary of the gray region in the plots of figure 5.5. In passing, we note that the SM prediction (that coincides with the dashed blue line) is very close to the theoretical maximum of the forward-backward asymmetry.

Interestingly enough, the zero crossing of the forward-backward asymmetry does not change with new physics, but depends purely on form factor inputs.

It is always determined by the condition in equation (5.23). Our predictions in equation (5.24) therefore serve as an interesting experimental cross-check of the form factor calculations.

5.2.4 Sensitivity to Heavy New Physics

After the discussion in the previous section that focused on the qualitative impact that heavy new physics can have on the $\Lambda_b \to \Lambda \nu \bar{\nu}$ decay, we now determine quantitatively the sensitivity to heavy new physics.

As discussed above, new physics can modify the value of the branching ratio and the forward-backward asymmetry as well as their kinematic distributions (but not the location of the zero crossing of the forward-backward asymmetry). The new physics sensitivity of the $\Lambda_b \to \Lambda \nu \bar{\nu}$ observables will depend on the precision of the theory predictions and the uncertainties of the future experimental measurements. The uncertainty of a future $\Lambda_b \to \Lambda \nu \bar{\nu}$ branching ratio measurement at the FCC-ee was estimated to be around 10% in [124]. This is below the current theory uncertainty of $\sim 14\%$, see equation (5.20). So far, no estimates exist how well the forward-backward asymmetry could be measured at future Z-pole machines. In our study, we will take into account the current uncertainties on the theory side and will neglect the experimental uncertainties. This illustrates to which extent the current theory precision limits the sensitivity of $\Lambda_b \to \Lambda \nu \bar{\nu}$. We do expect improved theory predictions by the time the FCC-ee or CEPC would deliver results.

To incorporate new physics to the branching ratio and the forward-backward asymmetry, we find it convenient to normalize the new physics contributions to the Wilson coefficients by the SM Wilson coefficient

$$c_L^{\rm NP} = C_L^{\rm NP}/C_L^{\rm SM} \,, \qquad c_R^{\rm NP} = C_R^{\rm NP}/C_L^{\rm SM} \,. \tag{5.31}$$

The expressions for the branching ratio and the forward-backward asymmetry in the presence of new physics are then

$$\text{BR}(\Lambda_b \to \Lambda \nu \bar{\nu}) \;=\; \text{BR}(\Lambda_b \to \Lambda \nu \bar{\nu})_{\rm SM} \Big(r \big| 1 + c_L^{\rm NP} + c_R^{\rm NP} \big|^2 + (1-r) \big| 1 + c_L^{\rm NP} - c_R^{\rm NP} \big|^2 \Big) \tag{5.32}$$

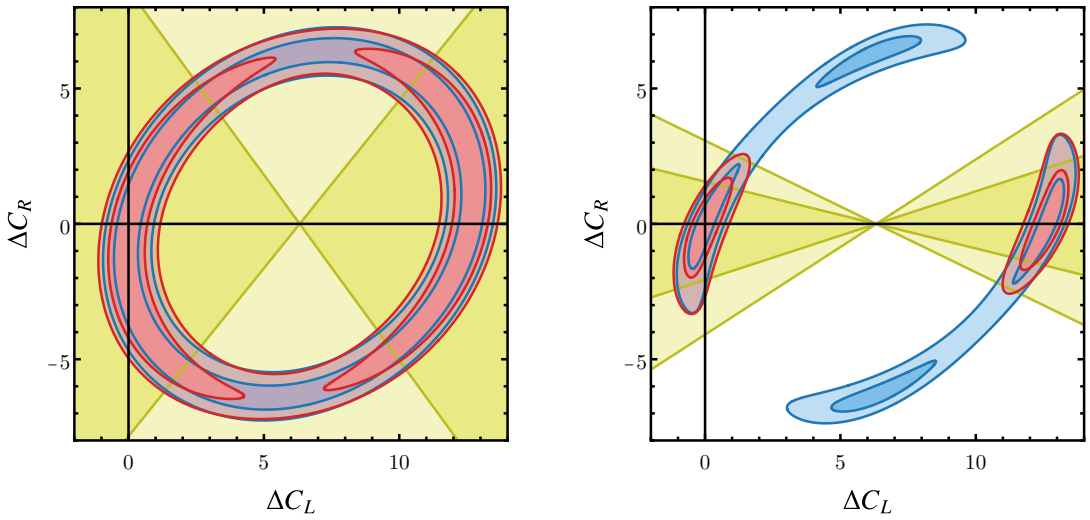

Figure 5.6: The expected sensitivity of $\Lambda_b \to \Lambda \nu \bar{\nu}$ to new physics parameterized by the Wilson coefficients $C_L^{\rm NP}$ and $C_R^{\rm NP}$. Left: taking into account a single large q^2 bin; Right: splitting the q^2 range into two bins, one above and one below the zero crossing of the forward-backward asymmetry. The blue, yellow, and red regions correspond to the constraints from the branching ratio, the forward-backward asymmetry, and their combination, respectively. Dark and light shaded regions indicate 1σ and 2σ constraints.

$$\langle A_{\rm FB}^{\uparrow} \rangle \;=\; \frac{\langle A_{\rm FB}^{\uparrow} \rangle_{\rm SM} \Big(\big|1 + c_L^{\rm NP}\big|^2 - \big|c_R^{\rm NP}\big|^2 \Big)}{r \big|1 + c_L^{\rm NP} + c_R^{\rm NP}\big|^2 + (1-r)\big|1 + c_L^{\rm NP} - c_R^{\rm NP}\big|^2} \;, \tag{5.33}$$

where the parameter r is given by

$$r = \frac{\int_{E_\Lambda^{\rm min}}^{E_\Lambda^{\rm max}} dE_\Lambda E_\Lambda^2 \sqrt{1 - \frac{m_\Lambda^2}{E_\Lambda^2}}\; \mathcal{F}_V}{\int_{E_\Lambda^{\rm min}}^{E_\Lambda^{\rm max}} dE_\Lambda E_\Lambda^2 \sqrt{1 - \frac{m_\Lambda^2}{E_\Lambda^2}}\; \big(\mathcal{F}_V + \mathcal{F}_A\big)} \;. \tag{5.34}$$

The expressions can be applied for any range of the Λ energy or q^2, respectively. In particular, we find for the total q^2 range and the low and high q^2 ranges

$$r_{\rm tot} \simeq 0.41 \;, \quad r_{\rm low} \simeq 0.55 \;, \quad r_{\rm high} \simeq 0.30 \;. \tag{5.35}$$

In figure 5.6, we show the allowed regions in $C_L^{\rm NP}$ vs. $C_R^{\rm NP}$ parameter space, assuming that the experimental measurements of the branching ration and the forward-backward asymmetry agree precisely with our SM predictions. The plot

on the left takes into account observables integrated over the full q^2 range, while in the plot on the right we include the low and high q^2 regions separately, taking into account their correlations. We assume that both $C_L^{\rm NP}$ and $C_R^{\rm NP}$ are real.

The blue regions correspond to the constraint we anticipate from a future branching ratio measurement at the 1σ and 2σ level, while the yellow regions correspond to a measurement of the forward-backward asymmetry. The red regions show the combination of both. More precisely, the dark and light shaded regions correspond to a $\Delta\chi^2$ of 1 and 4, when we consider the branching ratio or the forward backward asymmetry individually (blue and yellow regions), and to a $\Delta\chi^2$ of 2.3 and 6 in the combination (red regions). As expected, the branching ratio and the forward-backward asymmetry have complementary sensitivity. However, if the forward-backward asymmetry is integrated over the entire q^2 range, its constraining power is largely washed out. A much better sensitivity is obtained if the high-q^2 and low-q^2 regions are taken into account separately, which avoids cancellations in the forward-backward asymmetry.

In the right plot, we observe two clearly resolved regions of parameter space: one in the vicinity of the SM point $C_L^{\rm NP} = C_R^{\rm NP} = 0$, and one with $C_L^{\rm NP} \simeq -2C_L^{\rm SM} \simeq 12.6$, $C_R^{\rm NP} \simeq 0$. The second region corresponds to a total $b \to s\nu\nu$ amplitude with opposite sign compared to the SM, a scenario that cannot be distinguished from the SM using only $b \to s\nu\nu$ decays. We consider such a scenario contrived and do not discuss it further.

We can translate the allowed region around the point $C_L^{\rm NP} = C_R^{\rm NP} = 0$ into constraints on the new physics scale, using the parameterization

$$\frac{1}{\Lambda_L^2} = \frac{4G_F}{\sqrt{2}}\frac{\alpha}{4\pi}|V_{ts}^*V_{tb}|C_L^{\rm NP} \ , \quad \frac{1}{\Lambda_R^2} = \frac{4G_F}{\sqrt{2}}\frac{\alpha}{4\pi}|V_{ts}^*V_{tb}|C_R^{\rm NP} \ . \tag{5.36}$$

We find the following 2σ limits

$$\frac{-1}{\left(45\,\text{TeV}\right)^2} \lesssim \frac{1}{\Lambda_L^2} \lesssim \frac{1}{\left(44\,\text{TeV}\right)^2} \ , \quad \frac{-1}{\left(25\,\text{TeV}\right)^2} \lesssim \frac{1}{\Lambda_R^2} \lesssim \frac{1}{\left(33\,\text{TeV}\right)^2} \ . \tag{5.37}$$

These new physics scales are in the same ballpark as the scales that are probed by $b \to s\mu\mu$ decays (see e.g. [117, 283]) and by the rare meson decays with neutrinos in the final state $B \to K\nu\bar{\nu}$ and $B \to K^*\nu\bar{\nu}$ (see e.g. [163, 82]).

5.2.5 Differential Branching Ratio in the Lab Frame

As we have seen in the previous section, a measurement of the forward-backward asymmetry provides interesting sensitivity to new physics that is complementary to measurements of the branching ratio. We note that a measurement of $A_{\rm FB}^{\uparrow}$ requires access to the angle between the flight direction of the Λ in the Λ_b rest frame and the flight direction of the Λ_b in the lab frame. Reconstructing the Λ_b rest frame might be challenging due to the two neutrinos in the decay[2], and we therefore explore to which extent information about the forward-backward asymmetry (or, equivalently, information about the chirality structure of the $b \to s\nu\nu$ transition) can be extracted from lab frame observables alone. The approach is inspired by methods to determine the Λ_b polarization at LEP, using semi-leptonic decays [425, 437, 188].

For the following, it will be useful to introduce the shorthand notation

$$\hat{\beta}_{\Lambda_b} = \sqrt{1 - \frac{m_{\Lambda_b}^2}{\hat{E}_{\Lambda_b}^2}} \,, \quad \hat{\beta}_{\Lambda} = \sqrt{1 - \frac{m_{\Lambda}^2}{\hat{E}_{\Lambda}^2}} \,, \quad \beta_{\Lambda} = \sqrt{1 - \frac{m_{\Lambda}^2}{E_{\Lambda}^2}} \,, \tag{5.38}$$

where $\hat{\beta}_{\Lambda_b}$ is the velocity of the Λ_b in the lab frame, $\hat{\beta}_{\Lambda}$ the velocity of the Λ in the lab frame, and β_{Λ} the velocity of the Λ in the Λ_b restframe, respectively.

The relevant lab frame observable is the differential decay rate as a function of the Λ energy in the lab frame that we denote with $\hat{E}_{\Lambda}$. We find

$$\frac{d\mathrm{BR}(\Lambda_b \to \Lambda\nu\bar{\nu})}{d\hat{E}_{\Lambda}} = \int_{E_{\Lambda}^{\rm min}}^{E_{\Lambda}^{\rm max}} \frac{dE_{\Lambda}}{E_{\Lambda}} \frac{m_{\Lambda_b}}{\hat{E}_{\Lambda_b}} \frac{1}{\hat{\beta}_{\Lambda_b}\beta_{\Lambda}} \frac{d\mathrm{BR}(\Lambda_b \to \Lambda\nu\bar{\nu})}{dE_{\Lambda} d\cos\theta_{\Lambda}} \,, \tag{5.39}$$

where $\hat{E}_{\Lambda_b}$ is the energy of the Λ_b in the lab frame, and in the expression for the differential branching ratio in the Λ_b restframe (5.9), one needs to replace

$$\cos\theta_{\Lambda} = \frac{1}{\hat{\beta}_{\Lambda_b}\beta_{\Lambda}} \left(\frac{\hat{E}_{\Lambda}}{E_{\Lambda}} \frac{m_{\Lambda_b}}{\hat{E}_{\Lambda_b}} - 1 \right) \,. \tag{5.40}$$

The lower and upper integration boundaries in (5.39) are given by

$$E_{\Lambda}^{\rm min} = \frac{\hat{E}_{\Lambda}\hat{E}_{\Lambda_b}}{m_{\Lambda_b}} \left(1 - \hat{\beta}_{\Lambda_b}\hat{\beta}_{\Lambda}\right) \,, \tag{5.41}$$

[2] One could for example estimate the di-neutrino energy and momentum using the missing energy and momentum in the hemisphere containing the Λ_b.

$$E_\Lambda^{\max} \;=\; \text{Min}\left\{\frac{m_{\Lambda_b}}{2}\left(1+x_\Lambda^2\right),\; \frac{\hat{E}_\Lambda \hat{E}_{\Lambda_b}}{m_{\Lambda_b}}\left(1+\hat{\beta}_{\Lambda_b}\hat{\beta}_\Lambda\right)\right\}\;. \tag{5.42}$$

The physical range of the Λ energy in the lab frame is

$$\hat{E}_\Lambda^{\min} \;=\; \begin{cases} m_\Lambda & \text{if } \;\hat{\beta}_{\Lambda_b} < \dfrac{1-x_\Lambda^2}{1+x_\Lambda^2}\;, \\ \dfrac{\hat{E}_{\Lambda_b}}{2}\left(1+x_\Lambda^2-\left(1-x_\Lambda^2\right)\hat{\beta}_{\Lambda_b}\right) & \text{if } \;\hat{\beta}_{\Lambda_b} > \dfrac{1-x_\Lambda^2}{1+x_\Lambda^2}\;, \end{cases} \tag{5.43}$$

$$\hat{E}_\Lambda^{\max} \;=\; \frac{\hat{E}_{\Lambda_b}}{2}\left(1+x_\Lambda^2+\left(1-x_\Lambda^2\right)\hat{\beta}_{\Lambda_b}\right)\;. \tag{5.44}$$

The $\hat{E}_\Lambda$ spectrum depends on $\hat{E}_{\Lambda_b}$, the energy of the decaying Λ_b. The energy spectrum of B mesons produced on the Z-pole has been measured at LEP [58]. The average energy is around 70% of half the center of mass energy. As argued in [188] the average energies of mesons and baryons should be very similar and we therefore expect an average energy of Λ_b baryons of around (30-35) GeV, however, with a distribution that covers also much smaller and much larger values.

We find that the differential branching ratio (5.39) scales to a very good approximation with the Λ_b energy, i.e. its shape is approximately invariant if plotted as a function of $\hat{E}_\Lambda/\hat{E}_{\Lambda_b}$. For illustration, we show in figure 5.7 the differential branching ratio as a function of the Λ energy in the lab frame for a fixed $\hat{E}_{\Lambda_b} = 10\; m_{\Lambda_b} \simeq 56\,\text{GeV}$. The four panels correspond to four benchmark cases for the Wilson coefficients: $C_L = C_L^{\text{SM}}$, $C_R = 0$ (top left), $C_L = 0$, $C_R = C_L^{\text{SM}}$ (top right), $C_L = 2C_R = C_L^{\text{SM}}$ (bottom left), and $C_L = C_R = C_L^{\text{SM}}$ (bottom right). The peak of the distributions is at a Λ energy of around $\hat{E}_\Lambda \simeq 0.2 \times \hat{E}_{\Lambda_b}$ in all cases. The distribution is much broader if both C_L and C_R are present.

The distributions for purely left-chiral interactions (top left) and purely right-chiral interactions (top right) are very similar. This result indicates that the effect of the forward backward asymmetry (that maximally distinguishes between the left-chiral and right-chiral scenarios, see figure 5.5) is largely washed out in the lab frame. Dedicated sensitivity studies are required to determine to which extent a lab frame analysis could recover information about the chirality structure, or if a Λ_b rest frame analysis can provide much better sensitivity.

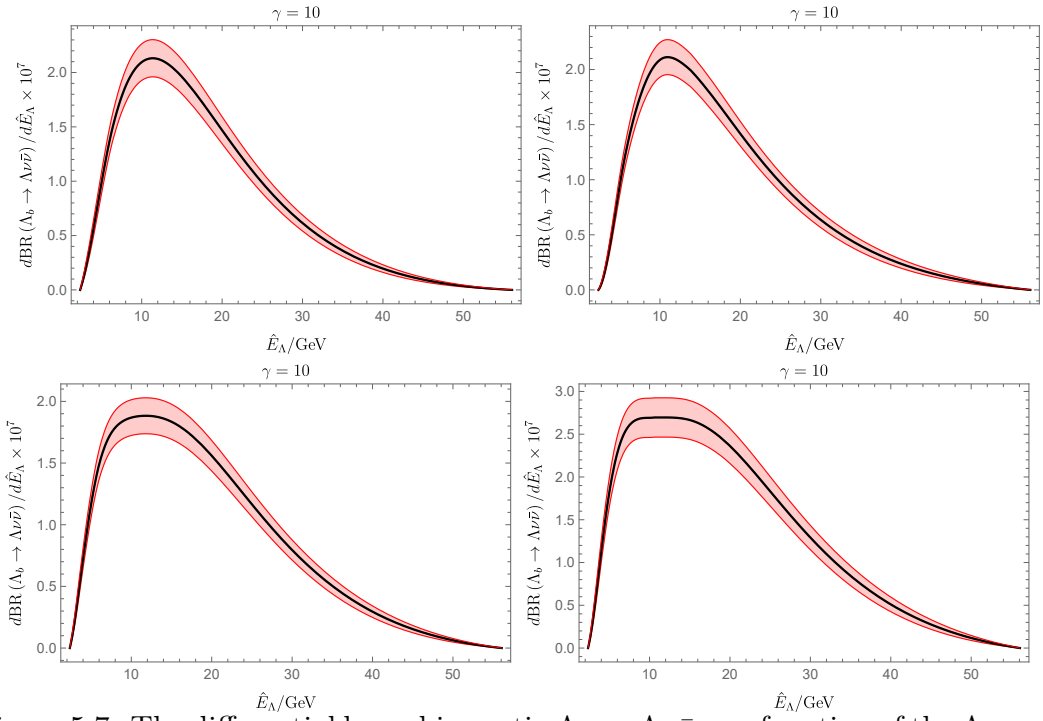

Figure 5.7: The differential branching ratio $\Lambda_b \to \Lambda\nu\bar{\nu}$ as a function of the Λ energy in the lab frame. For illustration, we set the Λ_b energy to $\hat{E}_{\Lambda_b} = 10\, m_{\Lambda_b} \simeq 56\,\mathrm{GeV}$. We show a few benchmark cases: $C_L = C_L^{\mathrm{SM}}$, $C_R = 0$ (top left), $C_L = 0$, $C_R = C_L^{\mathrm{SM}}$ (top right), $C_L = 2C_R = C_L^{\mathrm{SM}}$ (bottom left), and $C_L = C_R = C_L^{\mathrm{SM}}$ (bottom right). The shaded band corresponds to the 1σ theory uncertainty on the branching ratio.

5.2.6 Conclusions

In this paper, we explored the new physics sensitivity of the rare decay $\Lambda_b \to \Lambda\nu\bar{\nu}$. The decay has never been observed but can be accessed at future Z-pole machines like FCC-ee and CEPC. In contrast to the mesonic counterparts ($B \to K\nu\bar{\nu}$, $B \to K^*\nu\bar{\nu}$, and $B_s \to \phi\nu\bar{\nu}$), Λ_b baryons produced in Z decays are longitudinally polarized, which offers complementary novel observables to test the Standard Model.

The kinematics of the Λ baryon in the final state depends on two independent variables, its energy and the angle between its momentum and the spin of the Λ_b. We find that the corresponding angular decay distribution is characterized by a forward-backward asymmetry, $A_{\mathrm{FB}}^{\uparrow}$, that is proportional to the longitudinal

polarization of the Λ_b. We give state-of-the-art predictions for the integrated branching ratio, $\mathrm{BR}(\Lambda_b \to \Lambda \nu \bar{\nu})$, and the forward-backward asymmetry, $A_{\mathrm{FB}}^{\uparrow}$, in the Standard Model. The uncertainties are dominated by the current knowledge of $\Lambda_b \to \Lambda$ form factors, providing continued motivation to improve baryon form factor calculations on the lattice. We find that the forward-backward asymmetry has a zero crossing at a specific value of the Λ energy, E_Λ (or equivalently of the di-neutrino invariant mass, q^2). Interestingly, the location of the zero-crossing is independent of new physics and therefore can be used as an experimental test of form factor calculations. On the other hand, the q^2 shapes of the differential branching ratio and the forward-backward asymmetry do depend on new physics.

Parameterizing heavy new physics in $\Lambda_b \to \Lambda \nu \bar{\nu}$ by an effective Hamiltonian, we determine the expected new physics sensitivity of future precision measurements of $\Lambda_b \to \Lambda \nu \bar{\nu}$ on the Z-pole. We find that splitting the q^2 region into two bins, one above the $A_{\mathrm{FB}}^{\uparrow}$ zero crossing and one below, greatly enhances the new physics sensitivity, and allows one to break degeneracies in the new physics parameter space. We find that new physics scales of $\Lambda_{\mathrm{NP}} \sim (25 - 45)\,\mathrm{TeV}$ can be probed. This is comparable to the scales that can be probed with other $b \to s \nu \bar{\nu}$ decays and with $b \to s \ell^+ \ell^-$ decays. It would be interesting to extend our study to the $\Lambda_b \to \Lambda \ell^+ \ell^-$ decays on the Z-pole. Also in that case we expect that the longitudinal polarization of the Λ_b gives novel probes of new physics.

An experimental measurement of the forward-backward asymmetry requires reconstruction of the Λ_b rest frame. Because of the presence of the two neutrinos in the final state, this may be challenging. We therefore also explored to which extent information about the forward-backward asymmetry can be accessed from lab frame observables. We find that different values of the forward-backward asymmetry leave only a very mild imprint on the energy distribution of the Λ in the lab frame. More detailed studies are required to determine if a lab frame analysis or a Λ_b rest frame analysis would have better sensitivities.

Acknowledgements

We thank Howard Haber and Jason Nielsen for useful discussions. The research of WA, SAG, and KT is supported by the U.S. Department of Energy grant number DE-SC0010107.

Appendix

5.2.7 Form Factors

In this appendix we give details about our implementation of the $\Lambda_b \to \Lambda$ form factors. We follow [282] and parameterize the form factors using a z-expansion

$$f(q^2) = \frac{1}{1 - q^2/(m^f_{\text{pole}})^2} \sum_n a^f_n z^n \,, \qquad z = \frac{\sqrt{t_+ - q^2} - \sqrt{t_+ - t_0}}{\sqrt{t_+ - q^2} + \sqrt{t_+ - t_0}} \,. \tag{5.45}$$

The parameters t_0 and t_+ are chosen such that the kinematic endpoint q^2_{max} is mapped to $z = 0$, and q^2 values above the BK threshold are mapped onto the unit circle in the complex z plane

$$t_0 = (m_{\Lambda_b} - m_\Lambda)^2 \,, \qquad t_+ = (m_B + m_K)^2 \,. \tag{5.46}$$

The poles that correspond to the lowest relevant B_s mesons are factored out explicitly. The corresponding masses m^f_{pole} and the expansion coefficients a^f_n are taken from [282].

To obtain the form factor uncertainties, we follow the procedure recommended in [282] that takes into account the difference in the results based on z-expansions up to order $n = 1$ and $n = 2$. Figure 5.8 shows all the form factors relevant for our analysis with their 1σ and 2σ uncertainties.

5.3 Chapter Conclusion

This chapter has introduced a novel approach to probing new physics through the rare decay $\Lambda_b \to \Lambda \nu \bar{\nu}$at future Z-pole machines. This work extends the flavor

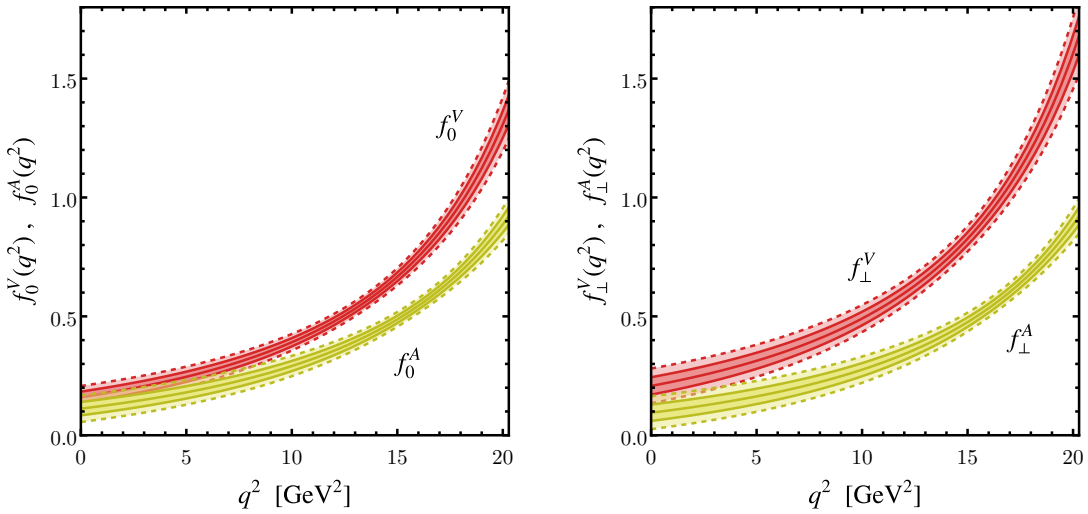

Figure 5.8: The relevant $\Lambda_b \to \Lambda$ form factors as a function of q^2. The colored bands correspond to the 1σ and 2σ uncertainties.

physics program discussed throughout this dissertation into the baryon sector, demonstrating the importance of exploring multiple complementary channels to build a comprehensive understanding of potential new physics affecting flavor-changing processes. The forward-backward asymmetry identified here provides unique sensitivity to the chirality structure of "New Physics" interactions, complementing the observables discussed in previous chapters. The finding that the zero-crossing of this asymmetry is independent of new physics offers a robust test of theoretical form factor calculations, addressing another important aspect of the flavor program: reducing theoretical uncertainties that limit our ability to identify "New Physics" effects.

Chapter 6

Conclusion

Throughout this dissertation, I have presented several novel approaches to probe physics beyond the Standard Model through precision flavor physics. The four studies included in this thesis collectively demonstrate the power of rare processes and precision measurements to provide insights into fundamental physics at energy scales far beyond the direct reach of current colliders.

In Chapter 2, I introduced the Flavorful Supersymmetric Standard Model (FSSM), which can explain the anomalous magnetic moment of the muon with superpartners at the multi-TeV scale. This work highlights how extended Higgs sectors with non-minimal flavor structure can significantly alter the phenomenology of supersymmetric models, providing viable solutions to experimental anomalies while maintaining consistency with direct search constraints.

Chapter 3 explored a supersymmetric implementation of the clockwork mechanism to address the flavor puzzle. This study demonstrated that the mechanism not only generates the observed hierarchical pattern of Standard Model fermion masses and mixings but also induces a characteristic flavor structure in the supersymmetric sector. The resulting constraints from flavor-changing neutral current processes, particularly kaon oscillations, push the scale of supersymmetry breaking into the PeV range, illustrating the power of indirect precision tests to probe extremely high energy scales.

In Chapter 4, I investigated the potential of a future high-energy muon collider

to directly probe the four-fermion contact interactions that might be responsible for the current anomalies in rare B meson decays. This work showed that measurements of the process $\mu^+\mu^- \to bs$ at a 10 TeV muon collider could provide sensitivity to new physics scales approaching 100 TeV, offering a complementary and potentially more powerful probe than rare B decays themselves.

Finally, Chapter 5 presented a novel strategy to search for new physics using the rare decay $\Lambda_b \to \Lambda\nu\bar{\nu}$ at future Z-pole machines. By exploiting the longitudinal polarization of Λ_b baryons produced in Z decays, this work introduced a new observable—the forward-backward asymmetry—that provides unique sensitivity to the chirality structure of potential new physics contributions. This study further enriches our toolkit for exploring physics beyond the Standard Model through precision measurements of rare decays.

The theories in this dissertation suggest specific experimental tests: Belle II and LHCb could probe the FSSM through improved $\tau \to \mu\gamma$ and $\tau \to 3\mu$ measurements reaching 10 sensitivity. Enhanced lattice QCD calculations combined with more precise measurements of kaon CP violation would test the supersymmetric clockwork model's predictions. A multi-TeV muon collider should include $\mu^+\mu^- \to bs$ measurements, using polarized beams to determine chiral structures in $b \to s$ transitions. A future FCC-ee or CEPC could measure the forward-backward asymmetry in $\Lambda_b \to \Lambda\nu\bar{\nu}$ with their expected $\sim 10^{10}$ Z bosons. These experiments would directly test the highlighted theoretical frameworks.

The works presented in this dissertation suggest a coherent roadmap for advancing the flavor physics program in the coming decades. The FSSM framework introduced in Chapter 2 demonstrates that extensions of minimal supersymmetric models can address existing anomalies while predicting specific signatures in lepton flavor violating processes, directing experimental efforts at future B-factories toward targeted measurements of $\tau \to \mu\gamma$ and $\tau \to 3\mu$. Meanwhile, the supersymmetric clockwork model of Chapter 3 establishes a deep connection between the observed pattern of fermion masses and specific signatures in kaon and B-meson oscillations, emphasizing the continued importance of precision measurements in these systems even as direct searches push to higher energies. The studies of

$\mu^+\mu^- \to bs$ production at a muon collider in Chapter 4 and $\Lambda_b \to \Lambda\nu\bar{\nu}$ decays at future Z-factories in Chapter 5 identify novel observables that can distinguish between different chirality structures of potential new physics, highlighting how complementary experiments across energy and intensity frontiers can work in concert to uncover the underlying nature of physics beyond the Standard Model. Together, these works indicate that a comprehensive flavor program requires pursuing multiple approaches simultaneously — from rare decay measurements at dedicated flavor facilities to direct production at high-energy colliders, to developing theoretical frameworks that can connect observations across these diverse experimental contexts.

Collectively, these works emphasize several key themes that will continue to guide the field of particle physics in the coming decades:

1. The complementarity of direct searches at high-energy colliders and precision measurements of rare processes.

2. The importance of developing theoretical frameworks that can connect different experimental anomalies and provide coherent explanations.

3. The potential of future facilities like muon colliders and Z-factories to provide transformative insights into fundamental physics.

4. The value of exploring novel observables and analysis techniques to maximize the physics reach of current and future experiments.

As the field of particle physics enters a new era, with the high-luminosity phase of the LHC on the horizon and plans for next-generation colliders taking shape, the approaches outlined in this dissertation will contribute to our ongoing quest to understand the fundamental laws of nature and uncover physics beyond the Standard Model.

Bibliography

[1] Snowmass muon collider forum. https://snowmass21.org/energy/muon_forum.

[2] Optimisation and performance studies of the ATLAS b-tagging algorithms for the 2017-18 LHC run. 7 2017.

[3] Measurement of $\mathrm{B}_\mathrm{s}^0 \to \mu^+\mu^-$ decay properties and search for the $\mathrm{B}^0 \to \mu\mu$ decay in proton-proton collisions at $\sqrt{s} = 13$ TeV. 2022.

[4] Morad Aaboud et al. Search for new phenomena in dijet events using 37 fb^{-1} of pp collision data collected at $\sqrt{s}$ =13 TeV with the ATLAS detector. *Phys. Rev. D*, 96(5):052004, 2017.

[5] Morad Aaboud et al. Angular analysis of $B_d^0 \to K^*\mu^+\mu^-$ decays in pp collisions at $\sqrt{s} = 8$ TeV with the ATLAS detector. *JHEP*, 10:047, 2018.

[6] Morad Aaboud et al. Measurement of the Higgs boson mass in the $H \to ZZ^* \to 4\ell$ and $H \to \gamma\gamma$ channels with $\sqrt{s} = 13$ TeV pp collisions using the ATLAS detector. *Phys. Lett. B*, 784:345–366, 2018.

[7] Morad Aaboud et al. Study of the rare decays of B_s^0 and B^0 mesons into muon pairs using data collected during 2015 and 2016 with the ATLAS detector. *JHEP*, 04:098, 2019.

[8] Georges Aad et al. Observation of a new particle in the search for the Standard Model Higgs boson with the ATLAS detector at the LHC. *Phys. Lett. B*, 716:1–29, 2012.

[9] Georges Aad et al. Combined Measurement of the Higgs Boson Mass in pp Collisions at $\sqrt{s} = 7$ and 8 TeV with the ATLAS and CMS Experiments. *Phys. Rev. Lett.*, 114:191803, 2015.

[10] Georges Aad et al. Combined measurements of Higgs boson production and decay using up to 80 fb^{-1} of proton-proton collision data at $\sqrt{s} = 13$ TeV collected with the ATLAS experiment. *Phys. Rev.*, D101(1):012002, 2020.

[11] Georges Aad et al. Search for electroweak production of charginos and sleptons decaying into final states with two leptons and missing transverse momentum in $\sqrt{s} = 13$ TeV pp collisions using the ATLAS detector. *Eur. Phys. J.*, C80(2):123, 2020.

[12] Georges Aad et al. Searches for electroweak production of supersymmetric particles with compressed mass spectra in $\sqrt{s} = 13$ TeV pp collisions with the ATLAS detector. *Phys. Rev.*, D101(5):052005, 2020.

[13] Georges Aad et al. A search for the dimuon decay of the Standard Model Higgs boson with the ATLAS detector. *Phys. Lett.*, B812:135980, 2021.

[14] R Aaij et al. Implications of LHCb measurements and future prospects. *Eur. Phys. J.*, C73(4):2373, 2013.

[15] R. Aaij et al. Test of lepton universality with $B^0 \to K^{*0}\ell^+\ell^-$ decays. *JHEP*, 08:055, 2017.

[16] R. Aaij et al. Measurement of lepton universality parameters in $B^+ \to K^+\ell^+\ell^-$ and $B^0 \to K^{*0}\ell^+\ell^-$ decays. *Phys. Rev. D*, 108(3):032002, 2023.

[17] Roel Aaij et al. Measurement of Form-Factor-Independent Observables in the Decay $B^0 \to K^{*0}\mu^+\mu^-$. *Phys. Rev. Lett.*, 111:191801, 2013.

[18] Roel Aaij et al. Differential branching fractions and isospin asymmetries of $B \to K^{(*)}\mu^+\mu^-$ decays. *JHEP*, 06:133, 2014.

[19] Roel Aaij et al. Test of lepton universality using $B^+ \to K^+\ell^+\ell^-$ decays. *Phys. Rev. Lett.*, 113:151601, 2014.

[20] Roel Aaij et al. Differential branching fraction and angular analysis of $\Lambda_b^0 \to \Lambda\mu^+\mu^-$ decays. *JHEP*, 06:115, 2015. [Erratum: JHEP 09, 145 (2018)].

[21] Roel Aaij et al. Search for the lepton flavour violating decay $\tau \to \mu\mu^+\mu$. *JHEP*, 02:121, 2015.

[22] Roel Aaij et al. Angular analysis of the $B^0 \to K^{*0}\mu^+\mu^-$ decay using 3 fb^{-1} of integrated luminosity. *JHEP*, 02:104, 2016.

[23] Roel Aaij et al. Measurements of the S-wave fraction in $B^0 \to K^+\pi^-\mu^+\mu^-$ decays and the $B^0 \to K^*(892)^0\mu^+\mu^-$ differential branching fraction. *JHEP*, 11:047, 2016. [Erratum: JHEP 04, 142 (2017)].

[24] Roel Aaij et al. Observation of the decay $\Lambda_b^0 \to pK^-\mu^+\mu^-$ and a search for *CP* violation. *JHEP*, 06:108, 2017.

[25] Roel Aaij et al. Test of lepton universality with $B^0 \to K^{*0}\ell^+\ell^-$ decays. *JHEP*, 08:055, 2017.

[26] Roel Aaij et al. Angular moments of the decay $\Lambda_b^0 \to \Lambda\mu^+\mu^-$ at low hadronic recoil. *JHEP*, 09:146, 2018.

[27] Roel Aaij et al. Physics case for an LHCb Upgrade II - Opportunities in flavour physics, and beyond, in the HL-LHC era. 8 2018.

[28] Roel Aaij et al. Search for lepton-universality violation in $B^+ \to K^+\ell^+\ell^-$ decays. *Phys. Rev. Lett.*, 122(19):191801, 2019.

[29] Roel Aaij et al. Measurement of CP-Averaged Observables in the $B^0 \to K^{*0}\mu^+\mu^-$ Decay. *Phys. Rev. Lett.*, 125(1):011802, 2020.

[30] Roel Aaij et al. Measurement of the $\Lambda_b^0 \to J/\psi\Lambda$ angular distribution and the Λ_b^0 polarisation in pp collisions. *JHEP*, 06:110, 2020.

[31] Roel Aaij et al. Test of lepton universality with $\Lambda_b^0 \to pK^-\ell^+\ell^-$ decays. *JHEP*, 05:040, 2020.

[32] Roel Aaij et al. Angular Analysis of the $B^+ \to K^{*+}\mu^+\mu^-$ Decay. *Phys. Rev. Lett.*, 126(16):161802, 2021.

[33] Roel Aaij et al. Angular analysis of the rare decay $B_s^0 \to \phi\mu^+\mu^-$. *JHEP*, 11:043, 2021.

[34] Roel Aaij et al. Branching Fraction Measurements of the Rare $B_s^0 \to \phi\mu^+\mu^-$ and $B_s^0 \to f_2'(1525)\mu^+\mu^-$ Decays. *Phys. Rev. Lett.*, 127(15):151801, 2021.

[35] Roel Aaij et al. Test of lepton universality in beauty-quark decays. 3 2021.

[36] Roel Aaij et al. Analysis of Neutral B-Meson Decays into Two Muons. *Phys. Rev. Lett.*, 128(4):041801, 2022.

[37] Roel Aaij et al. Differential branching fraction and angular moments analysis of the decay $B^0 \to K^+\pi^-\mu^+\mu^-$ at low hadronic recoil. *JHEP*, 05:044, 2022.

[38] Roel Aaij et al. Measurement of lepton universality parameters in $B^+ \to K^+\ell^+\ell^-$ and $B^0 \to K^{*0}\ell^+\ell^-$ decays. *Phys. Rev. D*, 108(3):032002, 2023.

[39] Roel Aaij et al. Measurement of the $\Lambda_b^0 \to \Lambda(1520)\mu^+\mu^-$ Differential Branching Fraction. *Phys. Rev. Lett.*, 131(15):151801, 2023.

[40] Roel Aaij et al. Test of lepton universality in $b \to s\ell^+\ell^-$ decays. *Phys. Rev. Lett.*, 131(5):051803, 2023.

[41] Roel Aaij et al. Amplitude Analysis of the $B^0 \to K^{*0}\mu^+\mu^-$ Decay. *Phys. Rev. Lett.*, 132(13):131801, 2024.

[42] Roel Aaij et al. Analysis of $\Lambda_b^0 \to pK^-\mu^+\mu^-$ decays. 9 2024.

[43] Roel Aaij et al. Comprehensive analysis of local and nonlocal amplitudes in the $B^0 \to K^{*0}\mu^+\mu^-$ decay. *JHEP*, 09:026, 2024.

[44] Roel Aaij et al. Determination of short- and long-distance contributions in $B^0 \to K^{*0}\mu^+\mu^-$ decays. *Phys. Rev. D*, 109(5):052009, 2024.

[45] Roel Aaij et al. Test of lepton flavour universality with $B_s^0 \to \phi\ell^+\ell^-$ decays. 10 2024.

[46] T. Aaltonen et al. Search for $B_s^0 \to \mu^+\mu^-$ and $B^0 \to \mu^+\mu^-$ Decays with CDF II. *Phys. Rev. Lett.*, 107:191801, 2011. [Addendum: Phys.Rev.Lett. 107, 239903 (2011)].

[47] S. Abachi et al. Search for high mass top quark production in $p\bar{p}$ collisions at $\sqrt{s} = 1.8$ TeV. *Phys. Rev. Lett.*, 74:2422–2426, 1995.

[48] A. Abada et al. FCC-ee: The Lepton Collider: Future Circular Collider Conceptual Design Report Volume 2. *Eur. Phys. J. ST*, 228(2):261–623, 2019.

[49] A. Abada et al. FCC-ee: The Lepton Collider: Future Circular Collider Conceptual Design Report Volume 2. *Eur. Phys. J. ST*, 228(2):261–623, 2019.

[50] Kevork N. Abazajian. Sterile neutrinos in cosmology. *Phys. Rept.*, 711-712:1–28, 2017.

[51] Kevork N. Abazajian et al. Light Sterile Neutrinos: A White Paper. 4 2012.

[52] G. Abbiendi et al. Measurement of the average polarization of b baryons in hadronic Z^0 decays. *Phys. Lett. B*, 444:539–554, 1998.

[53] J. Abdallah et al. Study of tau-pair production in photon-photon collisions at LEP and limits on the anomalous electromagnetic moments of the tau lepton. *Eur. Phys. J.*, C35:159–170, 2004.

[54] J. Abdallah et al. Determination of $A_{\rm FB}^b$ at the Z pole using inclusive charge reconstruction and lifetime tagging. *Eur. Phys. J. C*, 40:1–25, 2005.

[55] A. Abdesselam et al. Search for lepton-flavor-violating tau decays to $\ell\gamma$ modes at Belle. 2021.

[56] Murat Abdughani, Yi-Zhong Fan, Lei Feng, Yue-Lin Sming Tsai, Lei Wu, and Qiang Yuan. A common origin of muon g-2 anomaly, Galaxy Center GeV excess and AMS-02 anti-proton excess in the NMSSM. 4 2021.

[57] F. Abe et al. Observation of top quark production in $\bar{p}p$ collisions. *Phys. Rev. Lett.*, 74:2626–2631, 1995.

[58] K. Abe et al. Measurement of the B hadron energy distribution in Z0 decays. *Phys. Rev. D*, 56:5310–5319, 1997.

[59] T. Abe et al. Belle II Technical Design Report. 11 2010.

[60] B. Abi et al. Measurement of the Positive Muon Anomalous Magnetic Moment to 0.46 ppm. *Phys. Rev. Lett.*, 126(14):141801, 2021.

[61] Amin Aboubrahim, Michael Klasen, and Pran Nath. What Fermilab $(g-2)_\mu$ experiment tells us about discovering SUSY at HL-LHC and HE-LHC. 4 2021.

[62] P. Abreu et al. Λ_b polarization in Z^0 decays at LEP. *Phys. Lett. B*, 474:205–222, 2000.

[63] Fernando Abreu de Souza and Gero von Gersdorff. A Random Clockwork of Flavor. *JHEP*, 02:186, 2020.

[64] Chiara Accettura et al. Towards a Muon Collider. 3 2023.

[65] I. Adachi et al. Evidence for B+→K+$\nu\nu^-$ decays. *Phys. Rev. D*, 109(11):112006, 2024.

[66] Jason Aebischer, Christoph Bobeth, Andrzej J. Buras, and Jacky Kumar. SMEFT ATLAS of ΔF = 2 transitions. *JHEP*, 12:187, 2020.

[67] Jason Aebischer, Jacky Kumar, and David M. Straub. Wilson: a Python package for the running and matching of Wilson coefficients above and below the electroweak scale. *Eur. Phys. J. C*, 78(12):1026, 2018.

[68] Latika Aggarwal et al. Snowmass White Paper: Belle II physics reach and plans for the next decade and beyond. 7 2022.

[69] N. Aghanim et al. Planck 2018 results. I. Overview and the cosmological legacy of Planck. *Astron. Astrophys.*, 641:A1, 2020.

[70] N. Aghanim et al. Planck 2018 results. VI. Cosmological parameters. *Astron. Astrophys.*, 641:A6, 2020.

[71] Prateek Agrawal, Gustavo Marques-Tavares, and Wei Xue. Opening up the QCD axion window. *JHEP*, 03:049, 2018.

[72] Aqeel Ahmed and Barry M. Dillon. Clockwork Goldstone Bosons. *Phys. Rev. D*, 96(11):115031, 2017.

[73] Chiara Aime et al. Muon Collider Physics Summary. 3 2022.

[74] Hind Al Ali et al. The Muon Smasher's Guide. 3 2021.

[75] T. Albahri et al. Measurement of the anomalous precession frequency of the muon in the Fermilab Muon $g-2$ experiment. *Phys. Rev. D*, 103(7):072002, 2021.

[76] Marcel Algueró, Aritra Biswas, Bernat Capdevila, Sébastien Descotes-Genon, Joaquim Matias, and Martín Novoa-Brunet. To (b)e or not to (b)e: no electrons at LHCb. *Eur. Phys. J. C*, 83(8):648, 2023.

[77] Marcel Algueró, Bernat Capdevila, Sébastien Descotes-Genon, Joaquim Matias, and Martín Novoa-Brunet. $b \to s\ell^+\ell^-$ global fits after R_{K_S} and $R_{K^{*+}}$ LHCb measurements. *Eur. Phys. J. C*, 82(4):326, 2022.

[78] T. M. Aliev, K. Azizi, and M. Savci. Analysis of the $\Lambda_b \to \Lambda\ell^+\ell^-$ decay in QCD. *Phys. Rev. D*, 81:056006, 2010.

[79] T. M. Aliev and M. Savci. Unparticle physics effects in $\Lambda_b \to \Lambda+$ missing energy processes. *Phys. Lett. B*, 662:165–177, 2008.

[80] Ben Allanach and Joe Davighi. The Rumble in the Meson: a leptoquark versus a Z' to fit $b \to s\mu^+\mu^-$ anomalies including 2022 LHCb $R_{K^{(*)}}$ measurements. 11 2022.

[81] Ben Allanach and Anna Mullin. Plan B: New Z' models for $b \to sl^+l^-$ anomalies. 6 2023.

[82] Lukas Allwicher, Damir Becirevic, Gioacchino Piazza, Salvador Rosauro-Alcaraz, and Olcyr Sumensari. Understanding the first measurement of $B(B \to K\nu\bar{\nu})$. *Phys. Lett. B*, 848:138411, 2024.

[83] Lukas Allwicher, Marzia Bordone, Gino Isidori, Gioacchino Piazza, and Alfredo Stanzione. Probing third-generation New Physics with $K \to \pi\nu\bar{\nu}$ and $B \to K^{(*)}\nu\bar{\nu}$. 10 2024.

[84] Daniel Aloni, Pouya Asadi, Yuichiro Nakai, Matthew Reece, and Motoo Suzuki. Spontaneous CP Violation and Horizontal Symmetry in the MSSM: Toward Lepton Flavor Naturalness. 4 2021.

[85] R. Alonso, E. Fernandez Martinez, M. B. Gavela, B. Grinstein, L. Merlo, and P. Quilez. Gauged Lepton Flavour. *JHEP*, 12:119, 2016.

[86] Rodrigo Alonso, Adrian Carmona, Barry M. Dillon, Jernej F. Kamenik, Jorge Martin Camalich, and Jure Zupan. A clockwork solution to the flavor puzzle. *JHEP*, 10:099, 2018.

[87] Rodrigo Alonso, Benjamin Grinstein, and Jorge Martin Camalich. SU(2) $\times$ U(1) gauge invariance and the shape of new physics in rare B decays. *Phys. Rev. Lett.*, 113:241802, 2014.

[88] Rodrigo Alonso, Elizabeth E. Jenkins, Aneesh V. Manohar, and Michael Trott. Renormalization Group Evolution of the Standard Model Dimension Six Operators III: Gauge Coupling Dependence and Phenomenology. *JHEP*, 04:159, 2014.

[89] Cristiano Alpigiani, Alexander Belyaev, Andrzej J. Buras, Miguel Carrolo, Gloria Corti, Vincent Fortin-Martel, Dan Kelly, Ilya Komarov, Anastasiia Kozachuk, Alexey A. Petrov, and Yuri Shirman. Flavour physics and CP violation. 12 2018.

[90] Richard Altendorfer, Jonathan Bagger, and Dennis Nemeschansky. Supersymmetric Randall-Sundrum scenario. *Phys. Rev. D*, 63:125025, 2001.

[91] W. Altmannshofer et al. The Belle II Physics Book. *PTEP*, 2019(12):123C01, 2019. [Erratum: PTEP 2020, 029201 (2020)].

[92] Wolfgang Altmannshofer and Flavio Archilli. Rare decays of b and c hadrons. In *2022 Snowmass Summer Study*, 6 2022.

[93] Wolfgang Altmannshofer, Andrzej J. Buras, Stefania Gori, Paride Paradisi, and David M. Straub. Anatomy and Phenomenology of FCNC and CPV Effects in SUSY Theories. *Nucl. Phys. B*, 830:17–94, 2010.

[94] Wolfgang Altmannshofer, Andrzej J. Buras, and Diego Guadagnoli. The MFV limit of the MSSM for low tan(beta): Meson mixings revisited. *JHEP*, 11:065, 2007.

[95] Wolfgang Altmannshofer, Andrzej J. Buras, David M. Straub, and Michael Wick. New strategies for New Physics search in $B \to K^* \nu\bar{\nu}$, $B \to K \nu\bar{\nu}$ and $B \to X_s \nu\bar{\nu}$ decays. *JHEP*, 04:022, 2009.

[96] Wolfgang Altmannshofer, Andreas Crivellin, Huw Haigh, Gianluca Inguglia, and Jorge Martin Camalich. Light new physics in $B \to K^{(*)} \nu\bar{\nu}$? *Phys. Rev. D*, 109(7):075008, 2024.

[97] Wolfgang Altmannshofer, Joe Davighi, and Marco Nardecchia. Gauging the accidental symmetries of the standard model, and implications for the flavor anomalies. *Phys. Rev. D*, 101(1):015004, 2020.

[98] Wolfgang Altmannshofer, Joshua Eby, Stefania Gori, Matteo Lotito, Mario Martone, and Douglas Tuckler. Collider Signatures of Flavorful Higgs Bosons. *Phys. Rev.*, D94(11):115032, 2016.

[99] Wolfgang Altmannshofer et al. Evidence for $B^+ \to K^+ \nu\bar{\nu}$ decays. 12 2023.

[100] Wolfgang Altmannshofer, Claudia Frugiuele, and Roni Harnik. Fermion Hierarchy from Sfermion Anarchy. *JHEP*, 12:180, 2014.

[101] Wolfgang Altmannshofer and Sri Aditya Gadam. A Supersymmetric Flavor Clockwork. *JHEP*, 07:188, 2022.

[102] Wolfgang Altmannshofer, Sri Aditya Gadam, Stefania Gori, and Nick Hamer. Explaining $(g-2)_\mu$ with Multi-TeV Sleptons. *JHEP*, 07:164, 2021.

[103] Wolfgang Altmannshofer, Sri Aditya Gadam, and Stefano Profumo. Snowmass White Paper: Probing New Physics with $\mu^+\mu^- \to bs$ at a Muon Collider. In *2022 Snowmass Summer Study*, 3 2022.

[104] Wolfgang Altmannshofer, Sri Aditya Gadam, and Stefano Profumo. Probing new physics with $\mu^+\mu^- \to bs$ at a muon collider. *Phys. Rev. D*, 108(11):115033, 2023.

[105] Wolfgang Altmannshofer, Sri Aditya Gadam, and Kevin Toner. New Strategies for New Physics Search with $\Lambda_b \to \Lambda\nu\bar{\nu}$ Decays. 1 2024.

[106] Wolfgang Altmannshofer, Stefania Gori, Alexander L. Kagan, Luca Silvestrini, and Jure Zupan. Uncovering Mass Generation Through Higgs Flavor Violation. *Phys. Rev.*, D93(3):031301, 2016.

[107] Wolfgang Altmannshofer, Stefania Gori, Maxim Pospelov, and Itay Yavin. Quark flavor transitions in $L_\mu - L_\tau$ models. *Phys. Rev. D*, 89:095033, 2014.

[108] Wolfgang Altmannshofer, Stefania Gori, Dean J. Robinson, and Douglas Tuckler. The Flavor-locked Flavorful Two Higgs Doublet Model. *JHEP*, 03:129, 2018.

[109] Wolfgang Altmannshofer, Roni Harnik, and Jure Zupan. Low Energy Probes of PeV Scale Sfermions. *JHEP*, 11:202, 2013.

[110] Wolfgang Altmannshofer and Brian Maddock. Flavorful Two Higgs Doublet Models with a Twist. *Phys. Rev.*, D98(7):075005, 2018.

[111] Wolfgang Altmannshofer, Brian Maddock, and Douglas Tuckler. Rare Top Decays as Probes of Flavorful Higgs Bosons. *Phys. Rev.*, D100(1):015003, 2019.

[112] Wolfgang Altmannshofer, Christoph Niehoff, Peter Stangl, David M. Straub, and Jure Zupan. Status of the $B \to K^* \mu^+ \mu^-$ anomaly after Moriond 2017. *Eur. Phys. J. C*, 77(6):377, 2017.

[113] Wolfgang Altmannshofer, Christoph Niehoff, and David M. Straub. $B_s \to \mu^+ \mu^-$ as current and future probe of new physics. *JHEP*, 05:076, 2017.

[114] Wolfgang Altmannshofer, Paride Paradisi, and David M. Straub. Model-Independent Constraints on New Physics in $b \to s$ Transitions. *JHEP*, 04:008, 2012.

[115] Wolfgang Altmannshofer and Shibasis Roy. A joint explanation of the $B \to \pi K$ puzzle and the $B \to K \nu \bar{\nu}$ excess. 11 2024.

[116] Wolfgang Altmannshofer and Peter Stangl. New physics in rare B decays after Moriond 2021. *Eur. Phys. J. C*, 81(10):952, 2021.

[117] Wolfgang Altmannshofer, Peter Stangl, and David M. Straub. Interpreting Hints for Lepton Flavor Universality Violation. *Phys. Rev. D*, 96(5):055008, 2017.

[118] Wolfgang Altmannshofer and David M. Straub. Viability of MSSM scenarios at very large $\tan\beta$. *JHEP*, 09:078, 2010.

[119] Wolfgang Altmannshofer and David M. Straub. New Physics in $B \to K^* \mu\mu$? *Eur. Phys. J. C*, 73:2646, 2013.

[120] J. Alwall, R. Frederix, S. Frixione, V. Hirschi, F. Maltoni, O. Mattelaer, H. S. Shao, T. Stelzer, P. Torrielli, and M. Zaro. The automated computation of tree-level and next-to-leading order differential cross sections, and their matching to parton shower simulations. *JHEP*, 07:079, 2014.

[121] Y. Amhis et al. Averages of b-hadron, c-hadron, and τ-lepton properties as of 2018. *Eur. Phys. J. C*, 81:226, 2021.

[122] Yasmine Amhis, Marzia Bordone, and Méril Reboud. Dispersive analysis of $\Lambda_b \to \Lambda(1520)$ local form factors. *JHEP*, 02:010, 2023.

[123] Yasmine Amhis, Sébastien Descotes-Genon, Carla Marin Benito, Martín Novoa-Brunet, and Marie-Hélène Schune. Prospects for New Physics searches with $\Lambda_b^0 \to \Lambda(1520)\ell^+\ell^-$ decays. *Eur. Phys. J. Plus*, 136(6):614, 2021.

[124] Yasmine Amhis, Matthew Kenzie, Méril Reboud, and Aidan R. Wiederhold. Prospects for searches of $b \to s\nu\overline{\nu}$ decays at FCC-ee. *JHEP*, 01:144, 2024.

[125] Yasmine Sara Amhis et al. Averages of b-hadron, c-hadron, and τ-lepton properties as of 2021. *Phys. Rev. D*, 107(5):052008, 2023.

[126] Andrei Angelescu, Damir Bečirević, Darius A. Faroughy, Florentin Jaffredo, and Olcyr Sumensari. Single leptoquark solutions to the B-physics anomalies. *Phys. Rev. D*, 104(5):055017, 2021.

[127] Florian Angelescu, Damir Bečirević, Darius A. Faroughy, and Olcyr Sumensari. On the single leptoquark solutions to the B-physics anomalies. *JHEP*, 10:183, 2018.

[128] Charles M. Ankenbrandt et al. Status of muon collider research and development and future plans. *Phys. Rev. ST Accel. Beams*, 2:081001, 1999.

[129] Ignatios Antoniadis, Nima Arkani-Hamed, Savas Dimopoulos, and G.R. Dvali. New dimensions at a millimeter to a Fermi and superstrings at a TeV. *Phys. Lett. B*, 436:257–263, 1998.

[130] S. Aoki et al. FLAG Review 2019: Flavour Lattice Averaging Group (FLAG). *Eur. Phys. J. C*, 80(2):113, 2020.

[131] Y. Aoki et al. FLAG Review 2021. *Eur. Phys. J. C*, 82(10):869, 2022.

[132] T. Aoyama et al. The anomalous magnetic moment of the muon in the Standard Model. *Phys. Rept.*, 887:1–166, 2020.

[133] Tatsumi Aoyama, Masashi Hayakawa, Toichiro Kinoshita, and Makiko Nio. Complete Tenth-Order QED Contribution to the Muon g-2. *Phys. Rev. Lett.*, 109:111808, 2012.

[134] Tatsumi Aoyama, Toichiro Kinoshita, and Makiko Nio. Theory of the anomalous magnetic moment of the electron. *Atoms*, 7(1), 2019.

[135] F. Arias-Aragón, C. Bouthelier-Madre, J. M. Cano, and L. Merlo. Data Driven Flavour Model. *Eur. Phys. J. C*, 80(9):854, 2020.

[136] Nima Arkani-Hamed, Savas Dimopoulos, and Gia Dvali. The Hierarchy problem and new dimensions at a millimeter. *Phys. Lett. B*, 429:263–272, 1998.

[137] Nima Arkani-Hamed, Arpit Gupta, David E. Kaplan, Neal Weiner, and Tom Zorawski. Simply Unnatural Supersymmetry. 12 2012.

[138] Nima Arkani-Hamed and Martin Schmaltz. Hierarchies without symmetries from extra dimensions. *Phys. Rev. D*, 61:033005, 2000.

[139] Asimina Arvanitaki, Nathaniel Craig, Savas Dimopoulos, and Giovanni Villadoro. Mini-Split. *JHEP*, 02:126, 2013.

[140] Pouya Asadi, Rodolfo Capdevilla, Cari Cesarotti, and Samuel Homiller. Searching for leptoquarks at future muon colliders. *JHEP*, 10:182, 2021.

[141] Andreas Athenodorou and Emmanuel Tziligakis. MSSM predictions for the muon anomalous magnetic moment. *Phys. Rev. D*, 104(3):035009, 2021.

[142] Peter Athron, Csaba Balázs, Emanuele Bagnaschi, Andy Buckley, Marcin Chrząszcz, Jan Conrad, Jonathan M. Cornell, Lars A. Dal, Matthias Danninger, Benjamin Farmer, Tomás E. Gonzalo, Julia Harz, Prasanth S. Krishnamurthy, Anders Kvellestad, Farvah Mahmoudi, Gregory D. Martinez, Antje Putze, Are Raklev, Christopher Rogan, Aldo Saavedra, Christopher Savage, Pat Scott, Nishita Seif, Pranav Sharma, Christoph Weniger, Martin White, et al. Combined collider constraints on neutralinos and charginos. *Eur. Phys. J. C*, 81(11):992, 2021.

[143] Peter Athron, Csaba Balázs, Daniel H. Jacob, Wojciech Kotlarski, Dominik Stöckinger, and Hyejung Stöckinger-Kim. New physics explanations of a_μ in light of the FNAL muon $g-2$ measurement. *JHEP*, 09:080, 2021.

[144] Bernard Aubert et al. Searches for Lepton Flavor Violation in the Decays $\tau^\pm \to e^\pm\gamma$ and $\tau^\pm \to \mu^\pm\gamma$. *Phys. Rev. Lett.*, 104:021802, 2010.

[145] Christopher Aubin, Thomas Blum, Cheng Tu, Maarten Golterman, Chulwoo Jung, and Santiago Peris. Light quark vacuum polarization at the physical point and contribution to the muon $g-2$. *Phys. Rev.*, D101(1):014503, 2020.

[146] Anastasios Avgoustidis, Florian Niedermann, Antonio Padilla, and Paul M. Saffin. Deconstructing higher order clockwork gravity. 10 2020.

[147] Aleksandr Azatov, Francesco Garosi, Admir Greljo, David Marzocca, Julian Salko, and Sokratis Trifinopoulos. New physics in $b \to s\mu\mu$: FCC-hh or a muon collider? *JHEP*, 10:149, 2022.

[148] K. S. Babu and Shaikh Saad. Flavor Hierarchies from Clockwork in SO(10) GUT. *Phys. Rev. D*, 103(1):015009, 2021.

[149] K.S. Babu. TASI Lectures on Flavor Physics. 10 2009.

[150] K.S. Babu, Durga Das, and Sudip Jana. Two-Loop Neutrino Mass Generation and its Experimental Tests. *Phys. Rev. D*, 97(11):115037, 2018.

[151] Markus Bach, Jae-hyeon Park, Dominik Stöckinger, and Hyejung Stöckinger-Kim. Large muon $(g-2)$ with TeV-scale SUSY masses for $\tan\beta \to \infty$. *JHEP*, 10:026, 2015.

[152] Kyu Jung Bae and Sang Hui Im. Supersymmetric Clockwork Axion Model and Axino Dark Matter. *Phys. Rev. D*, 102(1):015011, 2020.

[153] Z. Bai, N. H. Christ, T. Izubuchi, C. T. Sachrajda, A. Soni, and J. Yu. $K_L - K_S$ Mass Difference from Lattice QCD. *Phys. Rev. Lett.*, 113:112003, 2014.

[154] Jon A. Bailey et al. $B \to Kl^+l^-$ Decay Form Factors from Three-Flavor Lattice QCD. *Phys. Rev. D*, 93(2):025026, 2016.

[155] Michael J. Baker and Andrea Thamm. Leptonic WIMP Coannihilation and the Current Dark Matter Search Strategy. *JHEP*, 10:187, 2018.

[156] B.S. Balakrishna, Alexander L. Kagan, and Rabindra N. Mohapatra. Quark Mixings and Mass Hierarchy From Radiative Corrections. *Phys. Lett. B*, 205:345–352, 1988.

[157] A. M. Baldini et al. Search for the lepton flavour violating decay $\mu^+ \to e^+\gamma$ with the full dataset of the MEG experiment. *Eur. Phys. J. C*, 76(8):434, 2016.

[158] Christopher Balzereit, Thomas Mannel, and Benedikt Plumper. The Renormalization group evolution of the CKM matrix. *Eur. Phys. J. C*, 9:197–211, 1999.

[159] Riccardo Barbieri, Christopher W. Murphy, and Ennio Salvioni. B-decay anomalies in a composite leptoquark model. *Phys. Lett. B*, 766:317–323, 2017.

[160] Martin Bauer, Marcela Carena, and Katrin Gemmler. Flavor from the Electroweak Scale. *JHEP*, 11:016, 2015.

[161] Sebastian Baum, Marcela Carena, Nausheen R. Shah, and Carlos E. M. Wagner. The Tiny (g-2) Muon Wobble from Small-μ Supersymmetry. 4 2021.

[162] Rigo Bause, Hector Gisbert, Marcel Golz, and Gudrun Hiller. Interplay of dineutrino modes with semileptonic rare B-decays. *JHEP*, 12:061, 2021.

[163] Rigo Bause, Hector Gisbert, and Gudrun Hiller. Implications of an enhanced $B \to K\nu\bar{\nu}$ branching ratio. *Phys. Rev. D*, 109(1):015006, 2024.

[164] Anja Beck, Thomas Blake, and Michal Kreps. Angular distribution of $\Lambda_b^0 \to pK^-\ell^+\ell^-$ decays comprising Λ resonances with spin $\leq 5/2$. *JHEP*, 02:189, 2023.

[165] G. W. Bennett et al. Final Report of the Muon E821 Anomalous Magnetic Moment Measurement at BNL. *Phys. Rev. D*, 73:072003, 2006.

[166] Alexander Berezhnoy and Dmitri Melikhov. $B \to K^* M_X$ vs $B \to K M_X$ as a probe of a scalar-mediator dark matter scenario. *EPL*, 145(1):14001, 2024.

[167] Gregorio Bernardi et al. The Future Circular Collider: a Summary for the US 2021 Snowmass Process. 3 2022.

[168] Gianfranco Bertone, Dan Hooper, and Joseph Silk. Particle dark matter: Evidence, candidates and constraints. *Phys. Rept.*, 405:279–390, 2005.

[169] Siegfried Bethke. World Summary of α_s (2012). *Nucl. Phys. B Proc. Suppl.*, 234:229–234, 2013.

[170] D. Bečirević, G. Piazza, and O. Sumensari. Revisiting $B \to K^{(*)}\nu\bar{\nu}$ decays in the Standard Model and beyond. *Eur. Phys. J. C*, 83(3):252, 2023.

[171] Damir Bečirević, Olcyr Sumensari, and Renata Zukanovich Funchal. Lepton flavor violation in exclusive $b \to s$ decays. *Eur. Phys. J. C*, 76(3):134, 2016.

[172] Simone Bifani, Sébastien Descotes-Genon, Antonio Romero Vidal, and Marie-Hélène Schune. Review of Lepton Universality tests in B decays. *J. Phys. G*, 46(2):023001, 2019.

[173] Innes Bigaran and Raymond R. Volkas. Getting chirality right: Single scalar leptoquark solutions to the $(g-2)_{e,\mu}$ puzzle. *Phys. Rev. D*, 102(7):075037, 2020.

[174] Johan Bijnens, Nils Hermansson-Truedsson, and Antonio Rodríguez-Sánchez. Short-distance constraints for the HLbL contribution to the muon anomalous magnetic moment. *Phys. Lett.*, B798:134994, 2019.

[175] K. M. Black et al. Muon Collider Forum Report. 9 2022.

[176] Thomas Blake and Michal Kreps. Angular distribution of polarised Λ_b baryons decaying to $\Lambda\ell^+\ell^-$. *JHEP*, 11:138, 2017.

[177] Thomas Blake, Gaia Lanfranchi, and David M. Straub. Rare B Decays as Tests of the Standard Model. *Prog. Part. Nucl. Phys.*, 92:50–91, 2017.

[178] Thomas Blake, Stefan Meinel, Muslem Rahimi, and Danny van Dyk. Dispersive bounds for local form factors in $\Lambda_b \to \Lambda$ transitions. *Phys. Rev. D*, 108(9):094509, 2023.

[179] Thomas Blake, Stefan Meinel, and Danny van Dyk. Bayesian Analysis of $b \to s\mu^+\mu^-$ Wilson Coefficients using the Full Angular Distribution of $\Lambda_b \to \Lambda(\to p\,\pi^-)\mu^+\mu^-$ Decays. *Phys. Rev. D*, 101(3):035023, 2020.

[180] Gianluca Blankenburg, John Ellis, and Gino Isidori. Flavour-Changing Decays of a 125 GeV Higgs-like Particle. *Phys. Lett. B*, 712:386–390, 2012.

[181] Andrew E. Blechman, Alexey A. Petrov, and Gagik Yeghiyan. The Flavor puzzle in multi-Higgs models. *JHEP*, 11:075, 2010.

[182] T. Blum, P. A. Boyle, V. Gülpers, T. Izubuchi, L. Jin, C. Jung, A. Jüttner, C. Lehner, A. Portelli, and J. T. Tsang. Calculation of the hadronic vacuum

polarization contribution to the muon anomalous magnetic moment. *Phys. Rev. Lett.*, 121(2):022003, 2018.

[183] Thomas Blum, Norman Christ, Masashi Hayakawa, Taku Izubuchi, Luchang Jin, Chulwoo Jung, and Christoph Lehner. The hadronic light-by-light scattering contribution to the muon anomalous magnetic moment from lattice QCD. *Phys. Rev. Lett.*, 124(13):132002, 2020.

[184] Arushi Bodas, Rupert Coy, and Simon J. D. King. Solving the electron and muon $g-2$ anomalies in Z' models. *Eur. Phys. J. C*, 81(12):1065, 2021.

[185] Philipp Böer, Thorsten Feldmann, and Danny van Dyk. Angular Analysis of the Decay $\Lambda_b \to \Lambda(\to N\pi)\ell^+\ell^-$. *JHEP*, 01:155, 2015.

[186] Patrick D. Bolton, Svjetlana Fajfer, Jernej F. Kamenik, and Martín Novoa-Brunet. Signatures of light new particles in $B \to K^{(*)} + E_{\rm miss}$. *Phys. Rev. D*, 110(5):055001, 2024.

[187] Quentin Bonnefoy, Emilian Dudas, and Stefan Pokorski. Axions in a highly protected gauge symmetry model. *Eur. Phys. J. C*, 79(1):31, 2019.

[188] G. Bonvicini and Lisa Randall. Optimized variables for the study of Lambda(b) polarization. *Phys. Rev. Lett.*, 73:392–395, 1994.

[189] Marzia Bordone. Heavy Quark Expansion of $\Lambda_b \to \Lambda^*(1520)$ Form Factors beyond Leading Order. *Symmetry*, 13(4):531, 2021.

[190] Marzia Bordone, Gino isidori, Sandro Mächler, and Arianna Tinari. Short- vs. long-distance physics in $B \to K^{(*)}\ell^+\ell^-$: a data-driven analysis. *Eur. Phys. J. C*, 84(5):547, 2024.

[191] Marzia Bordone, Gino Isidori, and Andrea Pattori. On the Standard Model predictions for R_K and R_{K^*}. *Eur. Phys. J. C*, 76(8):440, 2016.

[192] Sz. Borsanyi et al. Hadronic vacuum polarization contribution to the anomalous magnetic moments of leptons from first principles. *Phys. Rev. Lett.*, 121(2):022002, 2018.

[193] Sz. Borsanyi et al. Leading hadronic contribution to the muon magnetic moment from lattice QCD. *Nature*, 593(7857):51–55, 2021.

[194] F. J. Botella, G. C. Branco, M. N. Rebelo, and J. I. Silva-Marcos. What if the masses of the first two quark families are not generated by the standard model Higgs boson? *Phys. Rev.*, D94(11):115031, 2016.

[195] Chris Bouchard, G. Peter Lepage, Christopher Monahan, Heechang Na, and Junko Shigemitsu. Rare decay $B \to K\ell^+\ell^-$ form factors from lattice QCD. *Phys. Rev. D*, 88(5):054509, 2013. [Erratum: Phys.Rev.D 88, 079901 (2013)].

[196] Joachim Brod and Martin Gorbahn. Next-to-Next-to-Leading-Order Charm-Quark Contribution to the CP Violation Parameter ϵ_K and ΔM_K. *Phys. Rev. Lett.*, 108:121801, 2012.

[197] Joachim Brod, Martin Gorbahn, and Emmanuel Stamou. Two-Loop Electroweak Corrections for the $K \to \pi\nu\bar{\nu}$ Decays. *Phys. Rev. D*, 83:034030, 2011.

[198] Joachim Brod, Martin Gorbahn, and Emmanuel Stamou. Standard-Model Prediction of ϵ_K with Manifest Quark-Mixing Unitarity. *Phys. Rev. Lett.*, 125(17):171803, 2020.

[199] Joachim Brod, Martin Gorbahn, and Emmanuel Stamou. Updated Standard Model Prediction for $K \to \pi\nu\bar{\nu}$ and ϵ_K. *PoS*, BEAUTY2020:056, 2021.

[200] Thomas E. Browder, Nilendra G. Deshpande, Rusa Mandal, and Rahul Sinha. Impact of $B \to K\nu\bar{\nu}$ measurements on beyond the Standard Model theories. *Phys. Rev. D*, 104(5):053007, 2021.

[201] Gerhard Buchalla, Andrzej J. Buras, and Markus E. Lautenbacher. Weak decays beyond leading logarithms. *Rev. Mod. Phys.*, 68:1125–1144, 1996.

[202] W. Buchmuller, P. Di Bari, and M. Plumacher. Leptogenesis for pedestrians. *Annals Phys.*, 315:305–351, 2005.

[203] W. Buchmuller and D. Wyler. Effective Lagrangian Analysis of New Interactions and Flavor Conservation. *Nucl. Phys. B*, 268:621–653, 1986.

[204] Andrzej J. Buras, Jennifer Girrbach, Diego Guadagnoli, and Gino Isidori. On the Standard Model prediction for BR(Bs,d to mu+ mu-). *Eur. Phys. J. C*, 72:2172, 2012.

[205] Andrzej J. Buras, Jennifer Girrbach-Noe, Christoph Niehoff, and David M. Straub. $B \to K^{()}\nu\bar{\nu}$ decays in the Standard Model and beyond. *JHEP*, 02:184, 2015.

[206] Andrzej J. Buras, Martin Gorbahn, Sebastian Jäger, and Matthias Jamin. Improved anatomy of ε'/ε in the Standard Model. *JHEP*, 11:202, 2015.

[207] Andrzej J. Buras, Diego Guadagnoli, and Gino Isidori. On ϵ_K Beyond Lowest Order in the Operator Product Expansion. *Phys. Lett. B*, 688:309–313, 2010.

[208] Andrzej J. Buras, Julia Harz, and Martin A. Mojahed. Disentangling new physics in $K \to \pi\nu\overline{\nu}$ and $B \to K\,(K^*)\,\nu\overline{\nu}$ observables. *JHEP*, 10:087, 2024.

[209] Andrzej J. Buras, Sebastian Jager, and Jorg Urban. Master formulae for Delta F=2 NLO QCD factors in the standard model and beyond. *Nucl. Phys. B*, 605:600–624, 2001.

[210] Andrzej J. Buras, Mikolaj Misiak, and Jorg Urban. Two loop QCD anomalous dimensions of flavor changing four quark operators within and beyond the standard model. *Nucl. Phys. B*, 586:397–426, 2000.

[211] D. Buskulic et al. Measurement of Λ_b polarization in Z decays. *Phys. Lett. B*, 365:437–447, 1996.

[212] Dario Buttazzo, Admir Greljo, Gino Isidori, and David Marzocca. B-physics anomalies: a guide to combined explanations. *JHEP*, 11:044, 2017.

[213] Yusuf Buyukdag, Tony Gherghetta, and Andrew S. Miller. Partially composite supersymmetry. *Phys. Rev. D*, 99(3):035046, 2019.

[214] Yusuf Buyukdag, Tony Gherghetta, and Andrew S. Miller. Predicting the superpartner spectrum from partially composite supersymmetry. *Phys. Rev. D*, 99(5):055018, 2019.

[215] Nicola Cabibbo. Unitary Symmetry and Leptonic Decays. *Phys. Rev. Lett.*, 10:531–533, 1963.

[216] Lorenzo Calibbi, Andreas Crivellin, and Toshihiko Ota. Effective Field Theory Approach to $b \to s\ell\ell^{(\prime)}$, $B \to K^{(*)}\nu\bar{\nu}$ and $B \to D^{(*)}\tau\nu$ with Third Generation Couplings. *Phys. Rev. Lett.*, 115:181801, 2015.

[217] Anadi Canepa. Searches for Supersymmetry at the Large Hadron Collider. *Rev. Phys.*, 4:100033, 2019.

[218] Bernat Capdevila, Andreas Crivellin, Sebastien Descotes-Genon, Joaquim Matias, and Javier Virto. Patterns of New Physics in $b \to s\ell^+\ell^-$ transitions in the light of recent data. *JHEP*, 01:093, 2018.

[219] Rodolfo Capdevilla, David Curtin, Yonatan Kahn, and Gordan Krnjaic. Systematically Testing Singlet Models for $(g-2)_\mu$. 12 2021.

[220] Marcela Carena, M. Olechowski, S. Pokorski, and C. E. M. Wagner. Electroweak symmetry breaking and bottom - top Yukawa unification. *Nucl. Phys.*, B426:269–300, 1994.

[221] Bernard Carr and Florian Kuhnel. Primordial Black Holes as Dark Matter: Recent Developments. *Ann. Rev. Nucl. Part. Sci.*, 70:355–394, 2020.

[222] Bernard Carr, Florian Kuhnel, and Marit Sandstad. Primordial Black Holes as Dark Matter. *Phys. Rev. D*, 94(8):083504, 2016.

[223] N. Carrasco, P. Dimopoulos, R. Frezzotti, V. Lubicz, G. C Rossi, S. Simula, and C. Tarantino. ΔS=2 and ΔC=2 bag parameters in the standard model and beyond from N_f=2+1+1 twisted-mass lattice QCD. *Phys. Rev. D*, 92(3):034516, 2015.

[224] Massimo Casarsa, Marco Fabbrichesi, and Emidio Gabrielli. Monochromatic single photon events at the muon collider. 11 2021.

[225] CEPCStudyGroup. CEPC Conceptual Design Report: Volume 2 - Physics & Detector. 11 2018.

[226] Manimala Chakraborti, Sven Heinemeyer, and Ipsita Saha. The new "MUON G-2" result and supersymmetry. *Eur. Phys. J. C*, 81(12):1114, 2021.

[227] Manimala Chakraborti, Leszek Roszkowski, and Sebastian Trojanowski. GUT-constrained supersymmetry and dark matter in light of the new $(g-2)_\mu$ determination. 4 2021.

[228] B. Chakraborty et al. Strong-Isospin-Breaking Correction to the Muon Anomalous Magnetic Moment from Lattice QCD at the Physical Point. *Phys. Rev. Lett.*, 120(15):152001, 2018.

[229] Serguei Chatrchyan et al. Observation of a New Boson at a Mass of 125 GeV with the CMS Experiment at the LHC. *Phys. Lett. B*, 716:30–61, 2012.

[230] U. Chattopadhyay and Pran Nath. Probing supergravity grand unification in the Brookhaven g-2 experiment. *Phys. Rev.*, D53:1648–1657, 1996.

[231] Chuan-Hung Chen and C. Q. Geng. Study of $\Lambda_b \to \Lambda \nu \bar{\nu}$ with polarized baryons. *Phys. Rev. D*, 63:054005, 2001.

[232] Feng-Zhi Chen, Qiaoyi Wen, and Fanrong Xu. Correlating $B \to K^{(*)} \nu \bar{\nu}$ and flavor anomalies in SMEFT. *Eur. Phys. J. C*, 84(10):1012, 2024.

[233] Junmou Chen, Chih-Ting Lu, and Yongcheng Wu. Measuring Higgs boson self-couplings with $2 \to 3$ VBS processes. *JHEP*, 10:099, 2021.

[234] K. G. Chetyrkin, Johann H. Kuhn, and M. Steinhauser. RunDec: A Mathematica package for running and decoupling of the strong coupling and quark masses. *Comput. Phys. Commun.*, 133:43–65, 2000.

[235] S. Choudhury et al. Test of lepton flavor universality and search for lepton flavor violation in $B \to K\ell\ell$ decays. *JHEP*, 03:105, 2021.

[236] N. H. Christ, T. Izubuchi, C. T. Sachrajda, A. Soni, and J. Yu. Long distance contribution to the KL-KS mass difference. *Phys. Rev. D*, 88:014508, 2013.

[237] D. J. H. Chung, L. L. Everett, G. L. Kane, S. F. King, Joseph D. Lykken, and Lian-Tao Wang. The Soft supersymmetry breaking Lagrangian: Theory and applications. *Phys. Rept.*, 407:1–203, 2005.

[238] Marco Ciuchini et al. Delta M(K) and epsilon(K) in SUSY at the next-to-leading order. *JHEP*, 10:008, 1998.

[239] Marco Ciuchini, Marco Fedele, Enrico Franco, Ayan Paul, Luca Silvestrini, and Mauro Valli. Lessons from the $B^{0,+} \to K^{*0,+}\mu^+\mu^-$ angular analyses. *Phys. Rev. D*, 103(1):015030, 2021.

[240] Marco Ciuchini, Marco Fedele, Enrico Franco, Ayan Paul, Luca Silvestrini, and Mauro Valli. New Physics without bias: Charming Penguins and Lepton Universality Violation in $b \to s\ell^+\ell^-$ decays. *Phys. Rev. D*, 107(1):014025, 2023.

[241] Marco Ciuchini, E. Franco, V. Lubicz, G. Martinelli, I. Scimemi, and L. Silvestrini. Next-to-leading order QCD corrections to Delta F = 2 effective Hamiltonians. *Nucl. Phys. B*, 523:501–525, 1998.

[242] James M. Cline. Baryogenesis. pages 53–116, 1 2007.

[243] James M. Cline. B decay anomalies and dark matter from vectorlike confinement. *Phys. Rev. D*, 97(1):015013, 2018.

[244] Douglas Clowe, Marusa Bradac, Anthony H. Gonzalez, Maxim Markevitch, Scott W. Randall, Christine Jones, and Dennis Zaritsky. A direct empirical proof of the existence of dark matter. *Astrophys. J. Lett.*, 648:L109–L113, 2006.

[245] Gilberto Colangelo, Franziska Hagelstein, Martin Hoferichter, Laetitia Laub, and Peter Stoffer. Longitudinal short-distance constraints for the hadronic light-by-light contribution to $(g-2)_\mu$ with large-N_c Regge models. *JHEP*, 03:101, 2020.

[246] Gilberto Colangelo, Martin Hoferichter, Andreas Nyffeler, Massimo Passera, and Peter Stoffer. Remarks on higher-order hadronic corrections to the muon $g-2$. *Phys. Lett.*, B735:90–91, 2014.

[247] Gilberto Colangelo, Martin Hoferichter, Massimiliano Procura, and Peter Stoffer. Dispersion relation for hadronic light-by-light scattering: two-pion contributions. *JHEP*, 04:161, 2017.

[248] Gilberto Colangelo, Martin Hoferichter, and Peter Stoffer. Two-pion contribution to hadronic vacuum polarization. *JHEP*, 02:006, 2019.

[249] Gilberto Colangelo, Martin Hoferichter, and Peter Stoffer. Constraints on the two-pion contribution to hadronic vacuum polarization. *Phys. Lett. B*, 814:136073, 2021.

[250] Edvige Corbelli and Paolo Salucci. The Extended Rotation Curve and the Dark Matter Halo of M33. *Mon. Not. Roy. Astron. Soc.*, 311:441–447, 2000.

[251] Antonio Costantini, Federico De Lillo, Fabio Maltoni, Luca Mantani, Olivier Mattelaer, Richard Ruiz, and Xiaoran Zhao. Vector boson fusion at multi-TeV muon colliders. *JHEP*, 09:080, 2020.

[252] Peter Cox, Chengcheng Han, and Tsutomu T. Yanagida. Muon $g-2$ and Co-annihilating Dark Matter in the MSSM. 4 2021.

[253] Rupert Coy, Michele Frigerio, and Masahiro Ibe. Dynamical Clockwork Axions. *JHEP*, 10:002, 2017.

[254] Nathaniel Craig and Isabel Garcia Garcia. Rescuing Massive Photons from the Swampland. *JHEP*, 11:067, 2018.

[255] Nathaniel Craig, Isabel Garcia Garcia, and Dave Sutherland. Disassembling the Clockwork Mechanism. *JHEP*, 10:018, 2017.

[256] Andreas Crivellin and Momchil Davidkov. Do squarks have to be degenerate? Constraining the mass splitting with Kaon and D mixing. *Phys. Rev. D*, 81:095004, 2010.

[257] Andreas Crivellin, Javier Fuentes-Martin, Admir Greljo, and Gino Isidori. Lepton Flavor Non-Universality in B decays. *Phys. Rept.*, 856:1–24, 2020.

[258] Andreas Crivellin, Jennifer Girrbach, and Ulrich Nierste. Yukawa coupling and anomalous magnetic moment of the muon: an update for the LHC era. *Phys. Rev. D*, 83:055009, 2011.

[259] Andreas Crivellin, Christoph Greub, Francesco Saturnino, and Dario Müller. Importance of Loop Effects in Explaining the Accumulated Evidence for New Physics in B Decays with a Vector Leptoquark. *Phys. Rev. Lett.*, 122(1):011805, 2019.

[260] Andreas Crivellin, Martin Hoferichter, Claudio Andrea Manzari, and Marc Montull. Hadronic Vacuum Polarization: $(g-2)_\mu$ versus Global Electroweak Fits. *Phys. Rev. Lett.*, 125(9):091801, 2020.

[261] Andrzej Czarnecki and William J. Marciano. The Muon anomalous magnetic moment: A Harbinger for 'new physics'. *Phys. Rev. D*, 64:013014, 2001.

[262] Andrzej Czarnecki, William J. Marciano, and Arkady Vainshtein. Refinements in electroweak contributions to the muon anomalous magnetic moment. *Phys. Rev. D*, 67:073006, 2003. [Erratum: Phys.Rev.D 73, 119901 (2006)].

[263] Marco Cè, Antoine Gérardin, Georg von Hippel, Harvey B. Meyer, Kohtaroh Miura, Daniel San José, Hartmut Wittig, and Aaron Kuberski. Window observable for the hadronic vacuum polarization contribution to the muon $g-2$ from lattice QCD. *Phys. Rev. D*, 106(5):054502, 2022.

[264] Guido D'Amico, Marco Nardecchia, Paolo Panci, Francesco Sannino, Alessandro Strumia, Riccardo Torre, and Alfredo Urbano. Flavour anomalies after the R_{K^*} measurement. *JHEP*, 09:010, 2017.

[265] Igor Danilkin and Marc Vanderhaeghen. Light-by-light scattering sum rules in light of new data. *Phys. Rev.*, D95(1):014019, 2017.

[266] Luc Darmé, Luca Di Luzio, Maurizio Giannotti, and Enrico Nardi. Selective enhancement of the QCD axion couplings. *Phys. Rev. D*, 103(1):015034, 2021.

[267] Luc Darmé and Enrico Nardi. Exact accidental U(1) symmetries for the axion. 2 2021.

[268] Ashok K. Das and Chung Kao. A Two Higgs doublet model for the top quark. *Phys. Lett. B*, 372:106–112, 1996.

[269] Diganta Das and Jaydeb Das. The $\Lambda_b \to \Lambda^*(1520)(\to N\bar{K})\ell^+\ell^-$ decay at low-recoil in HQET. *JHEP*, 07:002, 2020.

[270] Nilakshi Das and Rupak Dutta. New physics analysis of $\Lambda_b \to (\Lambda^*(\to pK^-), \Lambda(\to p\pi))(\mu^+\mu^-, \nu\bar{\nu})$ baryonic decays under SMEFT framework. *Phys. Rev. D*, 108(9):095051, 2023.

[271] Alakabha Datta, Jiajun Liao, and Danny Marfatia. A light Z' for the R_K puzzle and nonstandard neutrino interactions. *Phys. Lett. B*, 768:265–269, 2017.

[272] Alakabha Datta, Danny Marfatia, and Lopamudra Mukherjee. $B \to K\nu\bar{\nu}$, MiniBooNE and muon g-2 anomalies from a dark sector. *Phys. Rev. D*, 109(3):L031701, 2024.

[273] Sacha Davidson, Enrico Nardi, and Yosef Nir. Leptogenesis. *Phys. Rept.*, 466:105–177, 2008.

[274] M. Davier, A. Hoecker, B. Malaescu, and Z. Zhang. A new evaluation of the hadronic vacuum polarisation contributions to the muon anomalous magnetic moment and to $\alpha(m_Z^2)$. *Eur. Phys. J.*, C80(3):241, 2020. [Erratum: Eur. Phys. J. **C80**, 410 (2020)].

[275] Michel Davier, Andreas Hoecker, Bogdan Malaescu, and Zhiqing Zhang. Reevaluation of the hadronic vacuum polarisation contributions to the Standard Model predictions of the muon $g-2$ and $\alpha(m_Z^2)$ using newest hadronic cross-section data. *Eur. Phys. J.*, C77(12):827, 2017.

[276] C. T. H. Davies et al. Hadronic-vacuum-polarization contribution to the muon's anomalous magnetic moment from four-flavor lattice QCD. *Phys. Rev.*, D101(3):034512, 2020.

[277] P. del Amo Sanchez et al. Search for the Rare Decay $B \to K\nu\bar{\nu}$. *Phys. Rev. D*, 82:112002, 2010.

[278] S. Descotes-Genon and Martín Novoa-Brunet. Angular analysis of the rare decay $\Lambda_b \to \Lambda(1520)(\to NK)\ell^+\ell^-$. *JHEP*, 06:136, 2019. [Erratum: JHEP 06, 102 (2020)].

[279] Sébastien Descotes-Genon, Lars Hofer, Joaquim Matias, and Javier Virto. Global analysis of $b \to s\ell\ell$ anomalies. *JHEP*, 06:092, 2016.

[280] Sébastien Descotes-Genon, Joaquim Matias, and Javier Virto. Understanding the $B \to K^*\mu^+\mu^-$ Anomaly. *Phys. Rev. D*, 88:074002, 2013.

[281] William Detmold, C. J. David Lin, Stefan Meinel, and Matthew Wingate. $\Lambda_b \to \Lambda\ell^+\ell^-$ form factors and differential branching fraction from lattice QCD. *Phys. Rev. D*, 87(7):074502, 2013.

[282] William Detmold and Stefan Meinel. $\Lambda_b \to \Lambda\ell^+\ell^-$ form factors, differential branching fraction, and angular observables from lattice QCD with relativistic b quarks. *Phys. Rev. D*, 93(7):074501, 2016.

[283] Luca Di Luzio and Marco Nardecchia. What is the scale of new physics behind the B-flavour anomalies? *Eur. Phys. J. C*, 77(8):536, 2017.

[284] Stefano Di Noi and Luca Silvestrini. RGESolver: a C++ library to perform renormalization group evolution in the Standard Model Effective Theory. *Eur. Phys. J. C*, 83(3):200, 2023.

[285] C. Diaconu, M. Talby, J. G. Korner, and D. Pirjol. Improved variables for measuring the Λ_b polarization. *Phys. Rev. D*, 53:6186–6194, 1996.

[286] J. Lorenzo Diaz-Cruz, R. Noriega-Papaqui, and A. Rosado. Measuring the fermionic couplings of the Higgs boson at future colliders as a probe of a non-minimal flavor structure. *Phys. Rev. D*, 71:015014, 2005.

[287] Michael Dine and Alexander Kusenko. The Origin of the matter - antimatter asymmetry. *Rev. Mod. Phys.*, 76:1–30, 2003.

[288] A.D. Dolgov. NonGUT baryogenesis. *Phys. Rept.*, 222:309–386, 1992.

[289] Mingyi Dong et al. CEPC Conceptual Design Report: Volume 2 - Physics & Detector. 11 2018.

[290] Ilja Doršner, Svjetlana Fajfer, and Nejc Košnik. Leptoquark mechanism of neutrino masses within the grand unification framework. *Eur. Phys. J. C*, 80(2):97, 2020.

[291] Herbert K. Dreiner, Julian Y. Günther, and Zeren Simon Wang. The Decay $B \to K\nu\bar{\nu}$ at Belle II and a Massless Bino in R-parity-violating Supersymmetry. 9 2023.

[292] Bhaskar Dutta and Yukihiro Mimura. Yukawa Unification with Four Higgs Doublets in Supersymmetric GUT. *Phys. Lett.*, B790:589–594, 2019.

[293] Daniel Egana-Ugrinovic, Samuel Homiller, and Patrick Roddy Meade. Higgs bosons with large couplings to light quarks. *Phys. Rev. D*, 100(11):115041, 2019.

[294] Gernot Eichmann, Christian S. Fischer, and Richard Williams. Kaon-box contribution to the anomalous magnetic moment of the muon. *Phys. Rev.*, D101(5):054015, 2020.

[295] Motoi Endo, Koichi Hamaguchi, Sho Iwamoto, and Teppei Kitahara. Supersymmetric Interpretation of the Muon $g-2$ Anomaly. 4 2021.

[296] N. Escudero, C. Munoz, and A. M. Teixeira. FCNCs in supersymmetric multi-Higgs doublet models. *Phys. Rev. D*, 73:055015, 2006.

[297] Adam F. Falk and Michael E. Peskin. Production, decay, and polarization of excited heavy hadrons. *Phys. Rev. D*, 49:3320–3332, 1994.

[298] Marco Farina, Duccio Pappadopulo, Fabrizio Rompineve, and Andrea Tesi. The photo-philic QCD axion. *JHEP*, 01:095, 2017.

[299] Marco Fedele, Alessio Mastroddi, and Mauro Valli. Minimal Froggatt-Nielsen textures. *JHEP*, 03:135, 2021.

[300] Thorsten Feldmann and Matthew W.Y. Yip. Form Factors for $\Lambda_b \to \Lambda$ Transitions in SCET. *Phys. Rev. D*, 85:014035, 2012. [Erratum: Phys.Rev.D 86, 079901 (2012)].

[301] Tobias Felkl, Anjan Giri, Rukmani Mohanta, and Michael A. Schmidt. When energy goes missing: new physics in $b \to s\nu\nu$ with sterile neutrinos. *Eur. Phys. J. C*, 83(12):1135, 2023.

[302] Jonathan L. Feng. Dark Matter Candidates from Particle Physics and Methods of Detection. *Ann. Rev. Astron. Astrophys.*, 48:495–545, 2010.

[303] Ferruccio Feruglio. Pieces of the Flavour Puzzle. *Eur. Phys. J. C*, 75(8):373, 2015.

[304] Ferruccio Feruglio. Flavor Physics in the era of Precision Physics. *Prog. Part. Nucl. Phys.*, 131:104049, 2023.

[305] Ferruccio Feruglio and Andrea Romanino. Lepton Flavour Symmetries. *Eur. Phys. J. C*, 81(3):233, 2021.

[306] Kåre Fridell, Mitrajyoti Ghosh, Takemichi Okui, and Kohsaku Tobioka. Decoding the $B \to K\nu\bar{\nu}$ excess at Belle II: Kinematics, operators, and masses. *Phys. Rev. D*, 109(11):115006, 2024.

[307] C.D. Froggatt and Holger Bech Nielsen. Hierarchy of Quark Masses, Cabibbo Angles and CP Violation. *Nucl. Phys. B*, 147:277–298, 1979.

[308] Javier Fuentes-Martin, Pedro Ruiz-Femenia, Avelino Vicente, and Javier Virto. DsixTools 2.0: The Effective Field Theory Toolkit. *Eur. Phys. J. C*, 81(2):167, 2021.

[309] M. Fukugita and T. Yanagida. Baryogenesis Without Grand Unification. *Phys. Lett. B*, 174:45–47, 1986.

[310] F. Gabbiani, E. Gabrielli, A. Masiero, and L. Silvestrini. A Complete analysis of FCNC and CP constraints in general SUSY extensions of the standard model. *Nucl. Phys. B*, 477:321–352, 1996.

[311] Emidio Gabrielli, Luca Marzola, Kristjan Müürsepp, and Martti Raidal. Explaining the $B^+ \to K^+\nu\bar{\nu}$ excess via a massless dark photon. *Eur. Phys. J. C*, 84(5):460, 2024.

[312] Francesco Garosi, David Marzocca, and Sokratis Trifinopoulos. LePDF: Standard Model PDFs for High-Energy Lepton Colliders. 3 2023.

[313] M.B. Gavela, P. Hernandez, J. Orloff, and O. Pene. Standard model CP violation and baryon asymmetry. *Phys. Lett. B*, 326:247–251, 1994.

[314] M.B. Gavela, P. Hernandez, J. Orloff, O. Pene, and C. Quimbay. Standard model CP violation and baryon asymmetry. Part 2: Finite temperature. *Nucl. Phys. B*, 430:382–426, 1994.

[315] Li-Sheng Geng, Benjamín Grinstein, Sebastian Jäger, Shuang-Yi Li, Jorge Martin Camalich, and Rui-Xiang Shi. Implications of new evidence for lepton-universality violation in $b \to s\ell^+\ell^-$ decays. *Phys. Rev. D*, 104(3):035029, 2021.

[316] Antoine Gérardin, Marco Cè, Georg von Hippel, Ben Hörz, Harvey B. Meyer, Daniel Mohler, Konstantin Ottnad, Jonas Wilhelm, and Hartmut Wittig. The leading hadronic contribution to $(g-2)_\mu$ from lattice QCD with $N_\mathrm{f} = 2+1$ flavours of O(a) improved Wilson quarks. *Phys. Rev.*, D100(1):014510, 2019.

[317] Antoine Gérardin, Harvey B. Meyer, and Andreas Nyffeler. Lattice calculation of the pion transition form factor with $N_f = 2+1$ Wilson quarks. *Phys. Rev.*, D100(3):034520, 2019.

[318] Tony Gherghetta, Jörn Kersten, Keith Olive, and Maxim Pospelov. Evaluating the price of tiny kinetic mixing. *Phys. Rev. D*, 100(9):095001, 2019.

[319] Tony Gherghetta and Alex Pomarol. Bulk fields and supersymmetry in a slice of AdS. *Nucl. Phys. B*, 586:141–162, 2000.

[320] Diptimoy Ghosh, Rick Sandeepan Gupta, and Gilad Perez. Is the Higgs Mechanism of Fermion Mass Generation a Fact? A Yukawa-less First-Two-Generation Model. *Phys. Lett.*, B755:504–508, 2016.

[321] Jennifer Girrbach, Susanne Mertens, Ulrich Nierste, and Soren Wiesenfeldt. Lepton flavour violation in the MSSM. *JHEP*, 05:026, 2010.

[322] G. F. Giudice, P. Paradisi, and M. Passera. Testing new physics with the electron g-2. *JHEP*, 11:113, 2012.

[323] G.F. Giudice, Tao Lin, and A. Riotto. A Supersymmetric Standard Model from Extra Dimensions. *Nucl. Phys. B*, 800:264–276, 2008.

[324] Gian F. Giudice, Markus A. Luty, Hitoshi Murayama, and Riccardo Rattazzi. Gaugino mass without singlets. *JHEP*, 12:027, 1998.

[325] Gian F. Giudice and Matthew McCullough. A Clockwork Theory. *JHEP*, 02:036, 2017.

[326] Gian F. Giudice and Alessandro Strumia. Probing High-Scale and Split Supersymmetry with Higgs Mass Measurements. *Nucl. Phys. B*, 858:63–83, 2012.

[327] D. Giusti, V. Lubicz, G. Martinelli, F. Sanfilippo, and S. Simula. Electromagnetic and strong isospin-breaking corrections to the muon $g-2$ from Lattice QCD+QED. *Phys. Rev.*, D99(11):114502, 2019.

[328] D. Giusti and S. Simula. Lepton anomalous magnetic moments in Lattice QCD+QED. *PoS*, LATTICE2019:104, 2019.

[329] Sheldon L. Glashow. Partial Symmetries of Weak Interactions. *Nucl. Phys.*, 22:579–588, 1961.

[330] C. Gnendiger, D. Stöckinger, and H. Stöckinger-Kim. The electroweak contributions to $(g-2)_\mu$ after the Higgs boson mass measurement. *Phys. Rev. D*, 88:053005, 2013.

[331] Andreas Goudelis, Kirtimaan A. Mohan, and Dipan Sengupta. Clockworking FIMPs. *JHEP*, 10:014, 2018.

[332] Admir Greljo and David Marzocca. High-p_T dilepton tails and flavor physics. *Eur. Phys. J. C*, 77(8):548, 2017.

[333] Admir Greljo, Jakub Salko, Aleks Smolkovič, and Peter Stangl. Rare b decays meet high-mass Drell-Yan. 12 2022.

[334] Yuval Grossman and Matthias Neubert. Neutrino masses and mixings in nonfactorizable geometry. *Phys. Lett. B*, 474:361–371, 2000.

[335] Yuval Grossman and Yosef Nir. Lepton mass matrix models. *Nucl. Phys. B*, 448:30–50, 1995.

[336] J. Grygier et al. Search for $B \to h\nu\bar{\nu}$ decays with semileptonic tagging at Belle. *Phys. Rev. D*, 96(9):091101, 2017. [Addendum: Phys.Rev.D 97, 099902 (2018)].

[337] B. Grzadkowski, M. Iskrzynski, M. Misiak, and J. Rosiek. Dimension-Six Terms in the Standard Model Lagrangian. *JHEP*, 10:085, 2010.

[338] Yuchao Gu, Ning Liu, Liangliang Su, and Daohan Wang. Heavy Bino and Slepton for Muon g-2 Anomaly. 4 2021.

[339] Diego Guadagnoli, Camille Normand, Silvano Simula, and Ludovico Vittorio. Insights on the current semi-leptonic B-decay discrepancies and how $B_s \to \mu^+\mu^-\gamma$ can help. *JHEP*, 10:102, 2023.

[340] Nico Gubernari, Ahmet Kokulu, and Danny van Dyk. $B \to P$ and $B \to V$ Form Factors from B-Meson Light-Cone Sum Rules beyond Leading Twist. *JHEP*, 01:150, 2019.

[341] Nico Gubernari, Marco Reboud, Danny van Dyk, and Javier Virto. Improved theory predictions and global analysis of exclusive $b \to s\mu^+\mu^-$ processes. *JHEP*, 09:133, 2022.

[342] Nico Gubernari, Méril Reboud, Danny van Dyk, and Javier Virto. Dispersive analysis of $B \to K^{(*)}$ and $B_s \to \phi$ form factors. *JHEP*, 12:153, 2023.

[343] Nico Gubernari, Danny van Dyk, and Javier Virto. Non-local matrix elements in $B_{(s)} \to \{K^{(*)}, \phi\}\ell^+\ell^-$. *JHEP*, 02:088, 2021.

[344] Howard E. Haber and Laurel Stephenson Haskins. Supersymmetric theory and models. 2017.

[345] Howard E. Haber and Laurel Stephenson Haskins. Supersymmetric theory and models. In *Theoretical Advanced Study Institute in Elementary Particle Physics: Anticipating the Next Discoveries in Particle Physics*, pages 355–499. WSP, 2018.

[346] T. Hahn and M. Perez-Victoria. Automatized one loop calculations in four-dimensions and D-dimensions. *Comput. Phys. Commun.*, 118:153–165, 1999.

[347] Thomas Hahn. Generating Feynman diagrams and amplitudes with FeynArts 3. *Comput. Phys. Commun.*, 140:418–431, 2001.

[348] Lawrence J. Hall, Riccardo Rattazzi, and Uri Sarid. The Top quark mass in supersymmetric SO(10) unification. *Phys. Rev.*, D50:7048–7065, 1994.

[349] Thomas Hambye, Daniele Teresi, and Michel H. G. Tytgat. A Clockwork WIMP. *JHEP*, 07:047, 2017.

[350] Chengcheng Han. Muon g-2 and CP violation in MSSM. 4 2021.

[351] Tao Han, Yang Ma, and Keping Xie. High energy leptonic collisions and electroweak parton distribution functions. *Phys. Rev. D*, 103(3):L031301, 2021.

[352] Tao Han, Yang Ma, and Keping Xie. Quark and gluon contents of a lepton at high energies. *JHEP*, 02:154, 2022.

[353] D. Hanneke, S. Fogwell, and G. Gabrielse. New Measurement of the Electron Magnetic Moment and the Fine Structure Constant. *Phys. Rev. Lett.*, 100:120801, 2008.

[354] K. Hayasaka et al. New Search for $\tau \to \mu\gamma$ and $\tau \to e\gamma$ Decays at Belle. *Phys. Lett. B*, 666:16–22, 2008.

[355] K. Hayasaka et al. Search for Lepton Flavor Violating Tau Decays into Three Leptons with 719 Million Produced Tau+Tau- Pairs. *Phys. Lett. B*, 687:139–143, 2010.

[356] Aram Hayrapetyan et al. Angular analysis of the $B^0 \to K^*(892)^0\mu^+\mu^-$ decay in proton-proton collisions at $\sqrt{s} = 13$ TeV. 11 2024.

[357] Aram Hayrapetyan et al. Test of lepton flavor universality in $B^{\pm} \to K^{\pm}\mu^{+}\mu^{-}$ and $B^{\pm} \to K^{\pm}e^{+}e^{-}$ decays in proton-proton collisions at $\sqrt{s} = 13$ TeV. *Rept. Prog. Phys.*, 87(7):077802, 2024.

[358] Xiao-Gang He, Xiao-Dong Ma, Michael A. Schmidt, German Valencia, and Raymond R. Volkas. Scalar dark matter explanation of the excess in the Belle II $B^{+} \to K^{+}+$ invisible measurement. *JHEP*, 07:168, 2024.

[359] Xiao-Gang He, Xiao-Dong Ma, and German Valencia. Revisiting models that enhance $B^{+} \to K^{+}\nu\bar{\nu}$ in light of the new Belle II measurement. *Phys. Rev. D*, 109(7):075019, 2024.

[360] Sven Heinemeyer, Essodjolo Kpatcha, Iñaki Lara, Daniel E. López-Fogliani, Carlos Muñoz, and Natsumi Nagata. The new $(g-2)_{\mu}$ result and the $\mu\nu$SSM. 4 2021.

[361] Ralf Hempfling. Yukawa coupling unification with supersymmetric threshold corrections. *Phys. Rev.*, D49:6168–6172, 1994.

[362] Florian Herren and Matthias Steinhauser. Version 3 of RunDec and CRunDec. *Comput. Phys. Commun.*, 224:333–345, 2018.

[363] Christopher T. Hill and Elizabeth H. Simmons. Strong dynamics and electroweak symmetry breaking. *Phys. Rept.*, 381:235–402, 2003. [Erratum: Phys.Rept. 390, 553–554 (2004)].

[364] Gudrun Hiller and Alex Kagan. Probing for new physics in polarized Λ_b decays at the Z. *Phys. Rev. D*, 65:074038, 2002.

[365] Gudrun Hiller and Roman Zwicky. Endpoint relations for baryons. *JHEP*, 11:073, 2021.

[366] Shu-Yu Ho, Jongkuk Kim, and Pyungwon Ko. Recent $B^{+} \to K^{+}\nu\bar{\nu}$ Excess and Muon $g-2$ Illuminating Light Dark Sector with Higgs Portal. 1 2024.

[367] Martin Hoferichter, Bai-Long Hoid, and Bastian Kubis. Three-pion contribution to hadronic vacuum polarization. *JHEP*, 08:137, 2019.

[368] Martin Hoferichter, Bai-Long Hoid, Bastian Kubis, Stefan Leupold, and Sebastian P. Schneider. Dispersion relation for hadronic light-by-light scattering: pion pole. *JHEP*, 10:141, 2018.

[369] Sungwoo Hong, Gowri Kurup, and Maxim Perelstein. Clockwork Neutrinos. *JHEP*, 10:073, 2019.

[370] Gerard 't Hooft. Naturalness, chiral symmetry, and spontaneous chiral symmetry breaking. In G. 't Hooft et al., editors, *Recent Developments in Gauge Theories*, volume 59 of *NATO Sci. Ser. B*, pages 135–157. Plenum Press, 9 1980.

[371] R. R. Horgan, Z. Liu, S. Meinel, and M. Wingate. Rare B decays using lattice QCD form factors. *PoS*, LATTICE2014:372, 2015.

[372] Ronald R. Horgan, Zhaofeng Liu, Stefan Meinel, and Matthew Wingate. Calculation of $B^0 \to K^{*0}\mu^+\mu^-$ and $B_s^0 \to \phi\mu^+\mu^-$ observables using form factors from lattice QCD. *Phys. Rev. Lett.*, 112:212003, 2014.

[373] Biao-Feng Hou, Xin-Qiang Li, Meng Shen, Ya-Dong Yang, and Xing-Bo Yuan. Deciphering the Belle II data on $B \to K\nu\overline{\nu}$ decay in the (dark) SMEFT with minimal flavour violation. *JHEP*, 06:172, 2024.

[374] Howard Baer and Vernon Barger and Hasan Serce. Anomalous muon magnetic moment, supersymmetry, naturalness, LHC search limits and the landscape. 2021.

[375] Quan-Yi Hu. Are the new particles heavy or light in $b \to sE_{\rm miss}$? 12 2024.

[376] Guo-yuan Huang, Sudip Jana, Farinaldo S. Queiroz, and Werner Rodejohann. Probing the RK(*) anomaly at a muon collider. *Phys. Rev. D*, 105(1):015013, 2022.

[377] Guo-yuan Huang, Farinaldo S. Queiroz, and Werner Rodejohann. Gauged $L_\mu - L_\tau$ at a muon collider. *Phys. Rev. D*, 103(9):095005, 2021.

[378] Patrick Huet and Eric Sather. Electroweak baryogenesis and standard model CP violation. *Phys. Rev. D*, 51:379–394, 1995.

[379] T. Hurth, F. Mahmoudi, and S. Neshatpour. B anomalies in the post $R_{K^{(*)}}$ era. *Phys. Rev. D*, 108(11):115037, 2023.

[380] Tobias Hurth, Farvah Mahmoudi, David Martínez Santos, and Siavash Neshatpour. More indications for lepton nonuniversality in $b \to s\ell^+\ell^-$. *Phys. Lett. B*, 824:136838, 2022.

[381] Alejandro Ibarra, Ashwani Kushwaha, and Sudhir K. Vempati. Clockwork for Neutrino Masses and Lepton Flavor Violation. *Phys. Lett. B*, 780:86–92, 2018.

[382] Sang Hui Im, Hans Peter Nilles, and Andreas Trautner. Exploring extra dimensions through inflationary tensor modes. *JHEP*, 03:004, 2018.

[383] Gino Isidori, Davide Lancierini, Patrick Owen, and Nicola Serra. On the significance of new physics in $b \to s\ell^+\ell^-$ decays. *Phys. Lett. B*, 822:136644, 2021.

[384] Gino Isidori, Saad Nabeebaccus, and Roman Zwicky. QED corrections in $\overline{B} \to \overline{K}\ell^+\ell^-$ at the double-differential level. *JHEP*, 12:104, 2020.

[385] Gino Isidori, Yosef Nir, and Gilad Perez. Flavor Physics Constraints for Physics Beyond the Standard Model. *Ann. Rev. Nucl. Part. Sci.*, 60:355, 2010.

[386] Gino Isidori and Sokratis Trifinopoulos. Exploring the flavour structure of the high-scale MSSM. *Eur. Phys. J. C*, 80(3):291, 2020.

[387] Sho Iwamoto, Tsutomu T. Yanagida, and Norimi Yokozaki. Wino-Higgsino dark matter in the MSSM from the $g-2$ anomaly. 4 2021.

[388] Fred Jegerlehner and Andreas Nyffeler. The Muon g-2. *Phys. Rept.*, 477:1–110, 2009.

[389] Friedrich Jegerlehner. The Anomalous Magnetic Moment of the Muon. *Springer Tracts Mod. Phys.*, 274:1–693, 2017.

[390] Elizabeth E. Jenkins, Aneesh V. Manohar, and Peter Stoffer. Low-Energy Effective Field Theory below the Electroweak Scale: Anomalous Dimensions. *JHEP*, 01:084, 2018.

[391] Elizabeth E. Jenkins, Aneesh V. Manohar, and Peter Stoffer. Low-Energy Effective Field Theory below the Electroweak Scale: Operators and Matching. *JHEP*, 03:016, 2018.

[392] Elizabeth E. Jenkins, Aneesh V. Manohar, and Michael Trott. Renormalization Group Evolution of the Standard Model Dimension Six Operators II: Yukawa Dependence. *JHEP*, 01:035, 2014.

[393] Gerard Jungman, Marc Kamionkowski, and Kim Griest. Supersymmetric dark matter. *Phys. Rept.*, 267:195–373, 1996.

[394] Yoo-Jin Kang, Soonbin Kim, and Hyun Min Lee. The Clockwork Standard Model. *JHEP*, 09:005, 2020.

[395] David Elazzar Kaplan and Timothy M. P. Tait. New tools for fermion masses from extra dimensions. *JHEP*, 11:051, 2001.

[396] Hidetoshi Kawase. Light Neutralino Dark Matter Scenario in Supersymmetric four-Higgs Doublet Model. *JHEP*, 12:094, 2011.

[397] Alex Kehagias and Antonio Riotto. Clockwork Inflation. *Phys. Lett. B*, 767:73–80, 2017.

[398] Alex Kehagias and Antonio Riotto. The Clockwork Supergravity. *JHEP*, 02:160, 2018.

[399] Alexander Keshavarzi, Daisuke Nomura, and Thomas Teubner. Muon $g-2$ and $\alpha(M_Z^2)$: a new data-based analysis. *Phys. Rev.*, D97(11):114025, 2018.

[400] Alexander Keshavarzi, Daisuke Nomura, and Thomas Teubner. The $g-2$ of charged leptons, $\alpha(M_Z^2)$ and the hyperfine splitting of muonium. *Phys. Rev.*, D101:014029, 2020.

[401] Vardan Khachatryan et al. Precise determination of the mass of the Higgs boson and tests of compatibility of its couplings with the standard model predictions using proton collisions at 7 and 8 TeV. *Eur. Phys. J. C*, 75(5):212, 2015.

[402] Vardan Khachatryan et al. Angular analysis of the decay $B^0 \to K^{*0}\mu^+\mu^-$ from pp collisions at $\sqrt{s} = 8$ TeV. *Phys. Lett. B*, 753:424–448, 2016.

[403] Jihn E. Kim. Weak Interaction Singlet and Strong CP Invariance. *Phys. Rev. Lett.*, 43:103, 1979.

[404] Simon J. D. King and Stephen F. King. Fermion mass hierarchies from modular symmetry. *JHEP*, 09:043, 2020.

[405] Ryuichiro Kitano and Yasunori Nomura. Supersymmetry, naturalness, and signatures at the LHC. *Phys. Rev. D*, 73:095004, 2006.

[406] Simon Knapen and Dean J. Robinson. Disentangling Mass and Mixing Hierarchies. *Phys. Rev. Lett.*, 115(16):161803, 2015.

[407] M. Knecht, S. Narison, A. Rabemananjara, and D. Rabetiarivony. Scalar meson contributions to a_μ from hadronic light-by-light scattering. *Phys. Lett.*, B787:111–123, 2018.

[408] Makoto Kobayashi and Toshihide Maskawa. CP Violation in the Renormalizable Theory of Weak Interaction. *Prog. Theor. Phys.*, 49:652–657, 1973.

[409] Alexander Kurz, Tao Liu, Peter Marquard, and Matthias Steinhauser. Hadronic contribution to the muon anomalous magnetic moment to next-to-next-to-leading order. *Phys. Lett.*, B734:144–147, 2014.

[410] Jack Laiho and Ruth S. Van de Water. Pseudoscalar decay constants, light-quark masses, and B_K from mixed-action lattice QCD. *PoS*, LATTICE2011:293, 2011.

[411] Hyun Min Lee. Gauged $U(1)$ clockwork theory. *Phys. Lett. B*, 778:79–87, 2018.

[412] J. P. Lees et al. Limits on tau Lepton-Flavor Violating Decays in three charged leptons. *Phys. Rev. D*, 81:111101, 2010.

[413] J. P. Lees et al. Search for $B \to K^{(*)}\nu\overline{\nu}$ and invisible quarkonium decays. *Phys. Rev. D*, 87(11):112005, 2013.

[414] Christoph Lehner and Aaron S. Meyer. Consistency of hadronic vacuum polarization between lattice QCD and the R-ratio. *Phys. Rev. D*, 101(7):074515, 2020.

[415] Michael Leurer, Yosef Nir, and Nathan Seiberg. Mass matrix models. *Nucl. Phys. B*, 398:319–342, 1993.

[416] Michael Leurer, Yosef Nir, and Nathan Seiberg. Mass matrix models: The Sequel. *Nucl. Phys. B*, 420:468–504, 1994.

[417] Li Li, Manqi Ruan, Yaqian Wang, and Yue Wang. Analysis of $B_s \to \phi\nu\bar{\nu}$ at CEPC. *Phys. Rev. D*, 105(11):114036, 2022.

[418] Lingfeng Li, Manqi Ruan, Yudong Wang, and Yuexin Wang. Analysis of $B_s \to \phi\nu\bar{\nu}$ at CEPC. *Phys. Rev. D*, 105(11):114036, 2022.

[419] Qiang Li et al. The physics potential of the CEPC. Prepared for the US Snowmass Community Planning Exercise (Snowmass 2021). 5 2022.

[420] Yu-Shuai Li, Su-Ping Jin, Jing Gao, and Xiang Liu. Transition form factors and angular distributions of the $\Lambda_b \to \Lambda(1520)(\to NK)\ell^+\ell^-$ decay supported by baryon spectroscopy. *Phys. Rev. D*, 107(9):093003, 2023.

[421] Manfred Lindner, Moritz Platscher, and Farinaldo S. Queiroz. A Call for New Physics : The Muon Anomalous Magnetic Moment and Lepton Flavor Violation. *Phys. Rept.*, 731:1–82, 2018.

[422] Wei Liu, Ke-Pan Xie, and Zihan Yi. Testing leptogenesis at the LHC and future muon colliders: a Z' scenario. 9 2021.

[423] Andrew J. Long. Cosmological Aspects of the Clockwork Axion. *JHEP*, 07:066, 2018.

[424] O. Lutz et al. Search for $B \to h^{(*)}\nu\bar{\nu}$ with the full Belle $\Upsilon(4S)$ data sample. *Phys. Rev. D*, 87(11):111103, 2013.

[425] Thomas Mannel and Gerhard A. Schuler. Semileptonic decays of bottom baryons at LEP. *Phys. Lett. B*, 279:194–200, 1992.

[426] Schedar Marchetti, Susanne Mertens, Ulrich Nierste, and Dominik Stockinger. Tan(beta)-enhanced supersymmetric corrections to the anomalous magnetic moment of the muon. *Phys. Rev.*, D79:013010, 2009.

[427] Stephen P. Martin. A Supersymmetry primer. *Adv. Ser. Direct. High Energy Phys.*, 18:1–98, 1998.

[428] David Marzocca. Addressing the B-physics anomalies in a fundamental Composite Higgs Model. *JHEP*, 07:121, 2018.

[429] David Marzocca, Marco Nardecchia, Alfredo Stanzione, and Claudio Toni. Implications of $B \to K\nu\bar{\nu}$ under rank-one flavor violation hypothesis. *Eur. Phys. J. C*, 84(11):1217, 2024.

[430] I. Masina and Carlos A. Savoy. Sleptonarium: Constraints on the CP and flavor pattern of scalar lepton masses. *Nucl. Phys. B*, 661:365–393, 2003.

[431] Pere Masjuan and Pablo Sánchez-Puertas. Pseudoscalar-pole contribution to the $(g_\mu - 2)$: a rational approach. *Phys. Rev.*, D95(5):054026, 2017.

[432] Richard Massey, Thomas Kitching, and Johan Richard. The dark matter of gravitational lensing. *Rept. Prog. Phys.*, 73:086901, 2010.

[433] David McKeen, John N. Ng, and Douglas Tuckler. Higgs portal interpretation of the Belle II $B^+ \to K^+ \nu\bar{\nu}$ measurement. *Phys. Rev. D*, 109(7):075006, 2024.

[434] Anibal D. Medina, Nicolás I. Mileo, Alejandro Szynkman, and Santiago A. Tanco. The Elusive Muonic WIMP. 12 2021.

[435] Stefan Meinel and Gumaro Rendon. $\Lambda_b \to \Lambda^*(1520)\ell^+\ell^-$ form factors from lattice QCD. *Phys. Rev. D*, 103(7):074505, 2021.

[436] Stefan Meinel and Gumaro Rendon. $\Lambda_c \to \Lambda^*(1520)$ form factors from lattice QCD and improved analysis of the $\Lambda_b \to \Lambda^*(1520)$ and $\Lambda_b \to \Lambda_c^*(2595, 2625)$ form factors. *Phys. Rev. D*, 105(5):054511, 2022.

[437] Barbara Mele and Guido Altarelli. Lepton spectra as a measure of b quark polarization at LEP. *Phys. Lett. B*, 299:345–350, 1993.

[438] Kirill Melnikov and Arkady Vainshtein. Hadronic light-by-light scattering contribution to the muon anomalous magnetic moment revisited. *Phys. Rev.*, D70:113006, 2004.

[439] R. Mertig, M. Böhm, and A. Denner. Feyn Calc - Computer-algebraic calculation of Feynman amplitudes. *Computer Physics Communications*, 64(3):345–359, 1991.

[440] Hideki Miyake, Shinhong Kim, and Fumihiko Ukegawa. Precise Measurements of Exclusive $b \to s\mu\mu$ Decay Amplitudes Using the Full CDF Data Set. 7 2012.

[441] Léo Morel, Zhibin Yao, Pierre Cladé, and Saïda Guellati-Khélifa. Determination of the fine-structure constant with an accuracy of 81 parts per trillion. *Nature*, 588(7836):61–65, 2020.

[442] Takeo Moroi. The Muon anomalous magnetic dipole moment in the minimal supersymmetric standard model. *Phys. Rev.*, D53:6565–6575, 1996. [Erratum: Phys. Rev.D56,4424(1997)].

[443] L. Mott and W. Roberts. Lepton polarization asymmetries for FCNC decays of the Λ_b baryon. *Int. J. Mod. Phys. A*, 30(27):1550172, 2015.

[444] Priyamvada Natarajan et al. Mapping substructure in the HST Frontier Fields cluster lenses and in cosmological simulations. *Mon. Not. Roy. Astron. Soc.*, 468(2):1962–1980, 2017.

[445] Ann E. Nelson and Matthew J. Strassler. Suppressing flavor anarchy. *JHEP*, 09:030, 2000.

[446] Matthias Neubert. B Physics and Flavor Model Building. 12 2018.

[447] Hans Peter Nilles. Supersymmetry, Supergravity and Particle Physics. *Phys. Rept.*, 110:1–162, 1984.

[448] Yasunori Nomura, Michele Papucci, and Daniel Stolarski. Flavorful Supersymmetry from Higher Dimensions. *JHEP*, 07:055, 2008.

[449] Paride Paradisi. Higgs-mediated $\tau \to \mu$ and $\tau \to e$ transitions in II Higgs doublet model and supersymmetry. *JHEP*, 02:050, 2006.

[450] Richard H. Parker, Chenghui Yu, Weicheng Zhong, Brian Estey, and Holger Müller. Measurement of the fine-structure constant as a test of the Standard Model. *Science*, 360:191, 2018.

[451] Aaron K. Parrott and Aoife Bharucha. $B \to V\nu\overline{\nu}$ in the Standard Model: Phenomenology and Model Independent Analysis. *JHEP*, 03:209, 2023.

[452] Ketan M. Patel. Fermion mass hierarchies from supersymmetric gauged flavour symmetry in 5D. 9 2020.

[453] K.M. Patel. Clockwork mechanism for flavor hierarchies. *Phys. Rev. D*, 96(11):115013, 2017.

[454] Vladyslav Pauk and Marc Vanderhaeghen. Single meson contributions to the muon‘s anomalous magnetic moment. *Eur. Phys. J.*, C74(8):3008, 2014.

[455] R.D. Peccei and Helen R. Quinn. CP Conservation in the Presence of Instantons. *Phys. Rev. Lett.*, 38:1440–1443, 1977.

[456] Estel Perez Codina and Philipp Gerhard Roloff. Hit multiplicity approach to b-tagging in FCC-hh. CERN-ACC-2018-0023, LCD-Note-2018-001, Jul 2018.

[457] Damien M. Pierce, Jonathan A. Bagger, Konstantin T. Matchev, and Renjie Zhang. Precision corrections in the minimal supersymmetric standard model. *Nucl. Phys.*, B491:3–67, 1997.

[458] Oleg Popov, Michael A. Schmidt, and Graham White. R_2 as a single leptoquark solution to $R_{D^{(*)}}$ and $R_{K^{(*)}}$. *Phys. Rev. D*, 100(3):035028, 2019.

[459] Maxim Pospelov. Secluded U(1) below the weak scale. *Phys. Rev. D*, 80:095002, 2009.

[460] Sitian Qian, Congqiao Li, Qiang Li, Fanqiang Meng, Jie Xiao, Tianyi Yang, Meng Lu, and Zhengyun You. Searching for heavy leptoquarks at a muon collider. *JHEP*, 12:047, 2021.

[461] N. Rajeev and Rupak Dutta. Consequences of $b \to s\mu^+\mu^-$ anomalies on $B \to K^{(*)}\nu\bar{\nu}$ $B_s \to (\eta, \eta')\nu\bar{\nu}$ and $B_s \to \phi\nu\bar{\nu}$ decay observables. *Phys. Rev. D*, 105(11):115028, 2022.

[462] Lisa Randall and Raman Sundrum. A Large mass hierarchy from a small extra dimension. *Phys. Rev. Lett.*, 83:3370–3373, 1999.

[463] Antonio Riotto and Mark Trodden. Recent progress in baryogenesis. *Ann. Rev. Nucl. Part. Sci.*, 49:35–75, 1999.

[464] Pablo Roig and Pablo Sánchez-Puertas. Axial-vector exchange contribution to the hadronic light-by-light piece of the muon anomalous magnetic moment. *Phys. Rev.*, D101(7):074019, 2020.

[465] Shibasis Roy, Ria Sain, and Rahul Sinha. Lepton mass effects and angular observables in $\Lambda_b \to \Lambda(\to p\pi)\ell^+\ell^-$. *Phys. Rev. D*, 96(11):116005, 2017.

[466] Vera C. Rubin and Jr. Ford, W. Kent. Rotation of the Andromeda Nebula from a Spectroscopic Survey of Emission Regions. *Astrophys. J.*, 159:379–403, 1970.

[467] Vera C. Rubin, Jr. Ford, W. Kent, and N. Thonnard. Rotational Properties of 21 Sc Galaxies with a Large Range of Luminosities and Radii from NGC 4605 (R = 4kpc) to UGC 2885 (R = 122kpc). *Astrophys. J.*, 238:471, 1980.

[468] Maximilian Ruhdorfer, Ennio Salvioni, and Andrea Wulzer. Invisible Higgs boson decay from forward muons at a muon collider. *Phys. Rev. D*, 107(9):095038, 2023.

[469] Richard Ruiz, Antonio Costantini, Fabio Maltoni, and Olivier Mattelaer. The Effective Vector Boson Approximation in high-energy muon collisions. *JHEP*, 06:114, 2022.

[470] Suchismita Sahoo, Rukmani Mohanta, and Anjan K. Giri. Explaining the R_K and $R_{D^{(*)}}$ anomalies with vector leptoquarks. *Phys. Rev. D*, 95:035027, Feb 2017.

[471] Andrei D. Sakharov. Violation of CP Invariance, C asymmetry, and baryon asymmetry of the universe. *Sov. Phys. Usp.*, 34(5):392–393, 1991.

[472] Andrei D. Sakharov. Violation of CP Invariance, C asymmetry, and baryon asymmetry of the universe. *Sov. Phys. Usp.*, 34(5):392–393, 1991. Pisma Zh. Eksp. Teor. Fiz. 5, 32–35 (1967).

[473] Jun John Sakurai and Jim Napolitano. *Modern Quantum Mechanics*. Quantum physics, quantum information and quantum computation. Cambridge University Press, 10 2020.

[474] Abdus Salam. Weak and Electromagnetic Interactions. pages 367–377, 1968.

[475] Francesco Sannino, J. Smirnov, and Zhi-Wei Wang. Asymptotically safe clockwork mechanism. *Phys. Rev. D*, 100(7):075009, 2019.

[476] Matthias Schott and Monica Dunford. Review of single vector boson production in pp collisions at $\sqrt{s} = 7$ TeV. *Eur. Phys. J. C*, 79(7):563, 2019.

[477] Eigo Shintani and Yoshinobu Kuramashi. Study of systematic uncertainties in hadronic vacuum polarization contribution to muon $g-2$ with 2+1 flavor lattice QCD. *Phys. Rev.*, D100(3):034517, 2019.

[478] Vladyslav Shtabovenko, Rolf Mertig, and Frederik Orellana. New Developments in FeynCalc 9.0. *Comput. Phys. Commun.*, 207:432–444, 2016.

[479] Vladyslav Shtabovenko, Rolf Mertig, and Frederik Orellana. FeynCalc 9.3: New features and improvements. *Comput. Phys. Commun.*, 256:107478, 2020.

[480] Luca Silvestrini and Mauro Valli. Model-independent Bounds on the Standard Model Effective Theory from Flavour Physics. *Phys. Lett. B*, 799:135062, 2019.

[481] Neetu Raj Singh Chundawat. CP violation in $b \to s\ell\ell$: a model independent analysis. *Phys. Rev. D*, 107:075014, 2023.

[482] A. M. Sirunyan et al. Identification of heavy-flavour jets with the CMS detector in pp collisions at 13 TeV. *JINST*, 13(05):P05011, 2018.

[483] Albert M Sirunyan et al. Measurement of angular parameters from the decay $\mathrm{B}^0 \to \mathrm{K}^{*0}\mu^+\mu^-$ in proton-proton collisions at $\sqrt{s} = 8$ TeV. *Phys. Lett. B*, 781:517–541, 2018.

[484] Albert M Sirunyan et al. Measurement of the Λ_b polarization and angular parameters in $\Lambda_b \to J/\psi\,\Lambda$ decays from pp collisions at $\sqrt{s} = 7$ and 8 TeV. *Phys. Rev. D*, 97(7):072010, 2018.

[485] Albert M Sirunyan et al. Combined measurements of Higgs boson couplings in proton-proton collisions at $\sqrt{s} = 13\,\mathrm{TeV}$. *Eur. Phys. J.*, C79(5):421, 2019.

[486] Albert M Sirunyan et al. Search for heavy neutrinos and third-generation leptoquarks in hadronic states of two τ leptons and two jets in proton-proton collisions at $\sqrt{s} = 13$ TeV. *JHEP*, 03:170, 2019.

[487] Albert M Sirunyan et al. A measurement of the Higgs boson mass in the diphoton decay channel. *Phys. Lett. B*, 805:135425, 2020.

[488] Albert M Sirunyan et al. Measurement of properties of $\mathrm{B}_\mathrm{s}^0 \to \mu^+\mu^-$ decays and search for $\mathrm{B}^0 \to \mu^+\mu^-$ with the CMS experiment. *JHEP*, 04:188, 2020.

[489] Albert M Sirunyan et al. Search for supersymmetry in final states with two oppositely charged same-flavor leptons and missing transverse momentum in proton-proton collisions at $\sqrt{s} = 13$ TeV. 2020.

[490] Albert M Sirunyan et al. Evidence for Higgs boson decay to a pair of muons. *JHEP*, 01:148, 2021.

[491] Berin Belma Sirvanli. Semileptonic $\Lambda_b \to \Lambda\nu\bar{\nu}$ decay in the Leptophobic Z-prime model. *Mod. Phys. Lett. A*, 23:347–358, 2008.

[492] Aleks Smolkovič, Michele Tammaro, and Jure Zupan. Anomaly free Froggatt-Nielsen models of flavor. *JHEP*, 10:188, 2019.

[493] David M. Straub. flavio: a Python package for flavour and precision phenomenology in the Standard Model and beyond. 10 2018.

[494] Sichun Sun, Qi-Shu Yan, Xiaoran Zhao, and Zhijie Zhao. Constraining rare B decays by $\mu^+\mu^- \to tc$ at future lepton colliders. 2 2023.

[495] Leonard Susskind. Dynamics of Spontaneous Symmetry Breaking in the Weinberg-Salam Theory. *Phys. Rev. D*, 20:2619–2625, 1979.

[496] M. Tanabashi et al. Review of Particle Physics. *Phys. Rev. D*, 98(3):030001, 2018.

[497] Walter Tangarife, Kohsaku Tobioka, Lorenzo Ubaldi, and Tomer Volansky. Dynamics of Relaxed Inflation. *JHEP*, 02:084, 2018.

[498] Daniele Teresi. Clockwork without supersymmetry. *Phys. Lett. B*, 783:1–6, 2018.

[499] Mark Trodden. Electroweak baryogenesis: A Brief review. *Int. J. Mod. Phys. A*, 14:2069–2122, 1999.

[500] Melissa Van Beekveld, Wim Beenakker, Marrit Schutten, and Jeremy De Wit. Dark matter, fine-tuning and $(g-2)_\mu$ in the pMSSM. 4 2021.

[501] Gero von Gersdorff. Natural Fermion Hierarchies from Random Yukawa Couplings. *JHEP*, 09:094, 2017.

[502] Gero von Gersdorff. Realistic GUT Yukawa couplings from a random clockwork model. *Eur. Phys. J. C*, 80(12):1176, 2020.

[503] Bigeng Wang. Calculation of the $K_L - K_S$ mass difference for physical quark masses. *PoS*, LATTICE2019:093, 2019.

[504] Fei Wang, Lei Wu, Yang Xiao, Jin Min Yang, and Yang Zhang. GUT-scale constrained SUSY in light of E989 muon g-2 measurement. 4 2021.

[505] S. Wehle et al. Lepton-Flavor-Dependent Angular Analysis of $B \to K^* \ell^+ \ell^-$. *Phys. Rev. Lett.*, 118(11):111801, 2017.

[506] Steven Weinberg. A Model of Leptons. *Phys. Rev. Lett.*, 19:1264–1266, 1967.

[507] Steven Weinberg. Electromagnetic and weak masses. *Phys. Rev. Lett.*, 29:388–392, 1972.

[508] Steven Weinberg. Implications of Dynamical Symmetry Breaking. *Phys. Rev. D*, 13:974–996, 1976. [Addendum: Phys.Rev.D 19, 1277–1280 (1979)].

[509] Qiaoyi Wen and Fanrong Xu. The Global Fits of New Physics in $b \to s$ after $R_{K^{(*)}}$ 2022 Release. 5 2023.

[510] Julius Wess and Jonathan Bagger. *Supersymmetry and supergravity*. Princeton University Press, Princeton, NJ, USA, 1992.

[511] Frank Wilczek. Problem of Strong P and T Invariance in the Presence of Instantons. *Phys. Rev. Lett.*, 40:279–282, 1978.

[512] Kenneth G. Wilson. The Renormalization Group and Strong Interactions. *Phys. Rev. D*, 3:1818, 1971.

[513] R. L. Workman et al. Review of Particle Physics. *PTEP*, 2022:083C01, 2022.

[514] Tianyi Yang, Sitian Qian, Zhe Guan, Congqiao Li, Fanqiang Meng, Jie Xiao, Meng Lu, and Qiang Li. Longitudinally polarized ZZ scattering at a muon collider. *Phys. Rev. D*, 104(9):093003, 2021.

[515] Wen Yin. Muon $g-2$ Anomaly in Anomaly Mediation. 4 2021.

[516] P. A. Zyla et al. Review of Particle Physics. *PTEP*, 2020(8):083C01, 2020.